3-18-2019

Improving Coupled Enzyme Assays With Capillary Electrophoresis

Thu Hoai Nguyen
Louisiana State University and Agricultural and Mechanical College

IMPROVING COUPLED ENZYME ASSAYS WITH CAPILLARY ELECTROPHORESIS

A Dissertation

Submitted to the Graduate Faculty of the
Louisiana State University and
Agricultural and Mechanical College
in partial fulfillment of the
requirements for the degree of
Doctor of Philosophy

in

The Department of Chemistry

by
Thu Hoai Nguyen
B.S., Vietnam National University, 2013
May 2019

ACKNOWLEDGEMENTS

First and foremost, I would like to thank my advisor, Dr. Doug Gilman, for the support and guidance during my time in the Gilman Group. The critical discussions with Dr. Gilman, together with and feedback from my committee members, Dr. Grover Waldrop, Dr. McCarley, Dr. Daniel Kuroda, Dr. Wayne Newhauser, and Dr. Daniel Cohen, have been invaluable to my development as a scientist.

I would like to thank Dr. Alexander Scheeline (UIUC), Dr. Ta Thi Thao, and Ms. Nguyen Thi Thai (VNU), my teachers and mentors, for their support and advice. I would also like to thank my mentors, Dr. Funda Kizilkaya and Dr. Kresimir Rupnik, for their support during my time serving as a teaching assistant in the analytical and instrumental analysis labs. Dr. Robin McCarley and Dr. John Hopkins, thank you for showing me what it takes to make a great teacher. I am thankful to Dr. Isiah Warner for not only allowing me to audit his Organized Media class and generously lending us the CE instrument when ours were broken, but also inspiring me to become a better person and leader. I also appreciate the support from the faculty and staff at the Department of Chemistry, especially Dr. Carol Taylor and Ms. Kim Mollere, who genuinely cared and fought for the graduate students' rights.

I would like to thank my coworkers at SC Johnson, especially Chyree Batton, my mentors (Aldo Alvarado, Calistor Nyambo, Daniel Glatch), and the ICE committee for giving me the best opportunity to develop professionally.

I am thankful to my friends in Louisiana and elsewhere. Thank you chi Huong, anh Lai, cu Ti, and Trang Nguyen for being my family away from home, my refuge from crisis. Thank you to chi Nha, Dr. John Hopkins, Ethan, and Julia for welcoming me with open arms. Thank you co Huyen, chu Duc, co Linh, and chu An for treating me like one of your children. I am grateful to my Bulgarian mom, Valentina Marinova,

for being there for me through laughter and tears. I would also like to thank my British mom, Ms. Christine Cook, for the company, tasty Highland coffee, and the chats over our walks. Nimisha Bhattarai, Ansonia Badgett, and Deepthi de Silva, thank you for the late night group study, happy hours, and beyond all, our friendship. Drew Malina, thank you for training me on capillary electrophoresis, and keeping me company when I first joined the Gilman Group. To Della Saputra, Paul Abanador, Kieu Tran, Bao Pham, Truc Tran, Nga Nguyen, Huy Nguyen, Nha Tran, Doanh Do, Kathryn McKee, Manny and the chemists gang, and others I cannot mention, thank you for your support, gym time, LSU game time, the gatherings, and the great times that I dearly treasure. A big “Thank you” goes to my best friends Binh “Bun”, Dung Sh*t, Thanh Truong for being there for me. Though in different time zones, we still managed to make our friendship strong and our jokes corny ☺

Last but not least, I am grateful for my supportive family. Thank you dad and mom for setting me free to explore the world on my own. To my brother, my best friend and childhood foe, thank you for taking care of mom and dad when I was away. Grandma, please keep watching over me. I love and miss you every day.

Without y’all, I would not be who I am today. Thank you!

TABLE OF CONTENTS

LIST OF TABLES

LIST OF FIGURES

LIST OF SCHEMES

ABSTRACT

The goal of this project is to address limitations of coupled enzyme assays using capillary electrophoresis (CE). In some enzyme assays, it is ineffective to directly detect products and substrates spectroscopically (absorption or fluorescence). Coupling the enzyme-catalyzed reaction of interest with another enzyme-catalyzed reaction allows for indirect detection of product formation or substrate depletion for the target enzyme. While conventional coupled enzyme assays are facile for kinetic measurements, they can be problematic for inhibition screening due to spectral and inhibitor interferences. To address these limitations of coupled assays, CE has been used to develop enzyme assays for acetyl-coenzyme A carboxylase (ACC). The first approach is to utilize CE to separate assay components (substrates, products, and inhibitors) and avoid using coupling enzymes. In Chapter 2, a previously developed bacterial holo-ACC assay was optimized and applied to study the inhibition of bacterial holo-ACC, BC, and CT by five flavonols (myricetin, quercetin, anrantine osage orange, galangin, and DHF). The IC_{50} values for these inhibitors were determined using offline CE assays. A new offline assay developed for a human form of ACC, human ACC2, is presented in Chapter 3. This assay was used to detect inhibition of the human enzyme. The second approach is to use coupling enzymes, but in combination with CE separation to reduce spectral interference and inhibitor interference with the coupled reactions. The envisioned CE coupled enzyme assay will use a light emitting diode (LED) as the excitation source for fluorescence detection of NADH consumption. Although LEDs have been widely used as alternatives to lasers for fluorescence detection, studies on the stability and noise associated with LEDs for CE detection are limited. In Chapter 4, a 470-nm LED was quantitatively compared to argon ion laser lines as a source for fluorescence detection with CE. Appendix 1 presents progress in

the development of the CE online coupled assay for ACC. This assay will use magnetic beads as the solid support for immobilized the coupling enzymes, and the fluorescence detection of NADH with LED excitation.

CHAPTER 1. INTRODUCTION

1.1. Enzyme Catalysis, Inhibition and Assays

1.1.1. Enzyme Catalysis

Enzymes are biomolecules that catalyze chemical reactions to sustain life's critical functions in living entities. They are not only attractive targets for drug development but also important ingredients for chemical, food, and brewing industries. The vast majority of enzymes are proteins, except for catalytic ribonucleic acid enzymes, or ribozymes [1, 2]. Without enzyme catalysis, some biochemical reactions are too slow to maintain life functions. Protein enzymes accelerate reactions from 10^7- to 10^{19}-fold [3]. For example, orotidine 5'-monophosphate decarboxylase enhances the decarboxylation of orotidine monophosphate to form uridine monophosphate by a factor of 10^{17} [4]. Another enzyme, arginine decarboxylase, accelerates the decarboxylation of L-arginine to form agmatine by 10^{19}-fold [5].

Like all proteins, protein enzymes are built from amino acids. The assembling of amino acids into a protein is defined in four levels: primary, secondary, tertiary and quaternary structures. The primary structure is the linear polypeptide chain in which the amino acid residues are covalently linked through amide bonds. The secondary structure refers to the polypeptide chains folding into stable patterns such as alpha helices, beta sheets, and occasionally turns, loops, or hairpins. This arrangement is driven by hydrogen bonding between carboxyl groups and amino groups in close proximity. The tertiary structure is the three-dimensional arrangement of a single polypeptide chain. Finally, multiple polypeptide chains constitute subunits of the quaternary structure.

An enzyme derives its catalytic ability by catalyzing the conversion of substrates to products. The enzyme catalysis is initiated by the enzyme binding with a substrate

molecule to form an enzyme-substrate complex. This step takes place in a binding pocket or groove called the active site, which is relatively small compared to the total volume of the enzyme. Active sites are hydrophobic microenvironments that possess highly polarized functional groups [6]. Active sites usually have complementary shapes and structures to the substrates. The binding of a substrate to the active site is stabilized through weak noncovalent interactions such as electrostatic force, hydrogen bonding, hydrophobic interactions, and van der Waals interactions. Upon binding, the substrate is desolvated inside the active site and protected from the bulk aqueous solution. A chemically active portion of the active site then acts upon and distorts the enzyme-substrate bond. Consequently, changes in spatial orientation, bond length, or bond strength transform the substrate to product(s) [6].

Enzyme catalysis is regulated by not only the active sites but also cofactors which can be divided into two groups: metals and coenzymes. Metal ions such as Fe^{2+}, Mg^{2+}, Zn^{2+}, Ni^{2+}, and K^{+} which serve as Lewis acid or an electron acceptor/donator usually bind to either the enzyme or substrate. The metal-substrate complexes are actual substrates for the enzymatic reactions. For example, Mg^{2+} is needed for acetyl coenzyme A carboxylase-catalyzed reaction in which the Mg^{2+}-ATP complex is the actual substrate and Mg^{2+} also binds to the active site on the enzyme [7]. Coenzymes are small organic compounds derived from vitamins, exemplified by biotin, which is also known as vitamin B_7. Biotin is responsible for the transfer of the carboxyl group in carboxylase-catalyzed reactions [8]. A metal ion or a coenzyme that covalently bonds with the enzyme is called a prosthetic group. The holistic enzyme bound with metal ions or coenzymes is referred to as a holoenzyme [9].

1.1.2. Enzyme Kinetics

Equation 1.1 shows the progress of an enzyme-catalyzed reaction, provided that every step is reversible:

$$E + S \rightleftharpoons ES \rightleftharpoons ES^{\ddagger} \rightleftharpoons EP \rightleftharpoons E + P \qquad 1.1$$

An enzyme-catalyzed reaction starts with the formation of a binary encounter complex ES, also known as the Michaelis complex, by the binding of the enzyme (E) to the substrate (S). Subsequently, the binary encounter complex ES goes through the transition state ($ES^{\ddagger}$) and a bound product state (EP) before the product (P) and free enzyme (E) are released. The change in free energy over the course of an enzyme-catalyzed reaction is illustrated in Figure 1.1. Regardless of how negative the Gibbs free energy (ΔG) is, the substrates must overcome the activation energy (E_a) in order to be converted to the products. An enzyme functions through the formation of the transition complex between the enzyme and substrate to lower the activation energy (E_a'), leading to enhanced reaction rate while the reaction equilibrium remains unchanged.

The series of reactions after the formation of binary encounter complex ES are combined and represented as the conversion from ES to enzyme (E) and product (P). The corresponding rate constant for this process, k_2, predominantly depends on the formation of the transition state complex $ES^{\ddagger}$. Equation 1.2 shows the simplified enzymatic reaction:

$$E + S \underset{k_{-1}}{\overset{k_1}{\rightleftharpoons}} ES \xrightarrow{k_2} E + P \qquad 1.2$$

The Michaelis-Menten model of enzyme kinetics is based on several assumptions. First, the concentration of ES encounter complex is at steady state for a prolonged time period. In this condition, a balance between rate of ES formation and

rate of ES dissociation results in constant concentration of ES. Second, the reverse reaction to convert product back to substrate is negligible, provided that at the early stage of the enzymatic reaction, the concentration of product was relatively low. Therefore, the product formation is assumed to be an irreversible and rate-determining step. As a consequence, the change in ES concentration over time is calculated as:

$$\frac{d[ES]}{dt} = k_1[E][S] - k_{-1}[ES] - k_2[ES] = 0 \qquad 1.3$$

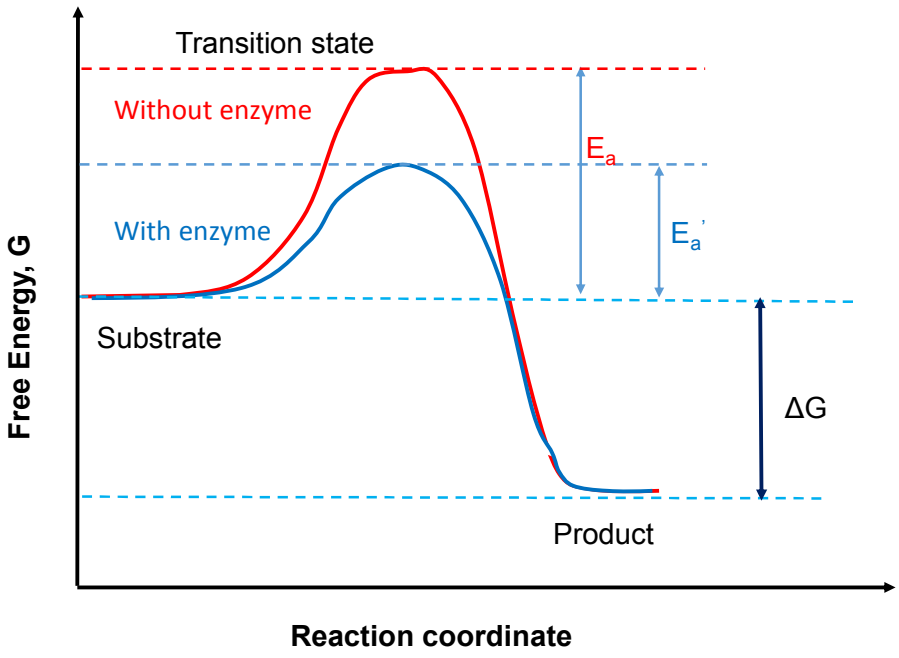

Figure 1.1. Energy diagram for enzymatic catalysis

The initial rate of reaction, measured as substrate depletion or product formation, is proportional to ES complex concentration:

$$v = -\frac{d[S]}{dt} = \frac{d[P]}{dt} = k_2[ES] \qquad 1.4$$

Provided that concentration of ES is constant under steady state conditions, the initial rate of reaction is also constant and can be calculated as the slope of the linear plot of [S[or [P] versus reaction time. The constant ES level is practically established

at high substrate concentration (micromolar to millimolar) relative to enzyme concentration (nanomolar). In the initial phase of the reaction, only a small portion of substrate depletes so the steady state condition is maintained. As the reaction proceeds, more substrate is consumed and converted to more products. After this point, the assumption of steady state does not apply, and the reaction rate slows down until the product formation reach equilibrium. The plot of product concentration as a function of time is shown in Figure 1.2.

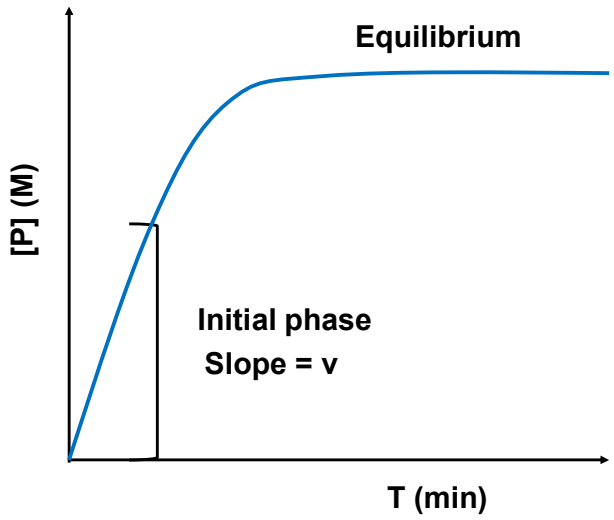

Figure 1.2. Schematic depiction of enzymatic reaction progress

At a fixed enzyme concentration, the dependence of the initial rate of reaction on substrate concentration is described by the Henri and Michaelis-Menten models:

$$v = \frac{V_{max}[S]}{K_m + [S]} \qquad 1.5$$

where v is the initial reaction rate, V_{max} is the maximum reaction rate at an infinite substrate concentration, [S] is the substrate concentration, and K_m is the Michaelis constant. Figure 1.3 illustrates the initial reaction rate as a function of substrate concentration when the enzyme concentration is kept constant.

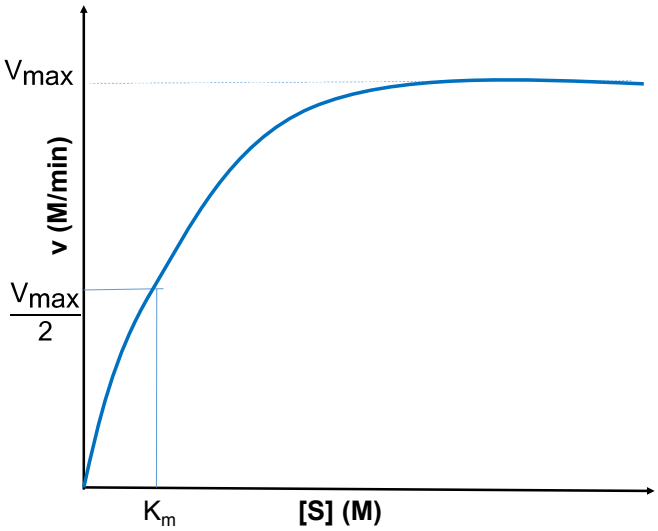

Figure 1.3. Schematic depiction of the dependence of reaction rate on substrate concentration

When the substrate is added at a negligible concentration relative to K_m, Equation 1.5 can be simplified as:

$$v = \frac{V_{max}}{K_m}[S] \qquad 1.6$$

As such, the initial reaction rate is linearly proportional to substrate concentration, and this linear portion has a slope of V_{max}/K_m. As the substrate concentration increases well above K_m, the initial rate of reaction reaches the maximum level, V_{max}. In this condition, the active sites of all enzyme molecules are likely saturated by the substrate. At substrate concentration equivalent to K_m, equation 1.5 becomes:

$$v = \frac{V_{max}[S]}{[S]+[S]} = \frac{V_{max}}{2} \qquad 1.7$$

Therefore, K_m is equal to the substrate concentration at which the initial rate of reaction equals half of the maximum rate.

1.1.3. Enzyme Inhibition

Enzymes are essential for all life, but enzyme inhibition is an attractive target for drug discovery. First of all, like other living entities, pathogens such as viruses, bacteria, and fungi rely on enzymes to maintain their functions. Selectively inhibiting certain enzymes in these pathogens is likely to disrupt their functions, weaken, and even kill them. As such, enzyme inhibition in infectious agents is effective for treatment of illness or infectious diseases of their hosts. In modern medicine, a plethora of antibiotics, antiviral and anti-parasitic drugs function based on selective enzyme inhibition [6]. Second, although enzymes are needed for biological functions, enzyme overexpression or exceedingly high enzyme activity is linked to disease stages. Mutation of genes encoding an enzyme can lead to abnormally high enzyme concentration (enzyme overexpression) and consequently generates excessive product concentrations. Alternatively, point mutations in an enzyme can result in aberrantly high enzyme activity, also giving rise to high product formation. Therefore, enzymes are an attractive target for intervention in many diseases [6].

In clinical use, a significant portion of drugs treat diseases through enzyme inhibition. According to Hopkins and Groom, about 47% of small molecule drugs available on market inhibit enzymes as their molecular targets [10]. Enzyme inhibitors are mostly small molecules that keep the substrates from being converted to products by binding to either the enzyme, substrate, or both. Enzymes are susceptible to reversible or irreversible inhibition. Reversible inhibitors bind to the enzymes via weak, non-covalent interactions such as hydrophobic interactions and hydrogen bonding. Alternatively, irreversible inhibitors form strong covalent bonds with enzymes that permanently alter the catalytic activity [6].

Most drugs inhibit their target enzymes through reversible interactions. Reversible enzyme inhibition proceeds in three modalities: competitive inhibition, uncompetitive inhibition, and noncompetitive inhibition. Figure 1.4 shows the possible pathways the inhibitor can take to inhibit an enzymatic reaction.

In competitive inhibition, the inhibitor shows exclusive affinity to the free enzyme. Typically, a competitive inhibitor is a compound that resembles the substrate with respect to chemical structure and molecular geometry. As a result, the inhibitor and substrate are mutually exclusive as they compete for the active site. Binding of the competitive inhibitor to the enzyme at the active site to form EI interferes with the interaction of substrate with the enzyme. However, the binding of the enzyme to either the inhibitor or substrate is reversible. Therefore, substrate at sufficiently high concentration can dominantly bind to the enzyme and minimize the enzyme inhibition. Consequently, competitive inhibition depends on concentrations of the substrate and product, and their affinity towards the enzyme.

Alternatively, uncompetitive inhibition indicates the case in which an inhibitor shows affinity to only the enzyme-substrate complex (ES). As such, the formation of ES is a prerequisite for the inhibition. Upon binding to the ES complex, the uncompetitive inhibitor prevents the subsequent transformation of the ES complex to the bound transition state of the substrate (ES^+). In uncompetitive inhibition, the apparent K_m and V_{max} decrease as the concentration of the uncompetitive inhibitor increases.

Lastly, a noncompetitive inhibitor exhibits affinity to both the free enzyme E and the enzyme-substrate complex ES, resulting in the formation of the enzyme-inhibitor (EI) and the enzyme-substrate-inhibitor (ESI) complexes. The dissociation constants of EI and ESI are K_i and αK_i, respectively. When $\alpha = 1$, the noncompetitive inhibitor

has equal affinity towards the free enzyme E and the ES complex. When α < 1, the binding of the noncompetitive inhibitor towards the ES complex is more favorable whereas with α > 1, the noncompetitive inhibitor shows stronger affinity to the free enzyme.

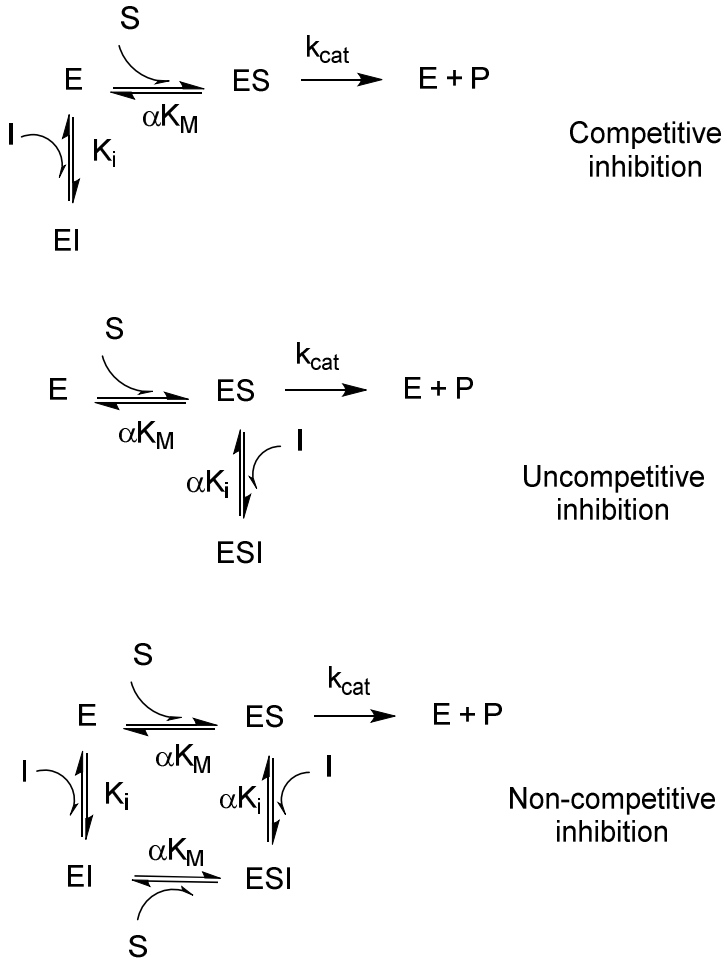

Figure 1.4. Enzyme inhibition mechanisms

1.1.4. Enzyme Assays

Enzyme assays are the measurement of substrate depletion or product formation for enzyme-catalyzed reactions to study the function of enzymes or quantify enzymes. Performing these assays allows for either qualitative or quantitative analysis of enzyme. Owing to enzyme's highly selective catalysis, the presence of one enzyme in an unknown sample can be confirmed by its catalyzed reaction. Meanwhile, for the

quantitative analysis of an enzyme, determining enzyme concentration is enabled by measuring substrate depletion or product formation.

An assay is initiated by mixing substrates, cofactors and the enzyme, followed by incubating the reaction mixture. In subsequence, the products or substrates can be monitored continuously as the reaction proceeds (continuous assays) or after the reaction is terminated (discontinuous assay). The incubation can be terminated by adding a quenching reagent to the reaction mixture, rapid freezing or heating without destroying the product. Acids such as perchloric acid and trichloroacetic acid are usually added to denature the enzyme, and consequently quench the reaction. For enzymes that require divalent metals as a cofactor, ethylenediaminetetraaceticc acid (EDTA) can be added to form chelate with metal ions and stop the reaction [6].

One of the conventional methods used for enzyme assays is radiochemical assay. This type of assay utilizes radiolabeled substrates containing radioactive isotopes, typically ^{14}C or ^{32}P, which are then incorporated in the products as the enzymatic reactions proceed. Radioactive isotopes are unstable, and they undergo radioactive decay to release energy through particle emission (alpha particles, beta particles) or electromagnetic radiation (gamma rays). In a radiochemical assay, after the incubation is quenched, a scintillation solution containing a solvent and a phosphor is added to the reaction mixture, followed by radioactivity measurement. Upon interacting with a phosphor, the energy emitted by radioactive decay can be absorbed by the phosphor which in turn emits light. This light emission, also known as scintillation, can be measured by a liquid scintillation counter, which is equipped with a photomultiplier tube. Depending on the stability of the products and substrates, quenching reagents are added to selectively remove the less stable components. Then either the remaining substrates or resulting products are measured by liquid

scintillation counting. For example, Tanabe and coworkers reported on a radiochemical assay for acetyl-coenzyme A carboxylase (ACC) where the substrate $KH^{14}CO_3$ is less stable than the product [^{14}C]malonyl-CoA. After HCl was added to the incubation mixture, the unreacted $KH^{14}CO_3$ was removed, and the concentration of the acid-stable [^{14}C]malonyl-CoA was subsequently measured based on its radioactivity [11]. Guchhait and coworkers demonstrated the carboxyltransferase radioactive assay in which the substrate [^{14}C]malonyl-CoA is acid-stable while the product N-[^{14}C]carboxybiotin methyl ester was destroyed upon the addition of HCl [12]. As a result, the enzyme activity was monitored based on the decrease in radioactivity of the product after incubation. Despite its application to plethora of enzymes, the radiochemical assay is limited in practice due to high cost, health risk, and issues related to waste regulation.

Simple, direct spectrophotometric assays were also developed to study enzyme kinetics and inhibition [13-15]. This type of assay is feasible if the difference in signal of the substrates and products can be detected. For example, dipeptidyl carboxypeptidase, an angiotensin converting enzyme (ACE), was assayed using the direct spectrophotometric assays [14, 15]. This enzyme catalyzes the conversion of angiotensin I (a decapeptide) to angiotensin II (an octapeptide) and a C-terminal His-Leu [14, 15]. Holmquist et al. used the artificial furanacryloyl-blocked tripeptides as substrates for the dipeptidyl carboxypeptidase-catalyzed reaction [14]. A blue shift of the absorption spectrum was observed owing to the hydrolysis of the substrates into funranacryloyl-amino acids and dipeptides. The reaction progress was monitored based on the decrease in absorbance of the reaction mixture at 328 and 352 nm [14]. Based on this assay, other spectrophotometric assays were modified and optimized to study kinetics and inhibition of ACE [15, 16]. Similarly, Hayre et al. assayed sialidase

using two artificial substrates [13]. The kinetic study was based on the red shift of absorption spectrum from 300 to 315 nm upon the hydrolysis of the substrate. Despite their applicability to various enzymes, direct spectrophotometric assays are limited to enzymatic reactions which result in a change in the absorbance.

For enzymatic reactions whose substrates or products are difficulty to detect directly, additional enzymes are often used for indirect monitoring of the reaction progress. Such cases are referred to as coupled enzyme assays. In this type of assay, either the product or substrate of the primary reaction becomes the substrate for the coupling enzymatic reaction whose progress is easily monitored. The most common coupling enzymes involve the oxidation of NAD(P)H or reduction of $NAD(P)^+$ which can be detected by UV-Vis absorption or fluorescence, typically carried out in cuvettes or well plates. Coupled enzyme assays offer the advantages of both continuous and discontinuous monitoring of reaction progress and applicability to high-throughput screening (HTS). There are some practical guidelines that need to be considered when carrying out coupled enzyme assays. First, the final signal should primarily correspond to the activity of the enzyme of interest and be independent of the coupling enzymes. This can be achieved by using relatively low concentration of the primary enzyme compared to the coupling enzymes, so that the primary enzyme is rate-limiting. Second, the inhibition detected upon screening should be due to inhibition of the primary enzyme, but not the coupling enzymes. As such, it is important to verify that the coupling enzymes do not give false positive by carrying out a control experiment with the coupling enzymes and in the absence of the primary enzyme. Third, the signal recorded should correspond to the product formation or substrate disappearance, and not be interfered with by the signal from the inhibitor or other enzyme assay components. Subtracting the attributed signal of control (not containing

the enzyme) from the final signal or using a proper detection method to selectively measure the substrate or product will enable monitoring of reaction progress with limited spectral interference. Fourth, for coupled enzyme assays, besides the reagents required for the primary reaction, additional reagents including the coupling enzymes, substrates and cofactors for the coupling reactions are also needed. Therefore, coupled enzyme assays can be costly, especially for high-throughput screening, which requires a large amount of reagents for a large library screening.

For reactions whose substrates and products cannot be quantified reliably during the reaction, it is desirable to perform the assay after the reaction is quenched and separate the assay mixture prior to analysis. Separation-based enzyme assays have been implemented, using high performance liquid chromatography (HPLC) or capillary electrophoresis (CE) [17, 18]. In such assays, the reaction should be stopped within the initial phase where the signal is linearly proportional to reaction time (Figure 1.2). In subsequence, the enzyme components are separated and quantified based on the area under their corresponding peaks. The typical detection methods used for HPLC and CE include UV-vis absorption and fluorescence.

1.2. Acetyl-Coenzyme A Carboxylase (ACC)

1.2.1. Overview on ACC

Acetyl-coenzyme A carboxylase (ACC) is an essential enzyme for fatty acid synthesis and metabolism [19]. Discovered by Wakil and Gibson 60 years ago, this enzyme was recognized for containing a high biotin concentration and its involvement in long-chain fatty acid synthesis from acetyl-CoA [20]. Between two enzymes required for long-chain fatty acid synthesis from acetyl-CoA (ACC and fatty acid synthase), ACC has lower catalytic capacity than fatty acid synthase [21]. This finding suggests that ACC is responsible for the rate-limiting step in fatty acid synthesis.

ACC is a biotin-dependent carboxylase made up of three components including biotin carboxylase (BC), carboxyltransferase (CT) and biotin carboxyl carrier protein (BCCP). Biotin, also known as vitamin H or vitamin B8, is a prosthetic group covalently attached to BCCP through an amide bond. ACC catalyzes the carboxylation of acetyl-coenzyme A (acetyl-CoA) to generate malonyl-coenzyme A (malonyl-CoA) in two half reactions (Figure 1.5). The first half-reaction, which is catalyzed by BC, involves the carboxylation of biotin at the 1'-N position, forming the 1'-N-carboxybiotinyl derivative. This half-reaction requires ATP, biotin, and bicarbonate as the substrates and Mg^{2+} as the cofactor. The reaction between ATP and bicarbonate to form an activated carboxyphosphate intermediate generates energy needed for the BC-catalyzed reaction [21, 22]. Divalent cations such as Mg^{2+} or Mn^{2+} are required to stabilize ATP. Meanwhile, bicarbonate is the source of carbonyl for the carboxylation reaction. The second half-reaction of the ACC catalysis, which is catalyzed by CT, involves transferring the carboxyl group from biotin to acetyl-CoA to form malonyl-CoA.

ACCs have been widely found in most living entities such as bacteria, viruses, fungi, plants, animals, and humans. In bacteria, plants chloroplasts, and other prokaryotes, ACCs are expressed as multi-subunits that readily dissociate [19]. In contrast, in humans, cytosols of plants, and most of eukaryotes, ACCs have been discovered in large multi-domains where BC, CT and BCCP are tightly incorporated in a polypeptide chain [22].

In *E. coli*, ACC is a multi-subunit form consisting of three components. The BC subunit is a 49.4 kDa protein made up of 449 amino acids and exists as a dimer in solution [19, 23]. The BCCP component (156 residues, 16.7 kDa) exists as either a dimer or higher oligomer [19, 23]. The CT component consists of α subunit (319 residues, 35.1 kDa) and β subunit (304 residues, 33.2 kDa), which form a stable $\alpha_2\beta_2$-

tetrameric complex [19, 23]. When in the same solution, the three components of ACC form an unstable holoenzyme (holo-ACC) which dissociates into individual subunits. Although the stoichiometry of the bacterial complex remains unknown, a complex of BCCP with BC was isolated from *E. coli,* which comprises two BCCP molecules per BC molecule [23]. Interestingly, in bacteria, either the BC or CT subunit can be isolated separately and exhibit catalytic ability without the other two ACC components. The reactions catalyzed by these two subunits make use of biotin or its derivatives as a substrate [7]. Malonyl-CoA, one of the products in the ACC-catalyzed reaction, is the building block for fatty acid biosynthesis. The bacteria use fatty acid for cell membrane biogenesis. As a consequence, inhibition of ACC results in cell death in bacteria, which suggests that ACC be a promising target for antibiotic drug development [24].

In humans and other mammals, the multi-domain ACCs have been identified in two forms: ACC1 and ACC2 [25]. These two isoforms are different in distribution, structure, and biological roles. ACC1, a 265 kDa protein consisting of 2346 amino acid residues, is localized in cytosol of lipogenic tissues such as liver, adipose and lactating mammary glands. Malonyl-CoA derived from the ACC1-catalyzed reaction provides the essential building blocks for fatty acid elongation. In contrast, ACC2 is a larger protein (280 kDa, 2483 amino acid residues), which is highly expressed in mitochondria of oxidative tissues such as heart, skeletal muscles and sparingly in liver [25]. While the two isoforms share about 70% amino acid sequence in common [25], ACC2 has an extra 136 amino acids, 114 of which form the N-terminus that enables ACC2 to target the outer mitochondria membrane [26]. In oxidative tissues, long chain acyl CoAs requires conversion to acylcartinines in order to cross mitochondrial membranes for fatty acid oxidation. This conversion is catalyzed by carnitine palmitoyltransferase 1 (CPT-I). The malonyl-CoA product of the ACC2-catalyzed

reaction is a potent allosteric inhibitor of CPT-I (IC_{50}=1.5 μM) and hence stimulates fatty acid oxidation in mitochondria [27].

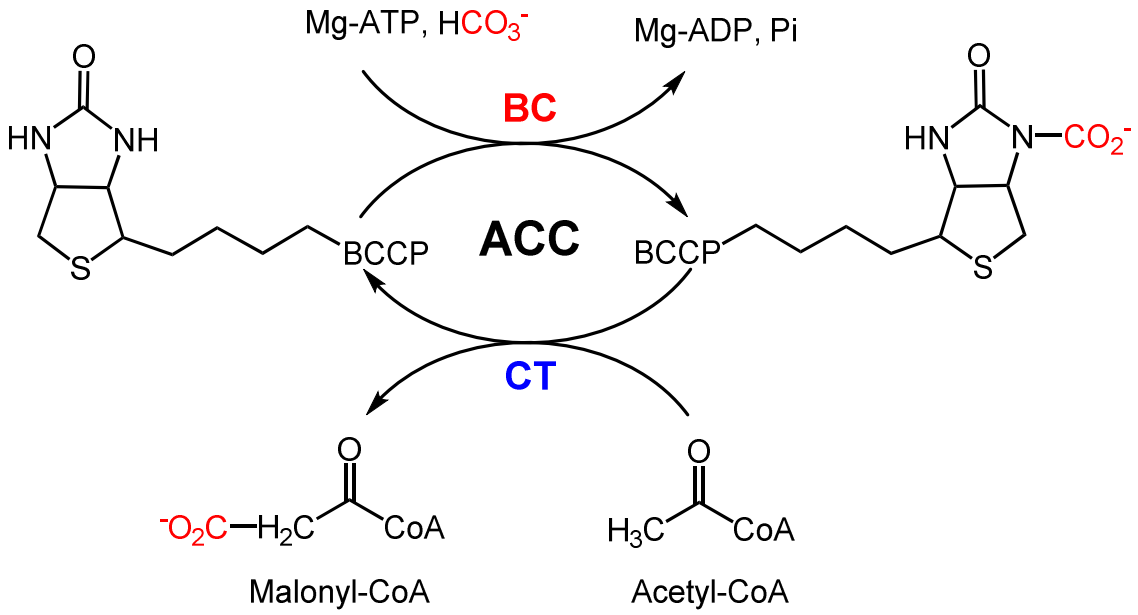

Figure 1.5. ACC-catalyzed reaction

The active form of ACCs in humans and mammals is a linear polymer with the molecular weight M_r of 4-8 million, and consists up to 20 protomers which are ACC dimers [28]. Multiple factors such as diet, hormones, and other feedforward and feedback regulators play an important role in regulating ACC activity. Particularly, citrate and long-chain acyl-CoAs were identified as regulators of mammalian ACCs. Citrate regulates these ACC isoforms through reversible phosphorylation and allosteric activation, and ultimately induces polymerization of ACC protomers [29]. Locke and coworkers discovered that citrate enhances the activities of recombinant human ACC1 and ACC2 by 1000-fold and 4-fold, respectively [30]. Interestingly, citrate activates both types human ACCs at low concentrations but inhibits at high concentration. Apparent K_d values (0.8±0.3 mM and 3.4±0.6 mM) and apparent K_i values (20±8 mM and 38±8 mM) were reported for ACC1 and ACC2, respectively [30].

The site of citrate action was previously reported to be on the BC domain where the dimerization site is located. The activation mechanism of citrate was evaluated by investigating the crystal structural of the phosphorylated BC domain of human ACC2 in presence of citrate [31]. In this structure, the phosphorylated Ser222 is known to disrupt ACC polymerization by binding to the dimer interface of BC. Citrate is responsible for removing the phosphorylated Ser222 from BC dimer interface; therefore, citrate promotes polymerization and activates ACC [31]. In contrast, long-chain acyl-CoAs are bound tightly to ACC, causing dissociation of ACC polymer into protomers.

The significance of ACC2 as a target for drug discovery to treat metabolic diseases was validated in ACC2-knockout mice [32, 33]. Compared to the wild type, ACC2-knockout mice had malonyl-CoA levels in heart and muscle reduced by 10- and 30-fold, respectively. In addition, these mutant mice had fatty acid oxidation rate accelerated by 30% and fat accumulation in adipose tissue decreased by 50% [32]. Even on high fat and high carbohydrate diets, compared to the wild type, ACC2 mutant mice gained less weight, accumulated less fat, and maintained normal insulin and glucose levels while the wild type exhibited type-2 diabetes [33]. Therefore, ACC2 is an attractive target for drug development to treat obesity, type-2 diabetes as well as other metabolic syndromes and associated diseases such as cardiovascular diseases, atherosclerosis, and hepatic steatosis [19, 34-37].

Recent studies have suggested that ACCs are attractive targets for anticancer therapy [38, 39]. Both isozymes are overexpressed in liver, lung, gastric, breast, and prostate cancer cells whose survival and invasiveness rely on fatty acids [38-42]. The use of small inhibitors of ACCs or RNA interference has proved to limit cancer cell proliferation and induce apoptosis [40, 42, 43]. This is exemplified by the work of

Beckers et al. in which soraphen A, a potent inhibitor of human ACC2 (IC_{50} = 3 nM) [44], was tested on prostate cancer cell lines [43]. It was reported that at nanomolar concentrations, soraphen A reduced fatty acid synthesis and enhanced fatty acid oxidation while causing limited formation of phospholipids in prostate cancer cells. Relative to normal cells, cancer cells exhibited selectively suppressed proliferation and induced cell death upon incubation with soraphen A. In another study, Sevensson et al. reported that ND-646, an allosteric inhibitor of ACC1 and ACC2, significantly reduced the growth of lung tumors [42]. In addition to small inhibitors of ACCs, the impact of RNA interference on ACC genes in cancer cells was also investigated [40]. Chajes et al. reported that silencing of ACC by the RNA is associated with the decrease of palmitic acid, which induced apoptosis in breast and prostate cancer cells. This discovery is consistent with the previous findings that cancer cell survival and invasive growth are strongly dependent on ACC activity.

Potent inhibitors of both ACC1 and ACC2 have been identified [44-46]. These can be categorized into three groups based on their inhibition mechanism. The first group is composed of long-chain fatty acid analogs which derive their efficacy through competing with acetyl-CoA in the CT-catalyzed half-reaction. Examples of inhibitors in this group include haloxyfop, sethoxydim, and TOFA (5-(tetradecyloxy)-2-furancarboxylic acid). The second group of ACC inhibitors is made up of bipiperidylcarboxamides which are potent, reversible, and isozyme-nonselective inhibitors of CT. For example, CP-610431 is a dual inhibitor of both ACC1 and ACC2 isozymes with IC_{50} (inhibitory concentration 50%) values of 50 nM [34]. Another analog, CP-640186, exhibited inhibition against both isozymes with IC_{50}'s of ~ 50 nM. Inhibition study of ACCs by both compounds demonstrated lower malonyl-CoA production, reduced fatty acid synthesis and stimulated fatty acid oxidation in cultured

cells as well as experimental animals [34]. Harriman and coworkers identified ND-630 as a potent inhibitor of ACC1 and ACC2 with IC_{50} values of 2.1 nM and 6.1 nM, respectively. This compound derives its efficacy by interacting with the phosphopeptide acceptor and interrupting ACC polymerization via its interaction with the dimerization site on the BC domain [37]. Cultured cells and animals treated with ND-630 exhibited reduced fatty acid synthesis and elevated fatty acid oxidation. Upon administration to the rats with diet-induced obesity, ND-630 was effective in enhancing insulin sensitivity, reducing weight gain, and lowering hepatic steatosis. The third group of ACC inhibitors includes polyketide natural product fungicides that inhibit ACC by disrupting the dimerization on the BC domain. Among this group, soraphen A, a compound isolated from *Sorangium celulosum*, has been reported as one of the most potent human ACC inhibitors (ACC1 IC_{50} ~1-5 nM, ACC2 IC_{50} = 3 nM) [44].

1.2.2. Enzyme Assays of ACC

1.2.2.1. Assays for bacterial enzymes

There have been assays developed for not only holo-ACC, but also the BC and CT subunits. While the holo-ACC assay required all three components (BC, CT, and BCCP), either the BC or CT subunit exhibited catalytic activity without the other two ACC components. The enzymatic reactions catalyzed by BC and CT usually utilize biotin or its derivatives as a substrate. Various assays have been reported including radioactive assays, spectrophotometric coupled assays, and separation-based assays. The radioactive assays utilize radiolabeled reagents and are based on measuring the radioactivity of the product formed or substrate depleted. The coupled assays require coupling reactions that involve the oxidation of NAD(P)H or reduction of $NAD(P)^+$ cofactors, followed by spectrophotometric detection at 340 nm. Recently, separation-based assays have been developed for ACC, BC, and CT, based on the

separation of reactants and substrates in prior to UV-Vis, fluorescence or mass spectrometry detection.

1.2.2.1.1. BC enzyme assays

The BC subunit catalyzes the ADP-dependent reaction in which the carboxyl group is transferred from the bicarbonate to biotin. The BC assays utilized ATP, Mg^{2+}, $KHCO_3$, and free biotin as the substrates. As the reaction proceeds, the products including ADP, the carboxylated biotin, and PO_4^{3-} were generated.

One of the earliest assays developed to study the BC subunit was based on the incorporation of $H^{14}CO_3^-$ into 1'-N-[^{14}C] carboxybiotin, which was often referred to as the ^{14}C bicarbonate fixation assay [12]. In this assay, the radio-labeled bicarbonate substrate $H^{14}CO_3^-$, which is also the source of carboxyl group for the ACC-catalyzed reaction, was incubated with other reagents including ATP, Mg^{2+}, biotin, and BC. The reaction was terminated the addition of ice-cold water and 1-octanol. Carbon dioxide bubbles were pumped through the reaction solution to remove the unreacted $H^{14}CO_3^-$. The resultant solution contained [^{14}C] carboxybiotin product whose radioactivity was measured using a liquid scintillator spectrometer.

Coupled enzyme assays have also been developed to eliminate the use of radioactivity. Eventually, the reactants and products in ACC-catalyzed reaction including ADP, ATP, acetyl-CoA, and malonyl-CoA all strongly absorb in the UV range at similar wavelengths. As a consequence, it is very difficult to detect one single component among others. Coupling the ACC-catalyzed reaction with secondary ones allows for indirect monitoring of reactant depletion or product formation. This concept was exemplified by the detection of ADP product when pyruvate kinase and lactate dehydrogenase were used as coupling enzymes, as presented in Scheme 1.1:

$$\text{ADP + phosph(enol)pyruvate} \xrightarrow{\text{Pyruvate kinase}} \text{ATP + Pyruvate}$$

$$\text{pyruvate + NADH} \xrightarrow{\text{Lactate Dehydrogenase}} \text{Lactate + NAD}^{+}$$

Scheme 1.1. Coupling reactions catalyzed by pyruvate kinase and lactate dehydrogenase

This coupled assay has been applied widely to study the forward reaction catalyzed by BC [12, 47, 48]. In this assay, the ADP product of ACC-catalyzed reaction becomes a reactant in the pyruvate kinase-catalyzed reaction where it reacts with phosph(enol)pyruvate to form ATP and pyruvate. In the subsequent reaction catalyzed by lactate dehydrogenase, pyruvate oxidizes NADH to produce lactate and NAD. As a result, the presence of ADP is accompanied with the depletion of NADH which is indicated by the decrease in absorbance at 334 nm or fluorescence at 460 nm.

1.2.2.1.2. CT enzyme assays

Similar to the BC subunit, the CT subunit also has catalytic activity as a standalone enzyme. CT catalyzes the transfer of the carboxyl group from biotin to acetyl-CoA to form malonyl-CoA. However, in practice, the CT-catalyzed reaction has frequently been monitored in the reverse, non-physiological direction (malonyl-CoA reacts to from acetyl-CoA). Biocytin or biotin methyl ester (BME), biotin analogs of higher reactivity (with maximal velocity V_{max} of 3 orders of magnitude higher than biotin) have been used as carboxyl acceptors for the reverse direction of the CT reaction [12, 24, 49, 50].

A radioactive assay for the CT subunit involves the use of [3-^{14}C-] or [2-^{14}C]malonyl-CoA and d-biotin methyl ester [12, 51]. The reaction was quenched by HCl, and the reaction mixture was then dried in the oven, followed by the addition of water and scintillator. Subsequently, the [2-^{14}C]acetyl-CoA, [^{14}C]O_2, and [^{14}C]carboxyl group in N-carboxybiotin methyl ester were all removed from the resultant mixture due

to their high volatility whereas the heat- and acid-stable [^{14}C]malonyl-CoA remained. The enzyme activity of CT is then calculated based on the decrease in radioactivity of [^{14}C]malonyl-CoA after the reaction completes.

In addition, another coupled assay using citrate synthase and malate dehydrogenase was reported by Guchhait et al. for the reverse direction of the half-reaction catalyzed by CT [12], as presented in Scheme 1.2:

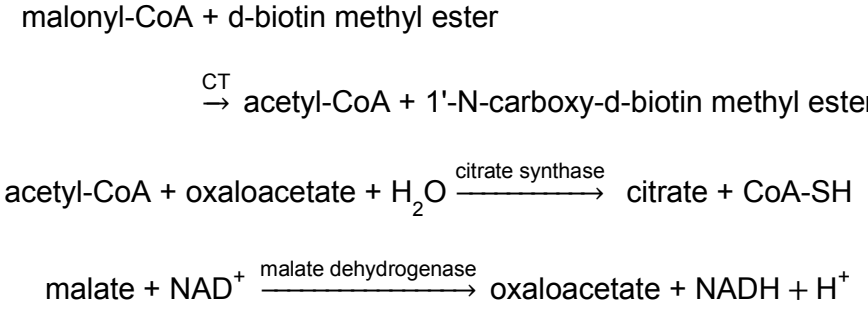

Scheme 1.2. Coupling reactions catalyzed by citrate synthase and malate dehydrogenase to study CT.

The activity of the enzyme was measured for the reverse direction of the CT-catalyzed reaction in which malonyl-CoA reacts with d-biotin methyl ester (an analog of biotin) to produce acetyl-CoA. Citrate synthase subsequently catalyzes coupling reaction where acetyl-CoA reacts with oxaloacetate to form citrate and free coenzyme A (CoA-SH). Oxaloacetate is also the product of the second coupling reaction between malate and NAD^+, catalyzed by malate dehydrogenase. The other product of this reaction, NADH, is detected spectrophotometrically at 340 nm. This coupled assay was applied to kinetic and inhibition study of CT in *E.coli* [12, 48, 50, 52, 53].

Another coupled assay utilizing malonyl-CoA reductase (MCR) was applied to study the CT unit via detection of malonyl-CoA [54], as presented in Scheme 1.3:

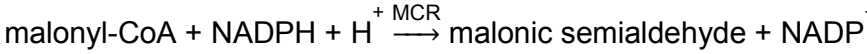

$$\text{malonic semialdehyde} + \text{NADPH} + \text{H}^{+} \xrightarrow{\text{MCR}} \text{3-hydroxypropionate} + \text{NADP}^{+}$$

Scheme 1.3. Coupling reactions catalyzed by malonyl-CoA reductase to study CT.

The coupling enzyme MCR isolated from *E. coli* catalyzes the reduction of malonyl-CoA to 3-hydroxypropionate via the two-step reactions that require two NADPH molecules. The decrease in NADPH concentration was monitored spectrophotometrically at 365 nm ($\epsilon_{365\,nm}$, 2NADPH = 6.8×10^3 M^{-1} cm^{-1}). This coupled assay was applied to assay ACCs isolated from *Metallosphaera sedula* [54].

Similarly, a coupled assay was developed by Santoro et al. and applied to study the CT subunit [24]:

$$\text{malonyl-CoA} + \text{biocytin} \xrightarrow{\text{CT}} \text{acetyl-CoA} + \text{carboxybiotin}$$

$$\text{acetyl-CoA} + \text{oxaloacetate} + \text{H}_2\text{O} \xrightarrow{\text{citrate synthase}} \text{citrate} + \text{CoA-SH}$$

$$\text{CoA-SH} + \text{DTNB} \rightarrow \text{TNB} + \text{CoA-S-S-TNB}$$

Scheme 1.4. Coupling reaction catalyzed by citrate synthase

Similar to the assay developed by Guchhait et al., the assay presented in Scheme 1.4 is applicable to the reverse direction of CT-catalyzed reaction, but using biocytin as the carboxyl receptor instead of d-biotin methyl ester. It also involves the conversion of acetyl-CoA and oxaloacetate to citrate and CoA-SH in the presence of citrate synthase. A second coupling enzyme malate dehydrogenase was omitted and 5,5'-dithiobis(2-nitrobenzoic acid) (DTNB, Ellman's reagent) was used instead to detect CoA-SH. The yellow product, thionitrobenzoate (TNB) absorbs in the visible range and is measurable at 412 nm. This coupled assay was performed with *C. glutamicum*, a gram positive bacterium, validated in an inhibition study of a known CT inhibitor, and further tested as a high-throughput assay for CT in *E.coli* [24, 55].

Recently, CE-based assays were developed and applied to study inhibition of CT [49, 52]. In these assays, acetyl-CoA and malonyl-CoA were separated based on their electrophoretic mobility and detected using UV-Vis absorption. Meades et al. successfully applied the CE assay to testing inhibition of *E. coli* CT by 1,4-hydroxy-3-methoxy-trans-cinnamaldehyde, an abundant compound in cinnamon bark extract [52].

1.2.2.1.3. Holo-ACC enzyme assays

Holo-ACC assays were adapted from either the BC or CT assays [47, 48, 51, 56]. One of the most common assays used for kinetics and inhibition studies of holo-ACC is the coupled assay in which pyruvate kinase and lactate dehydrogenase are used as the coupling enzymes [47, 56]. Alternatively, holo-ACC has been assayed by the incorporation of $^{14}CO_2$ from $H^{14}CO_3^-$ into the acid-stable product malonyl-CoA [48, 51].

Recently, a capillary electrophoresis-based assay for *E.coli* ACC was developed by Bryant and coworkers [49]. This assay involved the separation of substrates and products including ADP, ATP, acetyl-CoA, and malonyl-CoA, followed by UV-Vis detection at 256 nm without the need of either the coupling enzymes or radiolabeled reagents.

1.2.2.2. Mammalian ACC assays

Mammalian ACCs exist in two isoforms: ACC1 and ACC2. Both the isozymes require citrate as an enzyme activator. Therefore, in mammalian ACC assays, in addition to all reagents needed for the bacterial assay, citrate must be added to the reaction mixture.

Radiochemical assays of ACC have been adapted from the assays which were previously developed for bacterial ACCs. The commonly used radiochemical assays

were based on the ^{14}C fixation [11, 57-60]. Another radiochemical assay for ACC, but less common than the ^{14}C fixation assay, is based on the measurement of [^{32}P]Pi [29]. In such an assay, the radioactive [γ-^{32}P] ATP substrate was consumed while the [^{32}P]Pi product, a high-energy beta emitter, was generated, extracted by liquid-liquid extraction, then measured by the Cherenkov effect [29].

Coupled enzyme assays have been widely used to study kinetics and inhibition of human and mammalian ACCs [11, 29, 30, 61-63]. The most common coupled assays are based on the detection of ADP using pyruvate kinase and lactate dehydrogenase as the coupling enzymes [11, 29, 30]. Alternatively, other coupled assays which are based on indirect detection of malonyl-CoA [63] and inorganic phosphate [61, 62] were developed to study human and mammalian ACCs. In addition, Hashimoto et al also developed a coupled assay in which hexokinase and glucose-6-phosphate dehydrogenase (G6PD) are used as the coupling enzymes for indirect detection of ATP [29]:

$$\text{ATP + glucose} \xrightarrow{\text{hexokinase}} \text{ADP + G6P}$$

$$\text{G6P + NADP}^+ \xrightarrow{\text{G6PD}} \text{6-phospho-glucono-1,5-lactone + NADPH + H}^+$$

Scheme 1.5. Coupling reactions catalyzed by hexokinase and glucose-6-phosphate dehydrogenase.

The assay presented in Scheme 1.5 was based on the conversion of ATP and glucose to ADP and G6P with hexokinase, followed by the reduction of $NADP^+$ to its reduced form (NADPH) which was measurable by either UV absorption at 340 nm or fluorescence at 460 nm. This assay was applied to kinetic study of ACC isolated from rat liver [29].

Separation-based assays have been developed for mammalian ACCs. Spiegeleer et al. reported a direct assay for ACC based on HPLC separation of short-

chain CoAs including acetyl-CoA and malonyl-CoA, followed by absorbance measurement at 258 nm [64]. Similarly, Kim and coworkers described the HPLC assay to study kinetics of recombinant human ACC2 [65]. This assay allowed the separation and quantification of both acetyl-CoA and malonyl-CoA. However, both the substrate ([1-^{14}C]acetyl-CoA) and its corresponding product ([2-^{14}C]malonyl-CoA) were radioactive and detected by the radiometric detector. Alternatively, Kaushik and coworkers characterized recombinant human ACC2 kinetics using LC/MS/MS which offered sensitive detection of malonyl-CoA [66]. The need of the stable isotope labelled reagent ([3-^{13}C]malonyl-CoA) as an internal standard is a drawback of this assay.

1.3. Capillary Electrophoretic Enzyme Assays

1.3.1. Capillary Electrophoresis

Capillary electrophoresis (CE) is a separation technique used to separate small molecules as well as biological macromolecules such as DNA, proteins, and nucleotides. Characteristic advantages of CE include low sample consumption (nL), high separation efficiency, simple alteration of separation mechanisms, a wide variety of detection methods, short analysis time, and possibility of automation. The modes of CE separation that have been developed include capillary zone electrophoresis (CZE), capillary electrochromatography (CEC), micellar electrokinetic chromatography (MEKC), capillary isoelectric focusing (CIEF), capillary gel electrophoresis (CGE), and capillary isotachophoresis (CITP). Among these, CZE is the simplest and most commonly used form of CE. In 1981, Jorgenson and Lukacs were first to report CZE separation of derivatized amino acids, dipeptides, and amines with high efficiency using glass capillaries and fluorescence detection [67]. In 1991, Banke and coworkers pioneered using capillary electrophoresis to perform enzyme assay of alkaline protease [68]. Since then, CE-based enzyme assays have been developed to study

enzyme kinetics, enzyme inhibition, and screen for enzyme inhibitors [18].The number of publications on CE over the period from 1981 through 2018 is summarized in Figure 1.6.

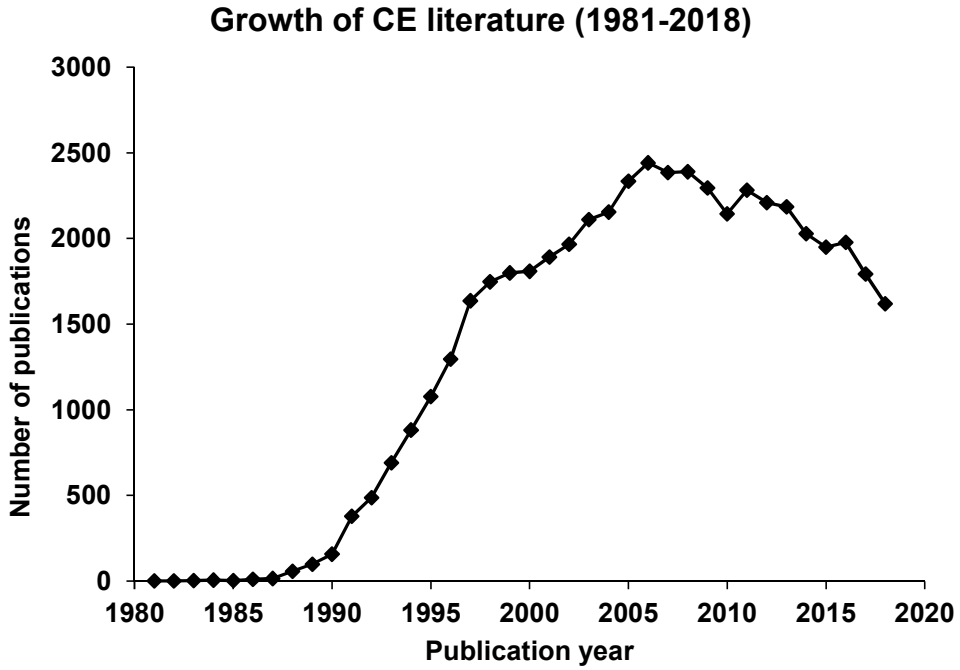

Figure 1.6. The growth of CE publications from 1981 to 2018. The Web of Science database was searched using the keyword “capillary electrophoresis”.

A typical CE system is illustrated in Figure 1.7 and includes a capillary, high voltage power supply, two buffer reservoirs, two electrodes and a detector. The capillary used in CE is typically made from fused-silica, with an inner diameter from 20 to 100 μm and an outer diameter of 150-360 μm. The outside of the capillary is coated with a protective layer (polyimide) to enhance its durability. A small portion of this coating is burned to create a detection window which is located near the capillary outlet. Both ends of the capillary and two electrodes connected to a high voltage power supply are immersed in two buffer vials.

At the beginning of a CE separation procedure, the capillary is usually conditioned by rinsing with a strong base such as NaOH to increase the negatively

charged silanol groups on the capillary inner surface. As the capillary is filled with buffer, the cations in buffer are attracted to the capillary wall, creating electrical double layer (Figure 1.8). The layer closest to the wall is referred to as Stern layer while the diffuse layer further away from the wall is called the Gouy layer. The cations making up the latter are mostly solvated cations which move towards the cathode under the applied voltage, dragging along the bulk solvent, creating electroosmotic flow (EOF). The EOF is calculated as follows:

$$v_{eof} = \frac{\varepsilon\zeta}{4\pi\eta}E \qquad 1.8$$

where v_{eof} is the electroosmotic velocity, ε is the dielectric constant, ζ is the zeta potential measured at capillary-buffer interface, E is the electric field, and η is the viscosity of the buffer.

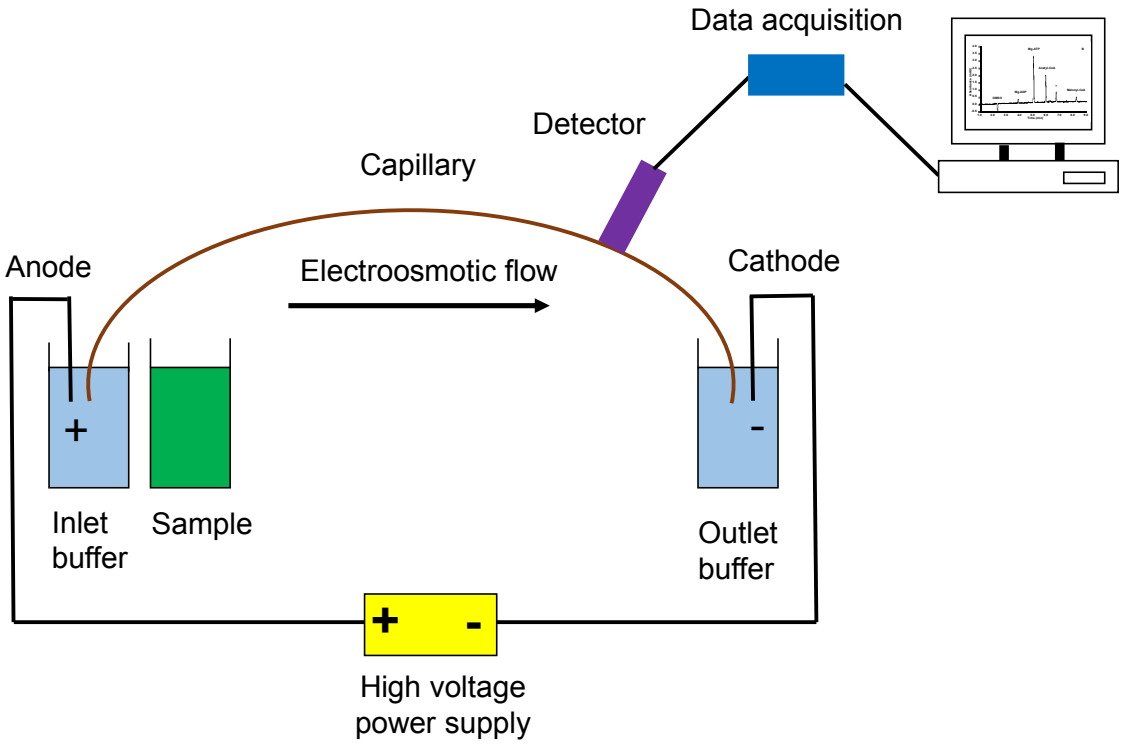

Figure 1.7. Scheme of a basic capillary electrophoresis system

The electroosmotic mobility is then calculated as:

$$\mu_{eof} = \frac{\nu_{eof}}{E} = \frac{\varepsilon\zeta}{4\pi\eta} \qquad 1.9$$

The EOF is important for electrokinetic separation in CZE since it acts as a pump to move all species regardless of their charge (cations, anions, neutral compounds) towards the capillary outlet. The magnitude of the EOF depends on the concentration of electrolytes and pH of the buffer solution. Since zeta potential is reversely proportional to the square root of the electrolyte concentration, increasing the electrolyte concentration decreases the zeta potential, and subsequently decreases the EOF. In a fused silica capillary, electroosmotic flow is reduced in buffer solution of low pH (<7.0) due to the conversion of SiO^- back to SiOH. In practice, EOF is measured based on the migration time of a neutral solute such as methanol, mesityl oxide, and DMSO. While EOF is desired for most CZE and MEKC separations, it is actively suppressed to perform IEF or ITP techniques. The EOF suppression is enabled by using Teflon capillary, properly coated capillary, or adding additives to the buffer solution.

In addition to the EOF, a more important factor affecting the migration in CZE is the electrophoresis which directs cations towards the cathode, anions towards the anode while the neutral analytes are not affected by the electric field. The rate at which the analytes migrate in the capillary under electric field, also referred to as electrophoretic velocity ν_{ep}, depends on the hydrodynamic size and charge of the species and is calculated as follows:

$$\nu_{ep} = \frac{q}{f}E = \mu_{ep}E = \mu_{ep}\frac{V}{L_t} \qquad 1.10$$

where v_{ep} is the electrophoretic velocity, q is the effective charge of the analyte, f is the friction coefficient, μ_{ep} is the electrophoretic mobility of the analyte, E is the electric field strength, V is the applied voltage, and L_t is the total length of the capillary.

The friction coefficient (f) depends on the hydrodynamic radius of the solute (r) and viscosity of the separation buffer:

$$f = 6r\eta \qquad 1.11$$

Because the friction coefficient is directly proportional to the hydrodynamic radius of the solute, the electropherotic velocity is inversely proportional to the size of the solute. A solute's electrophoretic mobility μ_{ep} is also proportional to the electrophoretic velocity.

$$\mu_{ep} = \frac{L_t v_{ep}}{V} \qquad 1.12$$

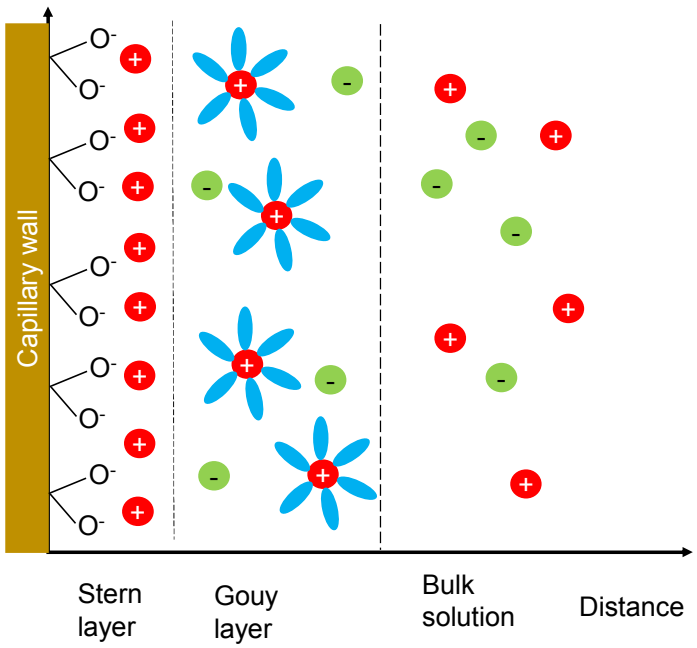

Figure 1.8. Scheme depiction of the EOF formation inside the capillary

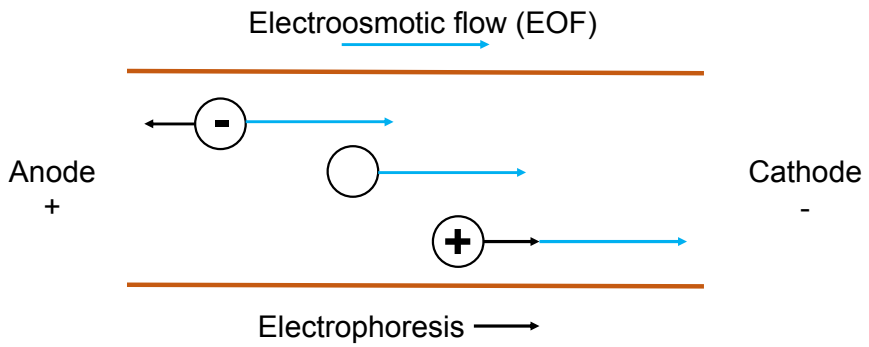

Figure 1.9. The order of migration under EOF and electrophoresis

Figure 1.9 summarizes the migration order of analytes in the capillary in the presence of both EOF and electrophoresis. The rate and direction of migration are governed by electrophoresis and EOF. The apparent mobility of the solute μ_{app} is a vector sum of the electroosmotic mobility of the buffer solution and the electrophoretic mobility of the solute.

$$\mu_{app} = \mu_{eof} + \mu_{ep} \qquad 1.13$$

When EOF is high relative to the electrophoresis, the cations migrate the fastest towards the cathode, followed by neutral molecules and anions. The migration time t_m is the time it takes for a solute to migrate from the capillary inlet to the detection window, which is also referred to as the effective length L_d.

$$t_m = \frac{L_d}{v_{app}} = \frac{L_d L_t}{\mu_{app} V} \qquad 1.14$$

The development of MEKC has enabled the CE separations of charged and neutral solutes through the use of micelles in the separation buffer [69]. Micelles are aggregates of surfactants such as SDS, CTAB, which have a hydrophilic head and a hydrophobic tail. The hydrophilic head can be cationic, anionic, zwitterionic, or nonionic while the hydrophobic tail is normally a chain of hydrocarbon. In aqueous solution, the hydrophilic heads interact with the surround solvent whereas the

hydrophobic tails cluster towards the center of the micelle. Above the critical micellar concentration (CMC), the micelles are fully formed. In CE separation, the micelles in the separation buffer act as the pseudo stationary phase similar to the stationary phase in reverse-phase HPLC. The separation in MEKC is based on the partition of solutes between the micelles and buffer solution, which can be controlled by the ionic strength, pH, temperature, and other additives in the separation buffer.

Depending on the properties of the analytes, CE can be coupled to different detection methods such as ultraviolet-visible (UV-Vis) absorption, fluorescence (FD), mass spectrometry (MS), or conductivity. Among these methods, UV-Vis absorption is the most commonly used due to a wide range of organic molecules absorbing in the UV-Vis region. However, high limits of detection (LOD) are a drawback for CE coupled with UV-Vis absorption detection due to narrow bore, and, thus, short optical path length provided by the capillary. This issue has been addressed by utilizing different detection cells such as bubble cell capillary or Z-cell capillary to increase the path length [70]. The limited optical path length is of less concern when using fluorescence detection. The laser, which is a high intensity, highly collimated, monochromatic and coherent light source, has been used widely as the excitation source for fluorescence detection in CE. Laser-induced fluorescence (LIF) is the second most common detection mode yet the lowest LOD for CE. [71]. In some cases, detection of a few to single molecules was possible with CE and LIF [72, 73].

Recently, light-emitting diodes (LEDs) have been used as an alternative to lasers as the excitation source for fluorescence detection in CE [74, 75]. A LED is a semiconductor device that emits light when an electric current flows through it. Most semiconductors are doped with impurities to add extra negatively charged electrons (n-type) or positively charged holes (p-type). An LED is made up of n-type and p-type

materials which are fused together and connected to electrodes on one end. Without the applied voltage to the diode, holes from the p-type material are filled by electrons from the n-type material, forming a depletion zone. When connecting the n-type material is to the negative end and the p-type material to the positive end of the electric circuit, the electrons from the n-type material move to the p-type material and the holes move in the opposite direction. The recombination of electron-hole generates energy in terms of photons. This effect is referred to as electroluminescence, and the wavelength of the emitted light depends on the energy band gap between the conduction band and the valence band of the semiconductor. The light beams emitted by the LEDs are multichromatic with broad bandwidth (20-30 nm full width at half maximum), noncoherent, and noncollimated. Lasers are monochromatic, coherent, and collimated. The associated small size, low cost, low energy consumption, long lifetime, and high stability make LEDs promising as light sources for fluorescence detection.

Capillary electrophoretic enzyme assays can be categorized based on two basic criteria. First, depending on where enzymatic reactions occur, enzyme assays are classified as offline and online assays. All steps involved in an online assay take place inside the capillary. However, in an offline assay, the incubation of reaction mixture is carried out outside the capillary prior to the subsequent in-capillary steps. Second, enzyme assays are either homogeneous or heterogeneous based on physical states of the substrates and enzyme in an assay. When all reagents needed for the assays including substrate, free enzyme, and cofactors are in solution, the assay is heterogeneous. However, when the enzyme is immobilized onto the capillary, within a sol-gel matrix, or onto a solid carrier while other assay components remain in

solution, the assay is referred to as heterogeneous. These two criteria are usually combined to specifically describe an enzyme assay.

Compared to traditional enzyme assays, CE-based assays have several advantages to offer. First, as a separation technique, CE is capable of separating and quantifying enzyme components including substrates, products, and inhibitors. Therefore, CE-based assays are not susceptible to spectral interference as the conventional plate reader- or cuvette-based assays. Second, relative to coupled enzyme assays, CE enzyme assays are simpler and free of inhibitor interference. Coupled enzyme reactions typically require coupling reactions which might be interfered with by the inhibitor to give false positive results for inhibition measurement. The majority of CE-based assays do not require coupling reactions, thus, inhibitor interference is not a problem. Third, CE assays require smaller sample amounts (nL) compare to plate reader- and cuvette-based coupled assays (μL-mL).

1.3.2. Offline Enzyme Assays

CE offline enzyme assay is the simplest CE-based assay. Offline enzyme assays have been developed to study enzyme activity, kinetics, and inhibition [18, 76]. In offline assays, the reaction mixture is incubated for a certain time, typically in a vial. After incubation, the resultant mixture is injected into the capillary, followed by separation by CE. Figure 1.10 illustrates typical separations for an offline CE assay. As the reaction proceeds, the substrate depletion and product formation can be quantified using the corresponding peak areas. At the same time, the separation and quantification of substrates and products makes CE-based assay less prone to spectral interference compared to the conventional cuvette- or plate reader-based assays.

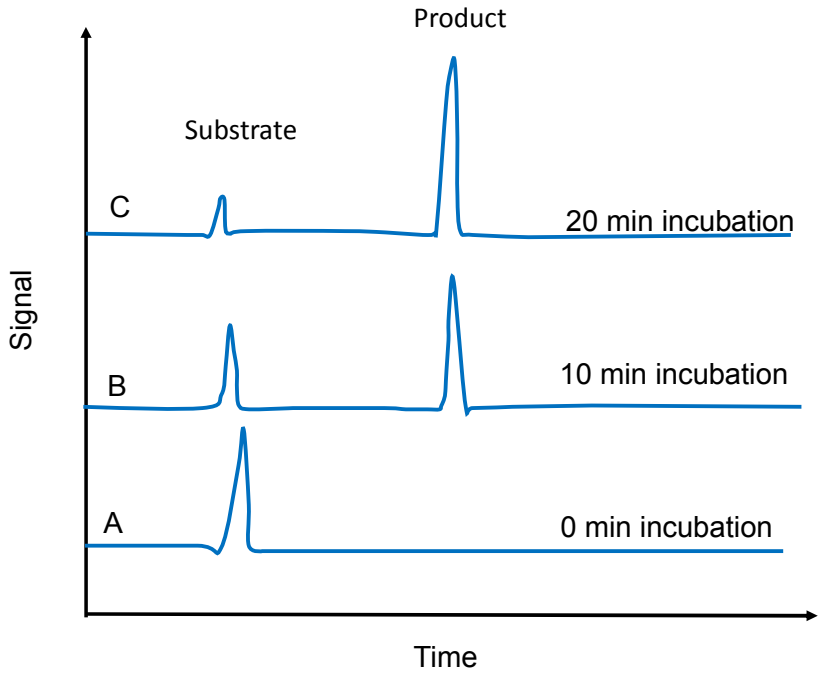

Figure 1.10. Schematic depiction of the progress of substrate depletion and product formation in an offline CE-based assay.

Banke and coworkers performed the first CE-based enzyme assay of an alkaline protease [68]. In this study, CE was used to separate the fermentation broth from *Aspergillius oryzae*, followed by collecting fractions of different peaks for further characterization. One of the fractions was then incubated with Suc-Ala-Ala-Pro-Phe-p-nitroanilide, and the reaction mixture was separated by CE. The formation of a proteolytic product p-nitroanilide suggested that the collected fraction contained an alkaline protease. The identity of the enzyme was specified by incubating the same fraction with casein, and a product peak was recorded by CE separation, indicating that the enzyme catalyzed hydrolysis of casein. The two CE-based assays confirmed that an endoprotease was present in the collected fraction. Since its first application to study enzyme, CE has been widely used to develop offline enzyme assays [18].

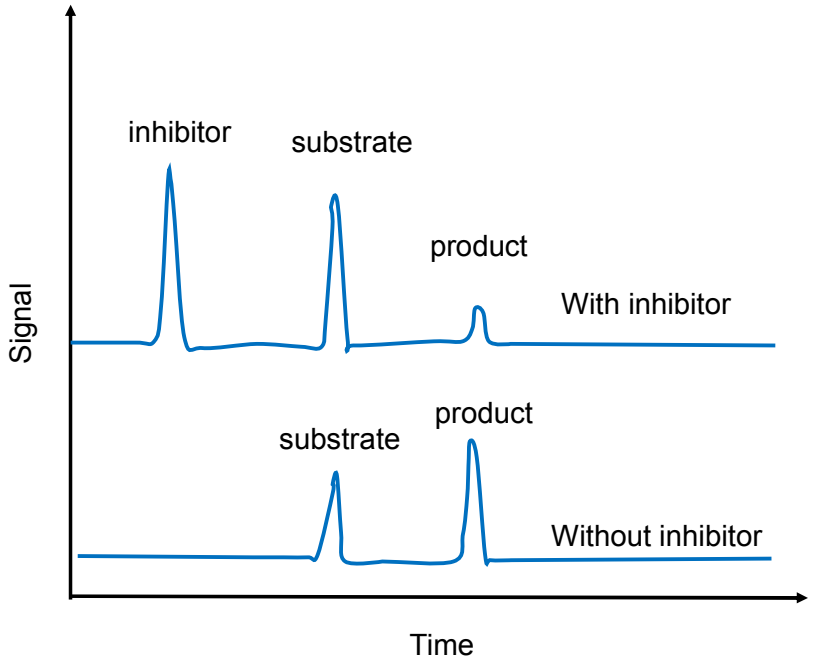

Figure 1.11. Schematic depiction of the separation of assay components with and without an inhibitor.

In enzyme inhibition studies, the inhibitor is added to the reaction mixture which contains the substrate, enzyme, and other cofactors. Figure 1.11 illustrates the CE separations for enzyme inhibition studies. Less product is formed in the inhibited reaction when compared to the control (without inhibitor). Also, the inhibitor can be observed as an extra peak, provided that it gives response to the detector used. This is an advantage of CE assay compared to the coupled enzyme assay. First, the separation of all assay components including the inhibitor prior to detection makes the CE less prone to spectral interference than the spectrophotometric coupled enzyme assay. Second, most CE assays do not require coupling enzymes, so false positive due to the compound inhibiting the coupling enzymes is not a concern. The applicability of CE assay to study enzyme inhibition is exemplified by the CE-based assay developed by Malina et al [77]. This was the study of phosphofructokinase-1 (PFK-1), which catalyzes the reaction of fructose 6-phosphate and ATP to form

fructose 1,6-biphosphate and ADP. In this CE assay, the ATP and ADP were separated and quantified at different incubation times to generate a reaction progress curve. The assay was then applied to determine the half maximum inhibitory concentration (IC_{50}) of aurintricarboxylic acid (ATA), a known inhibitor of PFK-1. This demonstrates that CE is suitable for qualitative and quantitative study of enzyme activity and enzyme inhibition.

1.3.3. Online Enzyme Assays

In an online or in-capillary enzyme assay, all assay steps such as mixing, incubation, and separation take place inside the capillary. Online assays are divided into homogeneous and heterogeneous assays, depending on the physical phase of the enzymes. A homogeneous online enzyme assay is typically referred to as electrophoretically mediated microanalysis (EMMA). The first EMMA assay, which was introduced in 1992 by Bao and Regnier, involved the study of glucose-6-phosphate dehydrogenase, and relied on the difference in electrophoretic motilities of the substrates, enzyme, and cofactors [78]. These components were injected in consecutive plugs and mixed in the capillary by either diffusion or under applied voltage. Alternatively, heterogeneous enzyme assays have been developed using three approaches, with enzymes immobilized on either the inner capillary wall, incorporated into a polymeric membrane or immobilized onto magnetic beads [79]. As a result, in heterogeneous assays, enzymes are fixed inside the capillary, forming immobilized enzyme microreactors (IMERs). Online enzyme assays offer some advantages relative to offline assays. First, all steps involved in online assays are carried out inside the capillary, which makes automation and miniaturization of the whole procedure easier. Second, the amount of reagents required is lower for online assay compared to offline approach. Consequently, online enzyme assays are

promising methods applicable for routine and high throughput screening in pharmaceutical studies and biochemical tests [80].

1.3.4. Electrophoretically Mediated Microanalysis

Electrophoretically mediated microanalysis (EMMA) is a homogeneous online assay in which all the involved steps including sample introduction, incubation, and separation take place inside the capillary. EMMA has been applied to study enzyme kinetics and inhibition [18, 80-83]. Compared to offline CE assays, EMMA-based assays offer significant advantages. First, only minute amount of reagents (nanoliter scale) is needed for EMMA because incubation proceeds inside the capillary. In addition, the automated procedure makes EMMA-based assays robust and applicable to analyzing multiple samples with less labor in comparison to offline assays.

Depending on the way the sample is introduced to the capillary, EMMA can be further categorized as either continuous engagement mode or transient engagement mode [81]. In the continuous engagement mode, also known as the long contact mode, the capillary is filled with a reagent, which often contains the buffer and the substrate. In the subsequent steps, the enzyme is introduced into the capillary and continuously mixes with the substrate as it migrates towards the capillary outlet under applied voltage. This process leads to continuous formation and separation of product. Other continuous EMMA assays were also developed in which the capillary was filled with enzyme in prior to substrate injection [84].

Regarding the introduction of sample to the capillary, EMMA can be operated in two ways: zonal injection or moving boundary. In zonal injection mode, the capillary is first filled with buffer solution prior to a brief enzyme injection as a plug. When the potential is applied across the capillary, the substrate contained in the inlet buffer reservoir migrates through the capillary, reacts with the enzyme and generate

products. On the other hand, moving boundary mode involves filling the capillary with the reagent of lower electrophoretic mobility, then electrokinetically injecting the reagent of higher electrophoretic mobility from the anodic buffer reservoir. As such, the two reagents are mixed when migrating under the applied potential, resulting in continuous product formation. Harmon et al. demonstrated the assay of leucine aminopeptidase (LAP) using moving boundary EMMA [84]. The substrate of the LAP-catalyzed reaction, L-leucine-p-nitroanilide, has higher electrophoretic mobility than the enzyme and was kept in the buffer reservoir at the capillary inlet. Meanwhile, the capillary was initially filled with LAP enzyme. Following the application of voltage, the substrate moved through the capillary full of enzyme and generated the product, p-nitroaniline.

Depending on how the reagents are incubated, continuous engagement assays can be further sub-categorized as either constant or zero potential. Bao et al. described the enzyme assays of glucose-6-phosphate dehydrogenase using both approaches [78]. Under constant potential throughout the separation, the product formed is detected as a flat plateau. Sensitivity of this mode is inversely proportional to the potential. At lower potential, the assay reagents migrate more slowly through the capillary, which leads longer incubation and higher product formation yield. Alternatively, in zero potential mode, after enzyme electrophoreses part way through the capillary, the applied potential is reduced to zero for a few minutes before returning to the original potential. This mode allows for longer incubation of the substrate and the enzyme, resulting in additional accumulated product and enhanced sensitivity. The corresponding electropherogram has a peak on top of a plateau. In another study, Xie et al. reported the measurement of NAD^+ and NADH in a single cell using EMMA in the zero potential mode [85]. The scheme of the recycling assay is illustrated in Figure

1.12. This is an enzymatic recycling assay that utilizes lactate dehydrogenase (LDH) and diaphorase (DIA) to generate a fluorescent product, resorufin, as an indicator of NAD^+ and NADH present. For the EMMA-based recycling assay, the capillary was initially filled with the Tris buffer solution containing lactate, resazurin, LDH and DIA. The sample containing NAD^+ and NADH was then introduced to the capillary and separated for 3 min into two bands. Subsequently, the applied voltage was stopped for up to 5 min for incubation. During this period, the enzymatic reactions took place, producing two plugs of resorufin corresponding to NAD^+ and NADH. Once the voltage was applied again, the plugs of resorufin migrated towards the capillary end and were detected using fluorescence detection. The recycling enzymatic assay offers sensitive detection of NAD^+ and NADH with the detection limits of 0.2 amol and 1.0 amol, respectively.

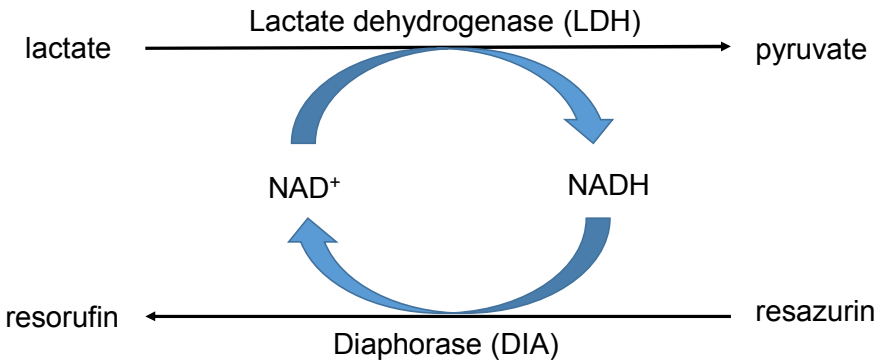

Figure 1.12. Enzymatic recycling reaction for the detection of NAD^+ and NADH.

The transient engagement format, also referred to as plug-plug mode, is an alternative to continuous engagement EMMA. In this mode, the capillary is initially filled with the buffer, followed by injecting the enzyme and substrate in separate small plugs in order of increasing electrophoretic mobilities. Once the electric field is applied, the plug of higher mobility faster than the plug of lower mobility towards the capillary outlet, causing the plugs to overlap and products to be generated. Relative to the

continuous engagement mode, the transient engagement mode consumes less reagents, and is the most cost-effective.

1.3.5. Immobilized-Enzyme Microreactors

In heterogeneous enzyme assays, the enzymes are immobilized onto insoluble supports through covalent bonds, ionic interaction, adsorption, entrapment, or cross-linking to form immobilized enzyme microreactors (IMERs) [82]. IMER-based assays are promising for pharmaceutical, bioanalytical studies and industrial applications thanks to the advantages they have to offer. First, properly immobilizing an enzyme leads to stabilizing its conformation and makes it less prone to denaturation by heat, extreme pH, or organic solvent. As such, immobilized enzymes are more stable compared to free enzyme solution although the reduction in enzyme activity is often reported [86, 87]. Second, unlike free enzymes, IMERs can be separated from the incubation mixture and used repeatedly. Third, it is possible to have the enzyme immobilized inside a capillary, reaction mixture incubated and assay reagents separated, all in one capillary. Collectively, IMERs are applicable for miniaturized, automated and cost-efficient enzyme assays.

IMERs have been fabricated using three main approaches. First, the enzyme is directly immobilized onto the capillary inner surface, creating open tubular capillary IMERs. CE-integrated open tubular IMERs are the simplest type of heterogeneous online assays owing to their easy fabrication [86]. In such assays, the enzymes are immobilized on the inner surface of the capillary through covalent bonds with silica or electrostatic immobilization. Low loading capacity and enzymatic catalysis efficiency are major drawbacks of open tubular IMERs owing to limited substrate-enzyme contact area. Second, the enzyme can be encapsulated within a porous polymer network inside the capillary to form monolithic IMERs. Compared to open tubular

IMERs, monolithic IMERs provide enhanced surface-to-volume ratio. However, time-consuming fabrication and the inability to remove IMERs from the capillary are limiting factors to applicability of monolithic IMERs. Third, the enzyme can be immobilized onto insoluble supports such as particles or membranes which are injected to and kept in place inside the capillary. Such fabrications are referred to as packed IMERs. The most popular case of packed IMERs involves the use of magnetic beads (MBs) which can be manipulated by an external magnetic field and easily removed from the capillary under high pressure or in the absence of magnetic field. In addition, the surface to volume ratio for MB-based IMERs is also higher than that of open tubular IMERs.

In conventional packed IMERs, the enzyme-immobilized particles are packed inside the capillary using frits. This inflexible design makes it difficult to replace IMERs. Recently, magnetic beads have emerged as the solid support for IMERs due to their commercial availability, the ease of manipulating the beads inside the capillary using external magnets and plethora of options of size (nanometer to micrometer scale) and functional groups. Basic composition of a magnetic bead used for IMERs is illustrated in Figure 1.13.

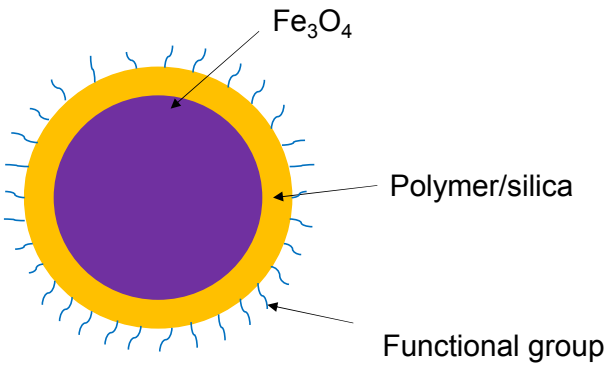

Figure 1.13. Composition of a typical magnetic bead

A magnetic bead has the core made from superparamagnetic iron oxide Fe_3O_4 that is attracted to the magnetic field. The core is covered with a shell of polymer or silica, which plays two important roles. First, the coating acts as the stabilizing material that prevents the Fe_3O_4 particles from aggregation, thus retaining paramagetic properties. Second, owing to the polymer coating, the surface of the magnetic beads can be functionalized with ligands such as epoxy, carboxylic acid, streptavidin, and antibody. The diversity of functionalized MBs enables the immobilization of various biomolecules including proteins, enzymes, antigens, nucleic acids and mRNA. Consequently, magnetic beads have been widely applied in life sciences, biotechnology, and healthcare [18, 86].

The first CE assays using magnetic bead-based IMERs (MB-IMERs) on a commercial CE instrument were developed by Rashkovetsky et al. [88]. This study made use of two round rare earth colbalt magnets that were placed directly on the capillary. In the alkaline phosphatase (AP) assay, the MBs (2.8 μm diameter) functionalized with streptavidin were used to immobilize biotinylated AP through the covalent streptavidin-biotin linkage. After the introduction of the AP-coated MBs into the capillary, the buffer containing AP substrate was injected to fill the capillary and let incubated for 30 min. Subsequently, the product was separated under low pressure and detected by absorbance at 405 nm. Rashkovetsky et al. also developed another MB-IMERs assay for HIV-protease [88]. In this assay, the substrate was immobilized on the MBs through streptavidin-biotin binding while the enzyme HIV-protease was later injected as a plug to the capillary. Following incubation, the product also migrated toward the detector under low pressure and wasthen detected by LIF. The inhibition of HIV-protease by acetyl-pepstatin resulted in the IC_{50} value that is consistent with

the reported value in literature, indicating that CE-based assays coupled with MB-IMERs are applicable to study not only enzyme activity but also enzyme inhibition.

Since its first application, CE assays coupled with MB-IMERs have been developed by many groups for various enzymes, especially to adapt to the commercial CE systems [18, 79, 82, 86]. Because the bead retention inside the capillary depends on the external magnets, the placement of MBs is the key factor to the performance of CE-integrated MB-IMERs. The magnet configurations of different shapes (square, bar, cylindrical), orientations (repulsive and attractive), angles (0-90 degrees), and different distances corresponding to different coolant systems were evaluated theoretically and experimentally. Several groups attempted to simulate the magnetic field and magnetic strength generated by single and double magnets using different software such as FEMM, Flux Expert, and Quickfield [89-91]. The simulation studies based on finite elements method by Bronzeau et al. and Gassner et al. both suggested that attractive arrangement of two magnets at 90˚ result in strong magnetic field, thus good MB plug formation [89, 90]. However, the microscopic images showed that the MB plugs formed using this configuration are not consistent. The images reported by Bronzeau et al. and Tarn et al., showed that the plug formed were not densely packed, which is opposite to the observations of Gassner et al. [89, 90, 92, 93]. In another simulation study using Quickfield software and Karlqvist method, Slovakova et al. concluded that the most efficient arrangement involved the two rectangular magnets in repulsive orientation, at angle of 30˚ to the separation channel. Imaging of the MBs immobilized using this arrangement and similar design (20˚) showed densely packed MB plugs [91, 94, 95]. Interestingly, Henken et al. reported that the formation and retention of MBs depends on the chemistry of the immobilized molecules on the beads [95]. Typically the reproducibility of enzyme assays developed using the repulsive

magnet configuration is at 20-25% [91, 96]. In most of the MB-based IMERs constructed using the air-based cooling system, the magnets are placed directly onto the capillary. Thus, the magnet-magnet and magnet-capillary distances are small, resulting in high magnetic field inside the capillary. However, for the P/ACE MDQ Beckman CE instrument that uses liquid-based cooling system, the capillary is inside a coolant tubing, making it difficult to place the magnets in close proximity to the capillary. As a result, it is more difficult to keep the MBs inside the capillary where the magnetic field is reduced. Ramana et al. attempted to assemble the magnets to adapt to this system in two ways [97, 98]. First, small cubic magnets were placed directly onto the capillary and kept in place by tape. Since both the magnets and capillary fit inside the tubing, this design enables the formation of MB plugs without having to remove the tubing. Second, a magnet holder was created to hold the magnets in attractive orientation, close to and at an angle of 30˚ to the coolant tubing. However, both configurations exhibited poor reproducibility and significant loss of enzyme activity.

1.4. Goals of this Dissertation

The goal of the research presented in this dissertation is to address limitations of coupled enzyme assays using capillary electrophoresis (CE). The first approach is to utilize CE to separate assay components (substrates, products, and inhibitors) for direct UV absorption detection thereby avoiding the use of coupling enzymes. Enzyme assays based on CE are less prone to spectral and inhibitor interferences relative to coupled assays. The second approach involves developing a CE coupled enzyme assay of ACC as a proof-of-concept, with fluorescence detection, using an LED to replace lasers as an excitation source.

Chapter 2. The goal of this project is to improve the CE enzyme assay and apply the improved assay to study inhibition of bacterial ACC. Previously, a CE enzyme assay was developed by Bryant et al. for bacterial holo-ACC [49], but it suffers from limited peak shape and peak area reproducibility. The first objective in this project is to improve the separation of ACC assay components including ADP, ATP, acetyl-CoA, and malony-CoA. The second objective is to apply the improved assay to inhibition study of bacterial holo-ACC. The third objective is to determine IC_{50} values of several inhibitors toward bacterial holo-ACC as well as the BC and CT subunits.

Chapter 3. The goal of this project is to develop a capillary electrophoretic assay of human ACC2. A simple off-column capillary electrophoresis (CE) assay for ACC2 was developed based on the separation of Mg-ADP, Mg-ATP, acetyl-CoA, and malonyl-CoA with detection by UV absorption at 256 nm. The main difference between human ACC2 and the bacterial holo-ACC is the requirement of citrate as an enzyme activator for human ACC2. The buffer containing 30.0 mM HEPES, 3.0 mM $KHCO_3$, 3.0 mM citrate, and 2.5 mM $MgCl_2$ at pH 7.50 was used as both the separation and sample buffers. When Mg^{2+} was absent from the separation buffer, the Mg-ADP and Mg-ATP zones both split and migrated as two separate peaks. With Mg^{2+} added to the separation buffer, Mg-ADP and Mg-ATP were detected as single peaks, and the reproducibility of peak shape and peak area for human ACC2 assay components was improved. To measure enzyme activity and screen for inhibitors of human ACC2, it is desirable to utilize a separation method to avoid spectral interference. Inhibition of human ACC2 by CP-640186, a known inhibitor, was studied using the CE assay.

Chapter 4. The goal of this project is to quantitatively compare a laser and LED for capillary electrophoresis with fluorescence detection. Lasers have been used as a common excitation source for fluorescence detection in CE owing to its powerful,

coherent, monochromatic, and highly collimated output. Recently, light emitting diodes have been used as an alternative to lasers due to their increasing commercial availability, compact design, lower power consumption, lower cost, longer life time (approximately 10,000 hours), and low maintenance. Signal-to-noise ratios (S/Ns) of visible fluorophores were quantitatively compared as an LED with a nominal output wavelength of 470 nm was used as an alternative to argon-ion laser lines at 488 nm, 472 nm, and 465 nm in laser-induced fluorescence detection with CE. Three fluorophores were used for this study: fluorescein, rhodamine 123, and 5-carboxyfluorescein. Optical fibers were used for excitation and collection of emission, so the collimation of the laser relative to the LED is not an issue for the fluorescence detector and comparison of sources. S/Ns were determined for all three fluorophores at several excitation intensities for each source tested. Fluorophore excitation and emission spectra, source spectra and the spectra of bandpass filters used for emission were all considered in the analysis and comparison of S/N for different sources

Chapter 5. Conclusion and future directions

Appendix 1. The goal of this project is to develop an online assay that uses coupling enzymes and CE separation. In the preliminary study, the CE online assay of the second coupling enzyme, lactate dehydrogenase, was developed on a liquid coolant-based CE system. The coolant tubing was modified with tubing of smaller size to shorten the magnet-magnet and magnet-capillary distances while not obstructing the coolant flow. The coupling enzymes lactate dehydrogenase was immobilized onto magnetics beads, which were held inside the capillary under the magnetic field generated by a pair of magnets. The NADH consumed in the assay was detected by fluorescence, using a 365-nm LED as the excitation source. The dependence of NADH

consumption on magnetic bead injection time, pyruvate concentration was investigated.

CHAPTER 2. INHIBITION STUDY OF BACTERIAL ACC

2.1. Introduction

Antibiotic resistance is a growing threat to the public's health worldwide [99]. This is an inevitable side effect of antibiotic usage due to the bacteria developing resistance to the drugs designed to kill them. Over years, the overuse and misuse of antibiotics in medical treatment and agricultural settings have attributed to the acceleration of antibiotic resistance. The bacteria can evolve and make the antibiotics impotent in multiple ways. Some bacteria can change the outer structure to prevent the antibiotic from permeating into the bacteria. Others modify or break down the antibiotics before any harm is caused. Some bacteria can change the proteins that are antibacterial targets in order to limit and block the effect of antibiotics [100, 101]. As a consequence, a new antibiotic is only effective for a limited period of time after its first introduction. After that, the bacteria still survive and multiply, causing untreatable fatal infections. Despite the urgent need to develop new antibiotics, only 30 new antibiotics and two new β-lactamase/β-lactam inhibitor combinations have been launched between 2000 and 2015 [102]. The slow progress in antibiotic drug discovery is due to the change in drug regulations, challenging commercialization, and the limited number of drug targets [99, 103]. Recently, new targets for antibiotic drug development have been identified, one of which is acetyl-coenzyme A carboxylase (ACC) [104].

ACC is an enzyme that catalyzes the first committed and rate-limiting step in fatty acid biosynthesis [28]. This enzyme can be found in bacteria, plants, animals, in which it catalyzes the biotin-dependent carboxylation of acetyl-CoA to form malonyl-CoA. ACC is composed of three components: biotin carboxylase (BC), carboxyltransferase (CT), and biotin carboxyl carrier protein (BCCP). In vivo, the biotin moiety is covalently bound to the BCCP subunit [7]. In bacteria, these three

components can be isolated as separate proteins, with BC and BCCP expressed as homodimers while CT is an $\alpha_2\beta_2$ tetramer [50]. The ACC-catalyzed reaction proceeds through two half-reactions. In the first half-reaction, BC catalyzes the ATP-dependent carboxylation of the biotin moiety on BCCP. This reaction requires two metal ions, typically Mg^{2+}. The first Mg^{2+} is chelated to magnesium to form the Mg^{2+}-ATP metal-nucleotide complex which is the actual substrate. The second Mg^{2+} is bound to the active site of the enzyme which interacts with the phosphate groups of ATP. As such, the metal ions are thought to direct Mg^{2+}-ATP to the active site cleft [7]. In the second half-reaction, under the catalysis of CT, the carboxyl group is transferred from biotin to acetyl-CoA to form malonyl-CoA. In bacteria, malonyl-CoA is the building block for the synthesis of fatty acids, which are crucial for cell wall biosynthesis [105]. Therefore, inhibiting ACC leads to limited bacterial cell wall synthesis and subsequently induces cell death. Interestingly, either BC or CT can derive their own efficacy without the other two ACC components, and the reactions catalyzed by these two subunits can utilize free biotin as a substrate rather than the biotinylated BCCP [7]. As a consequence, not only ACC but also BC and CT are attractive targets for antibacterial drug discovery.

Recently, antibacterial drug development has relied significantly on screening botanical extracts. To date, 100,000 plant species have been tested for medicinal purposes. Among 109 new antibiotics approved in 1981-2006, 69% were derived from natural products [106]. Botanical extracts exhibit antibacterial properties owing to the active compounds such as quinones, phenols, alkaloids, flavonoids [101]. Over 4000 flavonoids have been documented and classified into several sub-groups such as flavonols, flavones, flavanones, and flavon 3-ol [107]. Flavonols, among the most abundant flavonoids, are polyphenolic natural compounds frequently found in plants, vegetables, and fruits, especially berries [108]. They are beneficial to human health

owing to not only their antimicrobial activities but also antioxidant, anti-inflammatory, anticarcinogenic, and antiviral properties. Flavonols consist of two aromatic rings (A and B) linked by a 3-carbon chain that forms an oxygenated heterocyclic ring (C) and hydroxyl groups substituted in C3 position (Figure 2.1). The hydroxyl group at C-3 and hydroxyl groups on the aromatic rings attribute to the antimicrobial property of flavonols [108]. Flavonols were reported to exhibit antibacterial activities in multiple ways such as inhibition of nucleic acid synthesis, inhibition of cytoplasmic membrane function or inhibition of energy metabolism [109]. For example, galangin, quercetin, myricetin, and kaempferol demonstrated strong inhibition of DNA gyrase [109]. Quercetin was reported to disrupt membranes, decrease bilayer thickness, inhibit cell envelope synthesis, and inhibit fatty acid synthesis (FAS-I) in mycobacteria among others [106]. Similarly, myricetin inhibited FAS-I as well as DNA and RNA polymerases [106]. Galangin showed strong inhibition against penicillinase (a type of β-lactamase) from *E.cloacae*, and also altered the outer membrane permeability when combined with amoxicillin [110]. Being pigments responsible for the color of leaves and fruits in plants, flavonols strongly absorb in the UV range, which is a challenge for enzyme inhibition studies due to spectral interference. Therefore, a method that enables inhibitor screening with minimal spectral interference is needed.

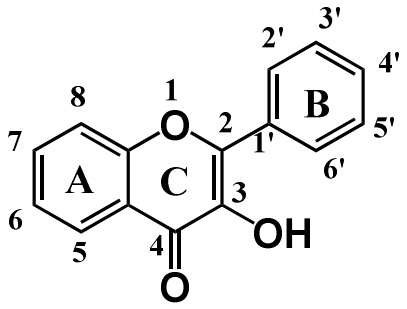

Figure 2.1. The skeleton structure of flavonols

Capillary electrophoresis (CE) has emerged as an analytical tool for pharmaceutical research [79, 86, 111]. Enzyme assays based on CE have been developed to study enzyme activity and applied to screen for enzyme inhibitors [76, 79, 111]. Compared to the conventional coupled enzyme assays, CE-based assays offer several advantages. First, in a CE enzyme assay, the assay components (substrates, products, inhibitors) are separated and quantified individually. This enables the detection of enzyme activity without the spectral interference, which is a drawback of coupled enzyme assays. Second, the CE assays allow for direct detection of the assay components without the need of coupling enzymes, thus avoid the complications from false positives in inhibitor screening. In addition, CE-based assays require minute sample (nL) and can be implemented in online assays, making CE more versatile a method to study enzymes.

Bryant et al. developed CE-based enzyme assays of not only the *Escherichia coli* (*E. coli*) holo-ACC but also BC and CT [49]. Bryant and coworkers previously studied the inhibition of botanical extracts and other flavonols towards holo-ACC, BC, and CT [112]. It was observed that extracts from cranberry resulted in strong inhibition of holo ACC, BC, and CT. Quercetin and myricetin, which are two abundant compounds in cranberry extract [113-116], were found to inhibit not only holo-ACC but also the BC and CT subunits [112]. These two compounds served as the structural leads for the ligand homology analysis to identify other potential inhibitors of ACC. Based on their commercially availability, three compounds: anrantine osage orange (also known as natural yellow 8,11), galangin and 3,6-dihydroxyflavone (DHF) were chosen for further study. Herein, the CE-based assays were used to study inhibition of holo-ACC, BC, and CT by five flavonols (quercetin, myricetin, anrantine osage orange, galangin and 3,6-dihydroxyflavone). The structures of these five compounds

are shown in Figure 2.2. The IC_{50} values (the inhibitory concentration at half maximum inhibition) for these five flavonols were measured to evaluate their potency towards *E. coli* ACC, BC, and CT inhibition.

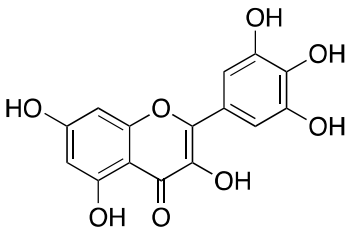

Myricetin

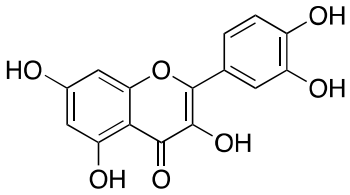

Quercetin

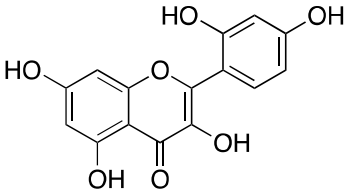

Anrantine osage orange

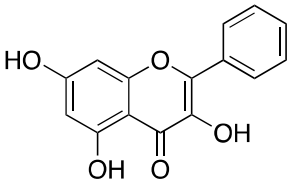

Galangin

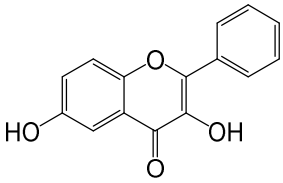

3,6-dihydroxyflavone

Figure 2.2. Strutures of five flavonols in the inhibition study of holo-ACC, BC, and CT

2.2. Materials and Methods

2.2.1. Chemicals

ADP, ATP, acetyl-CoA, malonyl-CoA, biotin, biocytin, DMSO, sodium hydroxide, potassium bicarbonate, magnesium chloride, sodium dedocyl sulfate, quercetin, myricetin, and galangin were purchased from Sigma-Aldrich (St Louis, MO, USA). Anrantine osage orange (natural yellow 8,11) was purchased from Aldrich (Milwaukee, WI, USA), and 3,6-dihydroxyflavone was purchased from Alfa Aesar (Heysham, Lancashire, UK). Potassium phosphate and sodium phosphate were purchased from Fisher (Fairlawn, NJ, USA). The *E. coli* BC, CT, holo-ACC enzymes, which were expressed following the procedures presented by Broussard et al. [47], were obtained from the Waldrop Research Group. All solutions were prepared using ultrapure water (>18 MΩ, Barnstead Nanopure, ThermoFisher, Marietta, Ohio, USA).

All buffer solutions were filtered through 0.2 μm membranes (Whatman, Hilsboro, OR, USA) before use.

2.2.2. Instrument

Capillary electrophoresis assays were performed using a P/ACE MDQ with a PDA detector from Beckman Coulter (Brea, CA, USA). The data were collected and analyzed using 32 Karat 5.0 software from Beckman Coulter. Fused-silica capillary (50 μm i.d., 360 μm o.d.) was purchased from Polymicro Technologies (Phoenix, Arizona, USA). A short segment of the polyimide coating on the capillary was removed to create a detection window using a MicroSolv CE window maker (Eatontown, NJ, USA). The IC_{50} values were calculated using Origin Pro 2016 software (OriginLab Corporation, Northampton, MA, USA).

2.2.3. CE Assays

At the beginning of each day, the capillary was conditioned by rinsing with 1.0 M NaOH, ultrapure water, and separation buffer at 20.0 psi for 10.0 min each. Before each run, the capillary was rinsed with the separation buffer at 20.0 psi for 1.0 min. The samples were introduced to the capillary by hydrodynamic injection at 1.0 psi for 10 s.

The BC and CT assays were adapted from the assays developed by Bryant et al. [49]. In the BC assay, the sample buffer contained 2.5 mM $MgCl_2$, 5.0 mM $KHCO_3$ and 5.0 mM potassium phosphate while the separation buffer contained 10.0 mM sodium phosphate and 20.0 mM SDS, both at pH 7.50. The reaction mixtures contain 50.0 μM ATP, 2.5 mM $MgCl_2$, 5.0 mM $KHCO_3$, 50.0 mM biotin, 0.25% DMSO, and 0.5 μM BC. The separation was carried out in a 54.0 cm capillary with an effective length of 44.0 cm, under the applied voltage of 30.0 kV (555 V/cm), with a current of 29.2 μA.

For the CT assay, both the reaction buffer and separation buffer were 5.0 mM potassium phosphate buffer at pH 7.50. The reaction mixture contained 100.0 μM malonyl-CoA, 4.0 mM biocytin, 0.25% DMSO, and 0.05 μM CT. The capillary total length was 38.6 cm, with an effective length of 28.6 cm (injection end to detection window) A potential of 30.0 kV was applied to the separation (777 V/cm), with a current of 16.6 μA.

The holo-ACC assay was based on the improved separation conditions presented in Chapter 3. For this assay, the sample buffer contained 5.0 mM potassium phosphate, 2.5 mM $MgCl_2$, and 5.0 mM $KHCO_3$ at pH 7.50 while the separation buffer contained 5.0 mM sodium phosphate, 10.0 mM SDS, and 2.0 mM $MgCl_2$ at pH 7.50. The reaction mixtures contained 25.0 μM ATP, 50.0 μM acetyl-CoA, 5.0 mM $KHCO_3$, 2.5 mM $MgCl_2$, 5.0 mM potassium phosphate, 0.25% DMSO, and 31.8 μg/ml holo-ACC. The capillary total length was 38.6 cm, with an effective length of 28.6 cm. The applied voltage was at 30.0 kV (777 V/cm), with a current of 30.6 μA.

2.2.4. Data Analysis

The inhibition of holo-ACC, BC, and CT by the flavonols was evaluated based on v/v_0 ratio in which v and v_0 are the enzyme activity with and without an inhibitor, respectively. The IC_{50} values were calculated by fitting the vi/vo ratios to the nonlinear Logistic Model (OriginPro 2016):

$$y = A_2 + \frac{(A_1 - A_2)}{1 + (x/x_0)^p} \qquad 2.1$$

where y is the parameter corresponding to v/v_0, A1 and A_2 are the maximum and minimum values of v/v_0 , x is the concentration of the inhibitor, x_0 is the concentration of the inhibitor at the inflection point of the curve, and p is the Hill's slope.

The adjusted r-square is used to evaluate the goodness of fit. This parameter is based on the coefficient of determination R^2, and accounts for the degrees of freedom.

2.3. Results and Discussion

2.3.1. BC Inhibition Study

For the BC assay, the reaction mixture contained 50.0 μM ATP, 2.5 mM $MgCl_2$, 5.0 mM $KHCO_3$, 50 mM biotin and 0.5 μM BC in a 5.0 mM sodium phosphate buffer solution at pH 7.50. The BC-catalyzed reaction (Scheme 2.1) is the first half-reaction in the ACC-catalyzed reaction. Herein, BC retains its catalytic activity using biotin as a substrate:

$$\text{ATP + biotin+ } HCO_3^- \xrightarrow{BC} \text{ADP + biotin-}COO^- + P_i$$

Scheme 2.1. Half-reaction catalyzed by BC

As the reaction proceeds, ATP depletes to produce ADP, both of which can be detected by UV absorption at 256 nm. Figure 2.3 shows the separation of the reaction mixture after 6.0 min incubation with and without the inhibitor (anrantine osage orange). DMSO was added to all reaction mixtures to the final concentration of 0.25% to help dissolve the flavonols. For the control sample to which 0.5 μM BC was added, in addition to the ATP substrate peak at 8.8 min, an additional peak corresponding to the ADP product was observed at 13.8 min. With 10^{-5} M anrantine osage orange added to the reaction mixture, no ADP peak was observed, indicating that anrantine osage orange inhibited the BC-catalyzed reaction.

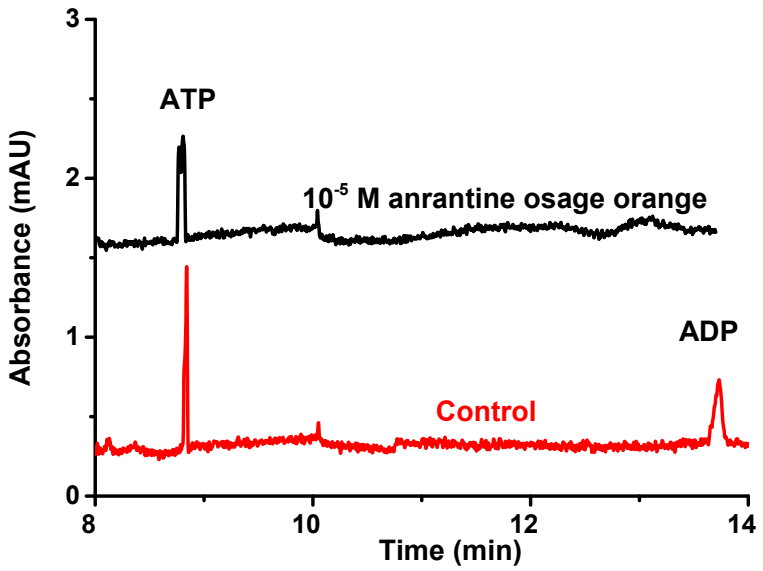

Figure 2.3. Electropherograms for the BC inhibition assay. The reaction mixtures contain 50.0 μM ATP, 2.5 mM $MgCl_2$, 5.0 mM $KHCO_3$, 50.0 mM biotin, 0.25% DMSO, and 0.5 μM BC without an inhibitor (control, solid red line) and with 10^{-5} M anrantine osage orange (solid black line). The reaction time was 6.0 min. The assay condition was described in Section 2.2.3.

The CE assay was applied to determine the IC_{50} values for the five flavonols. The enzyme activity (v) is defined as the peak area ratio of ADP/(ADP+ATP). As such, the precision of enzyme activity is improved by offsetting the fluctuation in sample injection [77]. The dose dependence of BC inhibition by the flavonols was evaluated based on the ratio v_i/v_o in which v_i and v_o are the enzyme activities in reactions with and without the inhibitor, respectively. Figure 2.4 presents the dose-response curves for the inhibition of BC by the 5 flavonols. Out of five compounds tested, only 3 compounds (myricetin, quercetin, and anratine osage orange) exhibited significant inhibition towards BC as the flavonol concentration was increased up to 2.5×10^{-4} M. The IC_{50} values calculated for myricetin, quercetin, and anrantine osage orange were $(5.3 \pm 1.7) \times 10^{-5}$ M, $(6.6 \pm 0.3) \times 10^{-5}$ M, and $(1.5 \pm 0.2) \times 10^{-5}$ M, respectively. It was not practical to determine IC_{50} for galagin and DHF. Galagin (10^{-8} – 5.0×10^{-4} M) did

not significantly inhibit BC whereas DHF slightly inhibited BC but its solubility (below 1.0×10^{-4} M) was too low for IC_{50} quantitation.

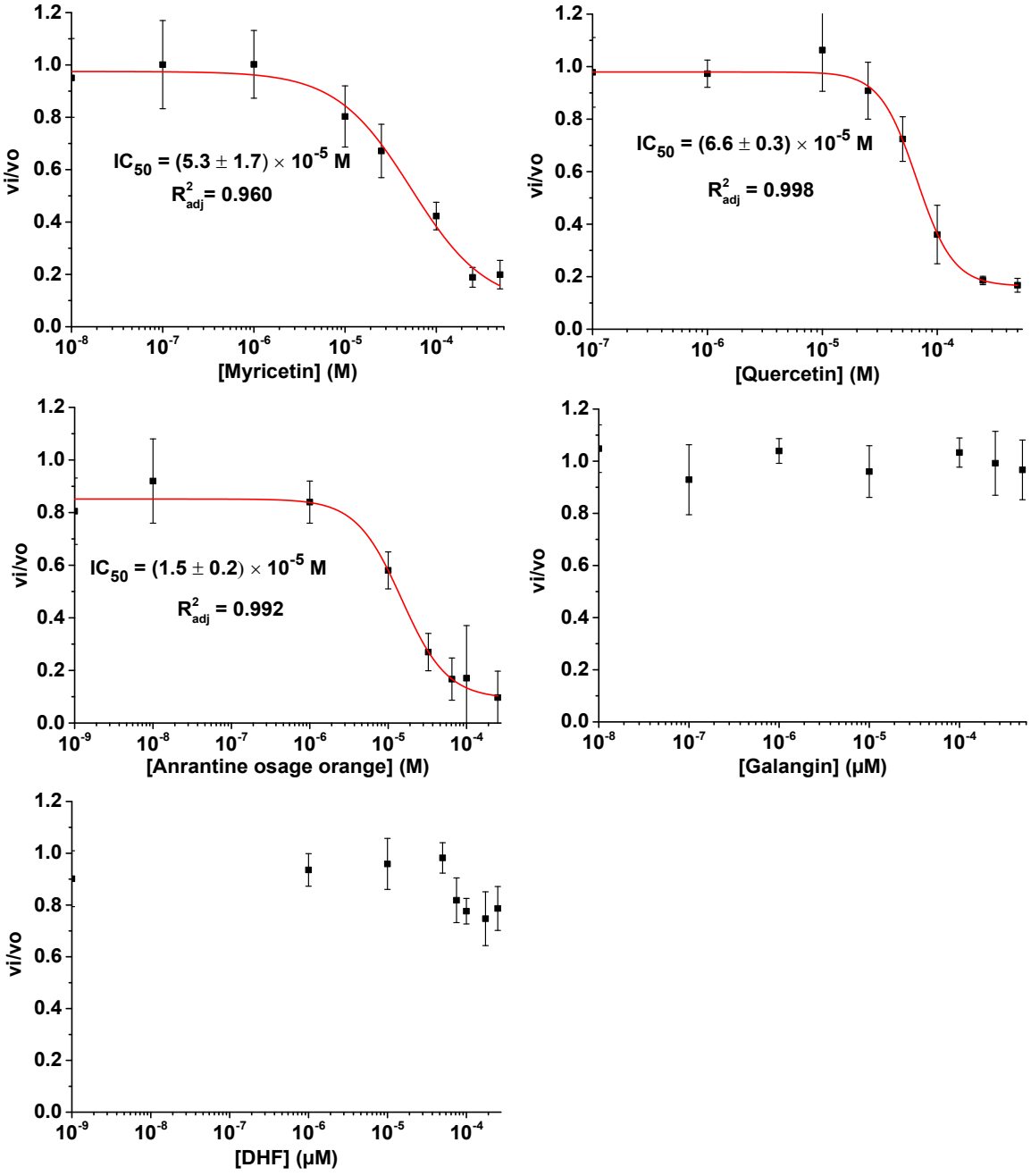

Figure 2.4. Dose dependence of BC inhibition by flavonols. The error bars present the standard deviations of vi/vo, each measured in triplicates.

2.3.2. CT Inhibition Study

The CT assay is used to study the second half-reaction in the ACC assay and proceeds in a non-physiological direction in which malonyl-CoA reacts to generate acetyl-CoA. Previously, the CE-based assays were developed and applied to inhibition study of CT [49, 52]. Biocytin, a more reactive analog of biotin (with maximal velocity 3 orders of magnitude higher than biotin), was used as a substrate for this assay [50]. The non-physiological reaction of malonyl-CoA and biocytin was catalyzed by CT as follow:

$$\text{malonyl-CoA} + \text{biocytin} \xrightarrow{\text{CT}} \text{acetyl-CoA} + \text{carboxybiocytin}$$

Scheme 2.2. Reverse half-reaction catalyzed by CT

For the CT assay, both the sample and the separation buffers contained 5.0 mM potassium phosphate at pH 7.50. The reaction mixtures contained 100.0 μM malonyl-CoA, 4.0 mM biocytin, 0.25% DMSO, and 0.05 μM CT, which were allowed to react for 4.0 min before being introduced to the capillary. The electropherograms for the inhibition study of CT are shown in Figure 2.5. Compared to the control sample (red solid line), the reaction mixture containing 10^{-5} M anrantine osage orange generated a acetyl-CoA product peak of smaller area. This indicates that anrantine osage orange inhibited the CT reaction. The CE-based assay was further applied to study the inhibition of CT by 5 flavonols. Similar to the BC inhibition study, the IC_{50} value for each compound in the CT assay was determined by fitting the activity ratio v_i/v_o to the Logistic model, the nonlinear regression model on the OriginLab software. The activity in this assay is defined as the peak ratio acetyl-CoA/(acetyl-CoA + malonyl-CoA). Plots showing the dependence of CT inhibition on the concentration of the flavonols are shown in Figure 2.6.

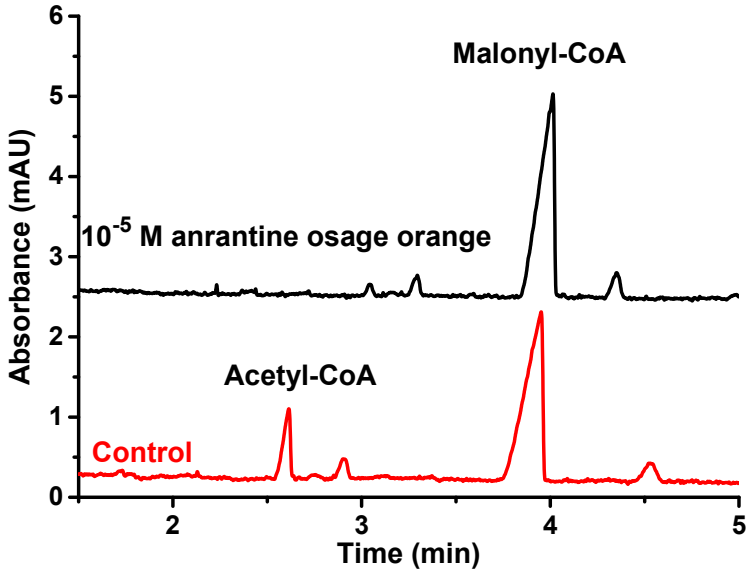

Figure 2.5. Electropherograms for the CT assay with anrantine osage orange. The reaction mixtures contained 100.0 μM malonyl-CoA, 4.0 mM biocytin, 0.25% DMSO, and 0.05 μM CT at reaction time of 4 min without an inhibitor (control, red solid line) and with 10^{-5} M anrantine osage orange (black solid line). The assay condition was described in Section 2.2.3.

Three compounds (myricetin, quercetin, and anrantine osage orange) inhibited CT and yielded the IC_{50}'s of $(4.6 \pm 1.4) \times 10^{-7}$ M, $(2.1 \pm 0.5) \times 10^{-6}$ M, and $(6.5 \pm 0.3) \times 10^{-7}$ M, respectively. These IC_{50}'s are 23-115 fold lower than the corresponding values for the BC assay, indicating that these inhibitors are more potent towards the CT component of ACC. Meanwhile, galagin and DHF did not significantly inhibit CT when tested up to 2.5×10^{-4} M and 1.0×10^{-4} M, respectively. Subsequently, only myricetin, quercetin, and anrantine osage orange were chosen for further testing of holo-ACC inhibition.

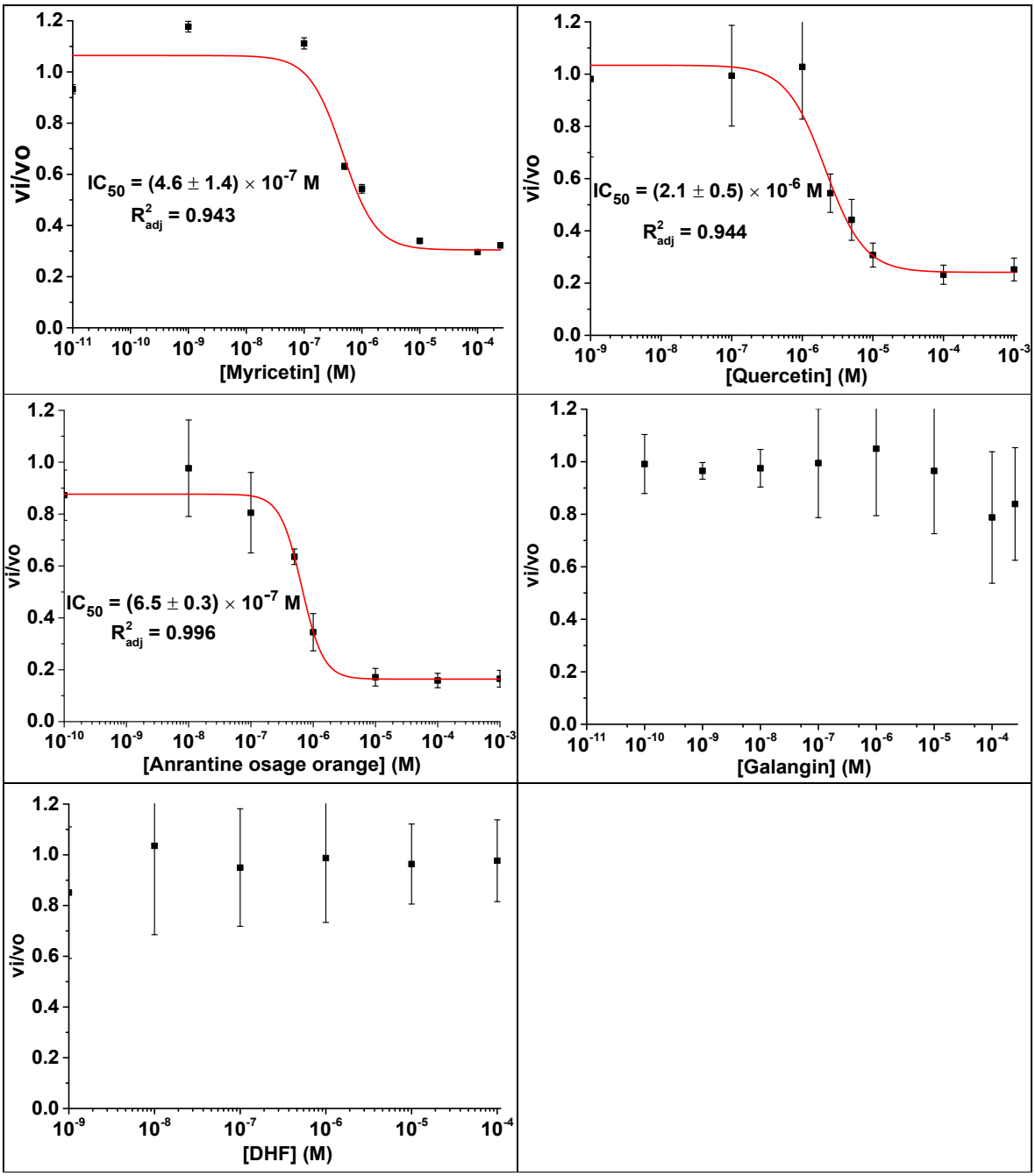

Figure 2.6. Dose dependence of CT inhibition by flavonols. The error bars present the standard deviations of vi/vo, each measured in triplicates.

2.3.3. Holo-ACC Inhibition Study

The separation conditions for the holo-ACC were modified from the assay previously developed by Bryant et al [49]. In this assay, the reaction buffer contained 5.0 mM $KHCO_3$, 2.5 mM $MgCl_2$, and 5.0 mM potassium phosphate at pH 7.50. Initially,

the separation buffer containing 10.0 mM sodium phosphate with 20.0 mM SDS at pH 7.50 was used, resulting in splitting peaks of ADP and ATP. The work of Malina et al. on the development of a PFK-1 assay, which also dealt with the separation of ADP and ATP, suggested that this problem is associated with the exclusion of Mg^{2+} from the separation buffer [77]. Upon the addition of Mg^{2+} to the separation buffer, ADP and ATP were separated and detected as single peaks, presumably due to the complexes Mg-ADP and Mg-ATP remaining at equilibrium when migrating in the separation buffer containing Mg^{2+}. The effect of Mg^{2+} on the separation of ACC assay components was discussed in more details in Chapter 3. For the holo-ACC assay, a buffer containing 5.0 mM sodium phosphate, 10.0 mM SDS, and 2.0 mM $MgCl_2$ was used as the separation buffer.

Figure 2.7 shows the electropherograms for inhibition study of holo-ACC. The reaction mixture contained 25.0 μM ATP, 50.0 μM acetyl-CoA, 5.0 mM $KHCO_3$, 2.5 mM $MgCl_2$, 5.0 mM potassium phosphate, 0.25% DMSO, and 31.8 μg/ml holo-ACC. The reaction mixtures were let to react for 4.0 min before being injected to the capillary. In the absence of an inhibitor, two peaks for the products, ADP and malonyl-CoA, were observed in addition to the ATP and acetyl-CoA peaks. When 10^{-4} M anrantine osage orange was added to the reaction mixture, holo-ACC was inhibited as evidenced by the absence of the ADP and malonyl-CoA peaks. The IC_{50}'s of the three flavonols were calculated based on the nonlinear fitting of the enzyme activity ratio v_i/v_o to the Logistic nonlinear regression model. The enzyme activity in this assay is defined as the peak ratio of malonyl-CoA/(malonyl-CoA + acetyl-CoA).

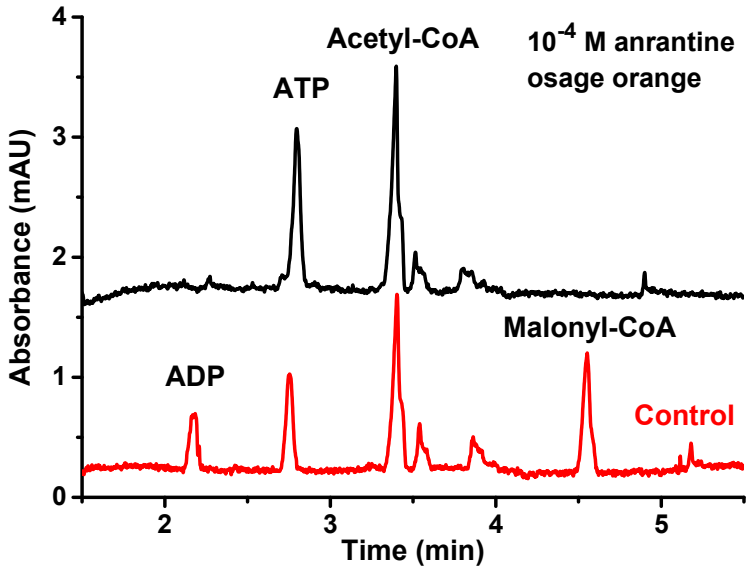

Figure 2.7. Electropherograms for holo-ACC inhibition study. Reaction mixtures containing 25.0 μM ATP, 50.0 μM acetyl-CoA, 5.0 mM $KHCO_3$, 2.5 mM $MgCl_2$, 5.0 mM potassium phosphate, 0.25% DMSO, and 31.8 μg/ml holo-ACC without an inhibitor (control, red solid line) and with 10^{-4} M anrantine osage orange (black solid line) were injected 4.0 min after incubation. The assay condition was described in Section 2.2.3.

Figure 2.8 shows the dependence of holo-ACC inhibition on the concentration of the flavonols. The IC_{50}'s calculated for myricetin, quercetin, and anrantine osage orange were $(6.7 \pm 0.3) \times 10^{-5}$ M, $(5.2 \pm 0.2) \times 10^{-5}$ M, and $(2.0 \pm 0.2) \times 10^{-5}$ M, respectively. Table 2.1 summarizes the IC_{50} values for the five flavonols studied in this project. Myricetin, quercetin, and anrantine osage orange inhibited not only holo-ACC but also the BC and CT components. Interestingly, for all three compounds, the IC_{50}'s for holo-ACC and BC are comparable, and 25-146 times higher than the IC_{50}'s for CT. As such, the inhibitors are more potent towards the CT subunit than the BC subunit.

Hydroxyl substitution in flavonols is an important factor associated with bacterial ACC inhibition. Tsuchiya et al. previously reported that the 5,7-dihydroxylation of the A ring was critical for antibacterial activity [117]. Our results with the five flavonols are in agreement with this hypothesis. Myricetin, quercetin, and anrantine osage orange showed inhibition towards BC, CT, and holo-ACC owing to the hydroxyl groups at the

C-4', C-3, C-5, and C-7 positions. Due to limited solubility, DHF was only tested up to 1.0 $\times 10^{-4}$ M. Even at the highest concentration tested, DHF, which only has one hydroxyl group at C-6 of the A ring did not significantly inhibit these enzymes. Meanwhile, galangin, which also has the hydroxyl groups at C-3, C-5, and C-7 positions did not show significant inhibition of the tested enzymes. This suggests that the 5,7-dihydroxylation of the A ring is not sufficient, and hydroxyl group substitution at C-4' is likely to enhance the inhibition of bacterial holo-ACC by flavonols. It was previously reported that 4'-OH in flavonols did not only enhance the antibacterial activity [109] but was also essential for the flavonols to inhibit influenza virus [118].

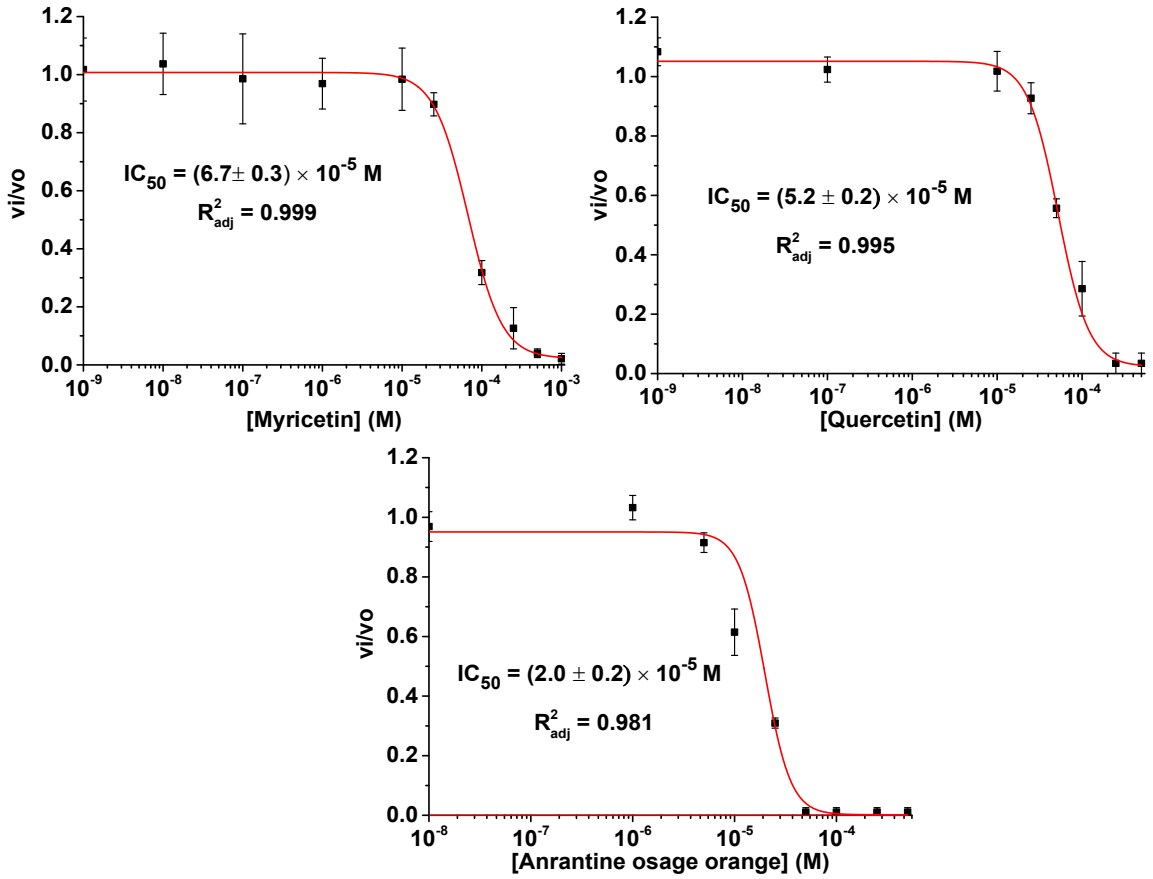

Figure 2.8. Dose dependence of holo-ACC inhibition by myricetin, quercetin, and anrantine osage orange. The error bars present the standard deviations of vi/vo, each measured in triplicates.

Myricetin, quercetin, and anrantine osage orange have the same hydroxyl groups in the A- and C- rings but different hydroxyl substitutions in the B-ring. Anrantine osage orange with two OH groups at C-2' and C-4' has the lowest IC_{50} values towards BC and holo-ACC relative to myricetin (with OH groups at C-3', C-4', C-5') and quercetin (with OH groups at C-4' and C-5'). This finding suggests two hypotheses. First, the hydroxyl substitutions at C-3' and C-5' are likely to decrease the potency of the flavonols towards bacterial holo-ACC inhibition. A previous report by Wu et al [109] also showed that the hydroxyl groups at these positions enhanced antibacterial activity. Second, the hydroxyl group at C-2' may enhance the inhibition of bacterial holo-ACC by flavonols. Though there is no further evidence to support this hypothesis on flavonols, the hydroxyl group at C-2' of chalcones was assumed to be essential for antibacterial activity [119]. Similarly, Tsuchiya et al. reported that the 2',4'-dihydroxylation in the B ring of the flavanones is important for anti-methicillin-resistant *S. aureus* activity [117].

Relative to quercetin, myricetin, which has an additional OH group at C-3', exhibits lower IC_{50} values towards the BC and CT subunits but higher IC_{50} value towards holo-ACC. This suggests that although the hydroxyl substitution at C-3' is associated with increased inhibitory efficiency of the BC and CT subunits, it still causes the decrease in activity of the holo-ACC as a whole.

In addition to the position of the hydroxyl groups on the phenolic rings, the degree of hydroxylation may also impact the inhibition of bacterial holo-ACC, BC, and CT by phenolic compounds [107]. In this study, strong inhibition of holo-ACC, BC, and CT was observed for myricetin, quercetin, and anrantine osage orange, which have 6, 5, and 5 hydroxyl groups, respectively whereas galangin and DHF with the corresponding 3 and 2 hydroxyl groups did not significantly inhibit when tested up to

2.5 ×10^{-4} M. This finding supports the hypothesis by Puupponen-Pimia et al. that the higher degree of hydroxylations is associated with the higher antibacterial activity of phenolic compounds [107]. However, myricetin has higher IC_{50} values for *E. coli* holo-ACC and BC, thus lower potency in inhibiting these enzymes compared to anrantine osage orange although the former has one hydroxyl group more in the B ring. Therefore, the structure-activity relationship associated with flavonols remains to be clarified.

2.4. Conclusion

Capillary electrophoretic enzyme assays were applied to study inhibition of holo-ACC, BC, and CT. Out of 5 flavonols tested, only myricetine, quercetin, and anrantine osage orange inhibited the three enzymes. Galangin did not show significant inhibition of holo-ACC, BC, and CT whereas DHF inhibited these three enzymes but its solubility (< 1.0 × 10^{-4} M) is too poor to get IC_{50} quantitation. The IC_{50} values of the flavonols depend on the position and number of hydroxyl groups. The 5,7-dihydroxylation of the A ring is essential but not efficient for the flavonols to inhibit bacterial holo-ACC. In addition, the hydroxyl groups C-4' and C-2' are likely to enhance the inhibition of bacterial-ACC by flavonols whereas the hydroxyl groups at the C-3' and C-5' decrease the potency of the flavonols towards holo-ACC inhibition.

Table 2.1. IC_{50} values of flavonols in BC, CT, and holo-ACC assays

Compounds	**Structure**	**IC_{50} (M) BC assay**	**IC_{50} (M) CT assay**	**IC_{50} (M) holo-ACC assay**
Myricetin	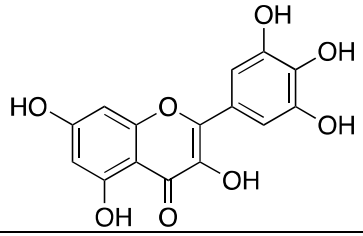	$(5.3 \pm 1.7) \times 10^{-5}$	$(4.6 \pm 1.4) \times 10^{-7}$	$(7.2 \pm 1.3) \times 10^{-5}$
Quercetin	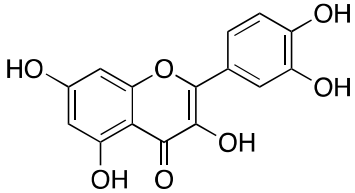	$(6.6 \pm 0.3) \times 10^{-5}$	$(2.0 \pm 0.3) \times 10^{-6}$	$(5.3 \pm 0.3) \times 10^{-5}$
Anrantine osage orange	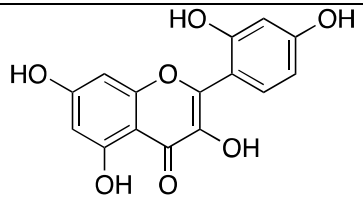	$(1.5 \pm 0.2) \times 10^{-5}$	$(6.5 \pm 0.3) \times 10^{-7}$	$(2.0 \pm 0.2) \times 10^{-5}$
Galangin	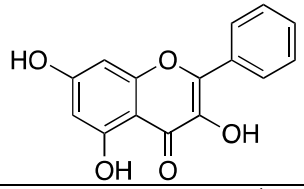	N/A (negligible inhibition)		
3,6-dihydroxyflavone	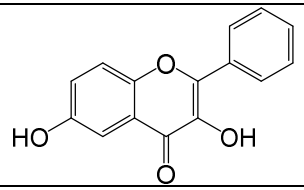	N/A (poor solubility)		

CHAPTER 3. CAPILLARY ELECTROPHORETIC ASSAY OF HUMAN ACETYL-COENZYME A CARBOXYLASE 2*

3.1. Introduction

Acetyl-CoA carboxylase (ACC) catalyzes the carboxylation of acetyl coenzyme A (CoA) to form malonyl-CoA in the committed step in fatty acid biosynthesis [45]. The reaction proceeds via two half-reactions catalyzed by biotin carboxylase (BC) and carboxyltransferase (CT), as shown in Scheme 3.1.

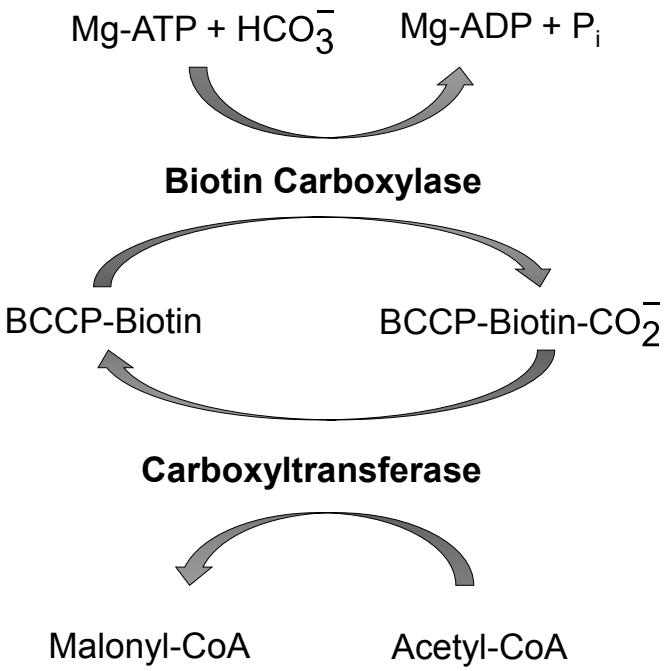

Scheme 3.1. ACC-catalyzed reaction

The first half-reaction, catalyzed by BC, uses magnesium-adenosine triphosphate complex (Mg-ATP) to activate HCO_3^- by forming a carboxyphosphate intermediate. The carboxyl group is transferred from carboxyphosphate to biotin, which is covalently attached to the biotin carboxyl carrier protein (BCCP). The first half-reaction requires two equivalents of Mg^{2+} for activity. One Mg^{2+} is bound to ATP

* Reprinted from Nguyen, T. H., Waldrop, G. L. and Gilman, S. D. (2019), Capillary electrophoretic assay of human acetyl-coenzyme A carboxylase 2. ELECTROPHORESIS. With permission from John Wiley and Sons.

so that the Mg-ATP metal-nucleotide complex is the substrate, while the other Mg^{2+} is bound in the active site where it interacts with the phosphate groups of ATP [120, 121]. In the second half-reaction, CT catalyzes the transfer of the carboxyl group from biotin-BCCP to acetyl-CoA to form malonyl-CoA. In most Gram-negative and Gram-positive bacteria, BC, CT, BCCP are separate proteins [122]. The active form of the enzyme is a complex of these three proteins (referred to hereafter as holo-ACC) [47]. In contrast, in eukaryotes, these three proteins are domains on a single polypeptide chain [123].

In mammals, including humans, ACC exists in two isoforms [45, 124]. The ACC1 isoform is a 265 kDa protein found in the cytosol of lipogenic tissues such as liver, mammary gland, and adipose where the product, malonyl-CoA, is a substrate for *de novo* fatty acid biosynthesis [45, 124, 125]. In contrast, the 280 kDa ACC2, is highly expressed only in the mitochondria of oxidative tissues such as skeletal muscle, cardiac muscle, and occasionally in liver [59, 60]. In these tissues, malonyl-CoA regulates fatty acid oxidation by inhibiting carnitine palmitoyltransferase I, and ultimately blocking the entry of fatty acids into the mitochondria for β-oxidation [27].

Both isoforms of human ACC are targets for the treatment of disease states. Knockout mice missing the gene for ACC2 do not gain weight even on a high-fat diet, suggesting that ACC2 is a target for anti-obesity agents [32]. Inhibition of ACC1 and ACC2 can be used to reduce hepatic *de novo* lipogenesis and treat metabolic disorders such as nonalcoholic steatohepatitis [37, 126]. Also, the expression of the gene coding for ACC1 is upregulated in several cancer types, indicating an increased need for fatty acids and thereby making ACC1 a target for anti-cancer drugs [43]. Despite both isoforms of ACC being targets for pharmaceutical intervention, there is a dearth of inhibitors of the enzymes for clinical testing. A robust and effective assay for screening inhibitors of ACC would be timely and useful.

Several different methodologies have been used to assay the activity of eukaryotic ACC. Early assays utilized radiochemicals such as $H^{14}CO_3$ [11, 30, 34, 60, 65] and [γ-^{32}P] ATP [29]; however, radiolabeled based assays have significant disadvantages, including safety and radioactive waste disposal regulation. In contrast, coupled enzyme assays are relatively benign. Coupled enzyme assays of ACC have been developed to measure the production of adenosine diphosphate (ADP) [11, 29, 30], inorganic phosphate (P_i) [61, 62], or malonyl-CoA [63]. While coupled enzyme assays are facile for many kinetic measurements, they can be problematic for inhibitor screening. The cost of the coupling enzymes can be prohibitive. More importantly, coupled enzyme assays, especially those utilizing NADH/NADPH, can be problematic for detecting enzyme inhibition due to spectral overlap with the inhibitors. Additionally, inhibition of the coupling enzymes is likely to cause false positive in inhibitor screening. Recently, LC-MS/MS has been used to detect the formation of malonyl-CoA [66]. While the LC-MS/MS assay is a direct, selective and sensitive measure of malonyl-CoA, it requires an expensive instrument run by highly-skilled personnel.

Capillary electrophoresis has emerged as a versatile separation-based platform for development of enzyme assays [18, 127, 128]. Using CE to measure enzyme activity and inhibition has several advantages, starting with the small amounts of enzyme, substrate, and inhibitors utilized for a typical CE-based enzyme assay. When the assay components can be separated and detected directly, coupled enzymes are not required, reducing complexity and the likelihood of false positives for enzyme inhibition studies. Electrophoretic separation of substrates, products, and inhibitors in CE-based assays minimizes the potential for spectral interference from inhibitors. Recently, a CE enzyme assay for ACC from *E. coli* was developed [49]. This assay can be used for holo-ACC-catalyzed reactions as well as the half-reactions catalyzed

by the isolated BC and CT components. The CE assay proved to be particularly useful for assessing inhibition of ACC by compounds that exhibited spectral interference with the coupled enzyme assay that utilizes NADH/NADPH [52]. Given the medical relevance of human ACC, a similar CE assay for the human enzyme would be useful; however, human ACC behaves differently than the bacterial form, in that, activity requires citrate to activate the enzyme via polymerization of the protomeric subunits into a filamentous form [129]. This aspect of human ACC2 makes the development of a CE assay for human ACC more challenging than for bacterial ACC. In this report, a CE assay for human ACC2 is described along with demonstration that the assay can detect ACC2 inhibition.

3.2. Materials and Methods

3.2.1. Chemicals

Human acetyl-CoA carboxylase 2, ADP, ATP, acetyl-CoA, malonyl-CoA, DMSO, sodium hydroxide, potassium bicarbonate, potassium citrate, magnesium chloride, and HEPES were purchased from Sigma-Aldrich (St Louis, MO, USA). Tris-HCl was purchased from Promega (Madison, MI, USA). Potassium phosphate and sodium phosphate were purchased from Fisher (Fairlawn, NJ, USA). The inhibitor [(3R)-1-[1-(anthracene-9-carbonyl)piperidin-4-yl]piperidin-3-yl]-morpholin-4-ylmethanone (CP-640186) was obtained from AdooQ Bioscience (Irvine, CA, USA). Solutions were prepared using ultrapure water (>18 MΩ, Barnstead Nanopure, ThermoFisher, Marietta, Ohio, USA). Buffer solutions were filtered through 0.2 μm membranes (Whatman, Hilsboro, OR, USA) before use.

3.2.2. Instrumentation

A P/ACE MDQ with a PDA detector from Beckman Coulter (Brea, CA, USA) was used for CE assays. Data were collected and analyzed using 32 Karat 5.0

software from Beckman Coulter. Fused-silica capillary (50 μm id, 360 μm od) was purchased from Polymicro Technologies (Phoenix, Arizona, USA). A short segment of the polyimide coating on the capillary was removed to create a detection window using a MicroSolv CE window maker (Eatontown, NJ, USA). The capillary total length was 38.6 cm, with an effective length of 28.6 cm (from the injection end to the detection window).

3.2.3. CE Conditions

At the beginning of each day, the capillary was rinsed with 1.0 M NaOH, ultrapure water, and separation buffer at 20.0 psi for 10.0 min each. Before each run, the capillary was rinsed with the separation buffer at 20.0 psi for 1.0 min. A buffer solution containing 30.0 mM HEPES, 3.0 mM $MgCl_2$, 2.5 mM $KHCO_3$, and 2.5 mM potassium citrate at pH 7.50 was used as both the sample and separation buffers unless noted. All enzyme-catalyzed reactions proceeded at room temperature, and the capillary temperature was kept constant at 25 °C. Human ACC2-catalyzed reaction mixtures were prepared in a total volume of 100 μL. All samples were hydrodynamically injected at 0.5 psi for 5.0 s, followed by separation at 19.5 kV (505 V/cm) with ultraviolet (UV) absorption detection at 256 nm.

3.3. Results and Discussion

3.3.1. Separation of Nucleotides using Capillary Electrophoresis

The ACC2 assay based on CE depends on the separation and quantification of the nucleotide substrates and products – ATP, ADP, acetyl-CoA, and malonyl-CoA. Previous CE assays for bacterial ACC [49] and phosphofructokinase-1 [77] included methods for the separation of nucleotides based on earlier published separations [130, 131]; however, the development of the ACC2 assay inspired a reexamination of those

previous nucleotide separations. This reexamination of the separation is relevant to the development of other CE-based assays for enzymes with nucleotide substrates.

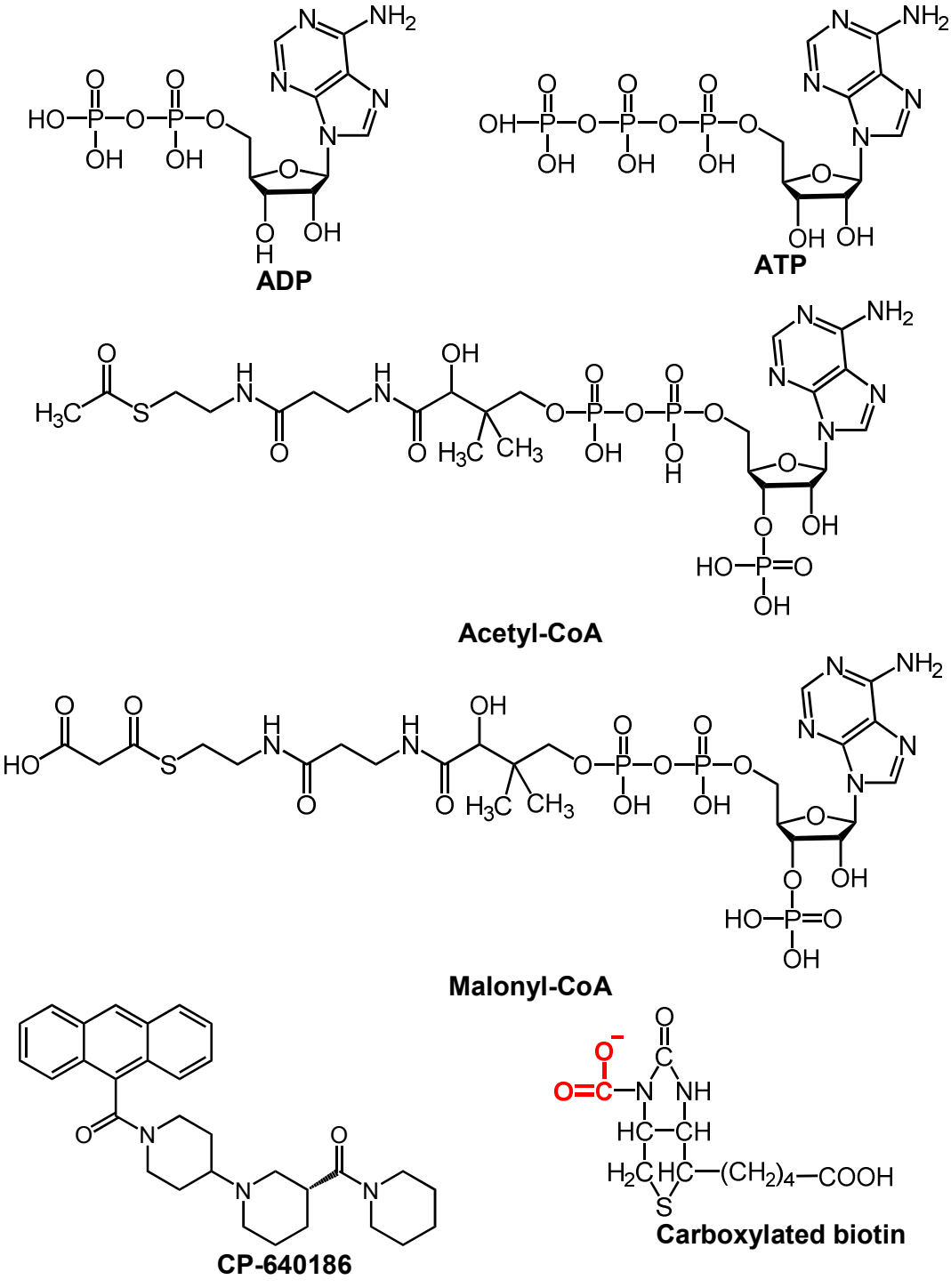

Figure 3.1. Structures of ADP, ATP, acetyl-CoA, malonyl-CoA, CP-640186 and carboxylated biotin. The added carboxyl group on carboxylated biotin is shown in red and boldface.

The separation approach presented here is still based on CE with UV absorption detection as ADP, ATP, acetyl-CoA, and malonyl-CoA all absorb strongly at 256 nm (Figure 3.1 and Figure 3.2).

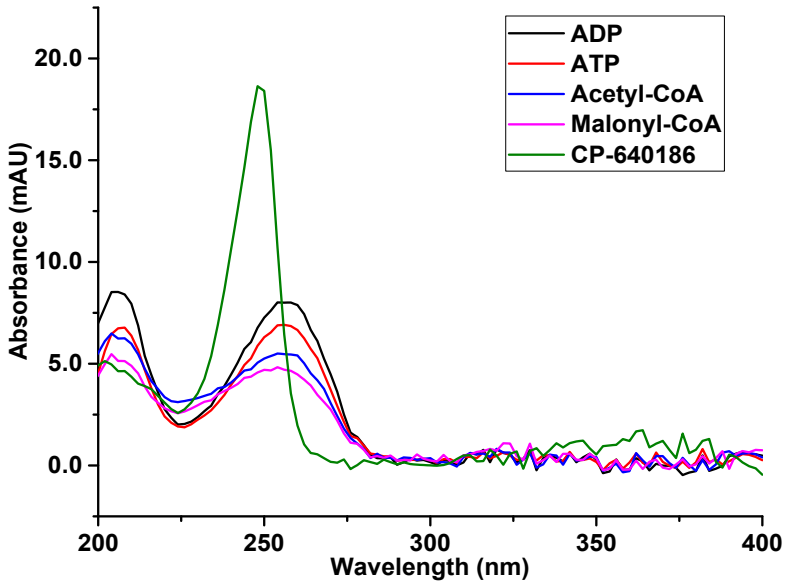

Figure 3.2. UV absorption spectra of 250 µM ADP, ATP, acetyl-CoA, malonyl-CoA, and CP-640186. The spectra were collected using CE with a PDA detector.

The separation method for an enzyme assay must strike a balance between optimal solution conditions for the enzyme-catalyzed reaction and conditions suitable for the reproducible separation of the substrates and products. The injected sample will contain the solution used for the enzyme-catalyzed reaction, and its injection must not degrade the CE separation. Separation of these four molecules has been demonstrated previously for an assay of a bacterial form of ACC [49], but the optimum solution conditions for bacterial ACC and human ACC2 are significantly different [30, 47, 49, 66, 129]. Therefore, the separation was revisited, taking into consideration the reaction requirements of human ACC2 and our experience working with bacterial ACC and phosphofructokinase-1 (PFK-1), another Mg^{2+}-dependent enzyme [77]. Figure 3.3 shows an electropherogram obtained using conditions developed for the bacterial

holo-ACC enzyme assay where the sample buffer was 5.0 mM potassium phosphate, 2.5 mM $MgCl_2$, and 5.0 mM $KHCO_3$ at pH 7.50, and the separation buffer was 10.0 mM sodium phosphate and 20.0 mM SDS at pH 7.50 [49].

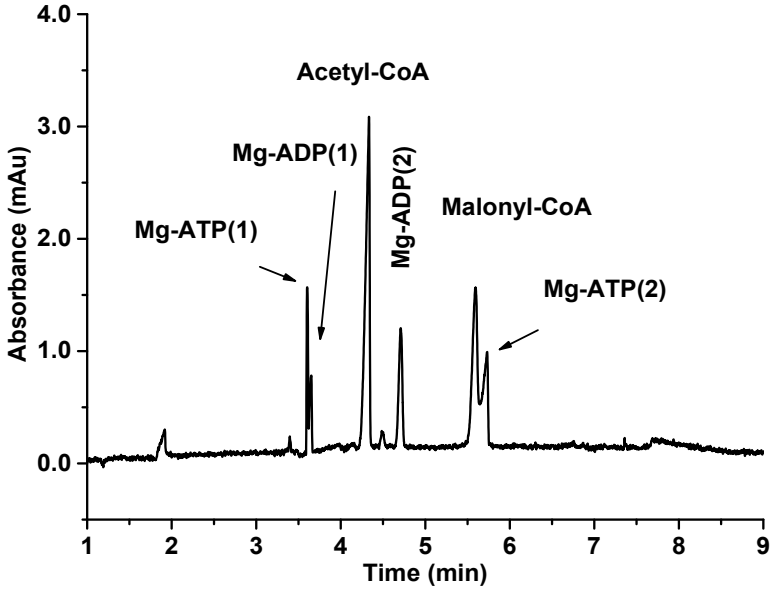

Figure 3.3. Electropherogram for the separation of holo-ACC assay components using the conditions from Bryant et al. [49]. The sample solution contained 50.0 μM ADP, 50.0 μM ATP, 100.0 μM acetyl-CoA, 100.0 μM malonyl-CoA in a buffer containing 5.0 mM potassium phosphate, 2.5 mM $MgCl_2$, and 5.0 mM $KHCO_3$ at pH 7.50. The separation buffer was 10.0 mM sodium phosphate and 20.0 mM SDS at pH 7.50. The sample was injected hydrodynamically at 0.5 psi for 5.0 s and then separated at 19.5 kV (505 V/cm) with a current of 26.7 μA.

Although this separation has been used successfully for quantitative assays of bacterial holo-ACC and its inhibition, this method occasionally suffered from reproducibility problems and peak splitting for ADP and ATP (Figure 3.3). Separation of ADP and ATP alone resulted in the formation of double peaks for each compound, similar to split peaks reported for naphthol separations in borate and attributed to multiple complexes formed by naphthols and borate [132]. Later work by Malina and coworkers on the development of a CE assay for PFK-1 shed light on the issue [77]. This assay also required separation of ATP and ADP, and similar problems were encountered. The substrate for both ACC and PFK-1 is ATP complexed to Mg^{2+}, so

Mg^{2+} must be included in the reaction solution, which is injected into the CE capillary for the enzyme assays. Separation reproducibility for PFK-1 was improved markedly by adding 1.0 mM Mg^{2+} to the separation buffer. The peaks in the CE separations were Mg-ATP and Mg-ADP complexes, and the additional peaks in the electropherograms with poor reproducibility were attributed to dissociation of Mg-ATP and Mg-ADP during the CE separations without Mg^{2+} in the separation buffer [77].

Based on this result for PFK-1, the conditions for the bacterial holo-ACC enzyme assay were modified to include 2.0 mM Mg^{2+} in the separation buffer, and Figure 3.4 shows a resulting electropherogram. The separation buffer contained 5.0 mM sodium phosphate, 10.0 mM SDS, and 2.0 mM $MgCl_2$ at pH 7.50, while the sample buffer still contained 5.0 mM potassium phosphate, 5.0 mM $KHCO_3$ and 2.5 mM $MgCl_2$ at pH 7.50. The separation buffer and sample buffer differ because of the conflicting requirements for the separation and enzyme assay (sample buffer). Potassium in the sample buffer increases the enzyme activity but causes SDS to precipitate, so potassium phosphate was used only in the sample buffer. The $KHCO_3$ in the sample buffer provides bicarbonate and potassium for the reaction but would precipitate SDS in the separation buffer. The concentrations of individual solution components were also adjusted to try to keep the ionic strengths of the two solutions similar in order to reduce deleterious effects (focusing, defocusing, system peaks, etc.) [133, 134].

The addition of Mg^{2+} to the separation buffer improved the separation of ACC assay components compared to previous results (Figure 3.4 vs. Figure 3.3). Peak splitting of ADP and ATP was eliminated, similar to the findings of Malina et al. [77]. The later migrating ATP and ADP peaks disappear, including the peak overlapping with malonyl-CoA (Figure 3.3). The remaining Mg-ATP and Mg-ADP peaks migrating before acetyl-CoA are better resolved with Mg^{2+} in the separation buffer (Figure 3.4).

Based on dissociation constants for Mg^{2+} complexes with ADP and ATP of 0.30 mM and 0.019 mM [135], about 91% of ADP and 99% of ATP will exist as Mg-ADP^{-} and Mg-ATP^{2-} in the sample solution containing 3.0 mM $MgCl_2$, 50.0 µM ADP and 50.0 µM ATP. The migration of acetyl-CoA and malonyl-CoA are largely unaffected by the addition of Mg^{2+} to the separation buffer, indicating they are not complexed to Mg^{2+}.

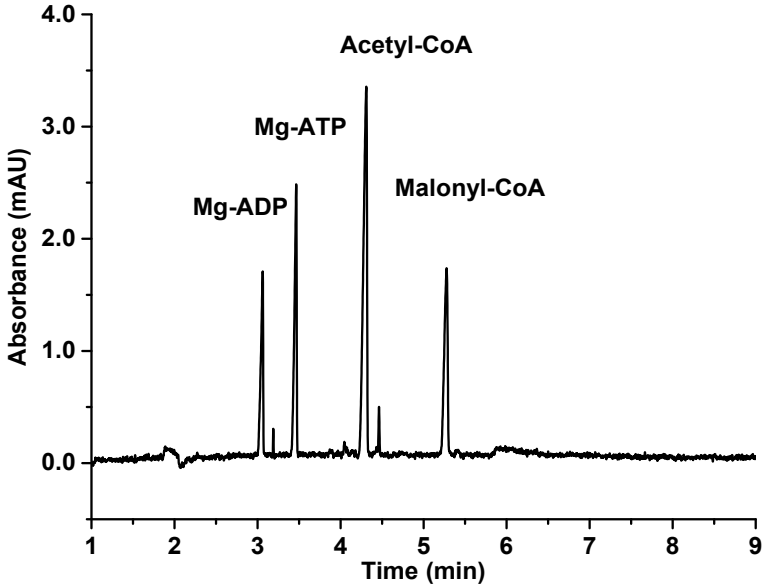

Figure 3.4. Electropherogram for the improved separation of holo-ACC assay components. The sample solution contained 50.0 µM ADP, 50.0 µM ATP, 100.0 µM acetyl-CoA, and 100.0 µM malonyl-CoA in a buffer containing 5.0 mM potassium phosphate, 2.5 mM $MgCl_2$, and 5.0 mM $KHCO_3$ at pH 7.50. The separation buffer was 5.0 mM sodium phosphate, 10.0 mM SDS, and 2.0 mM $MgCl_2$ at pH 7.50. The sample was injected hydrodynamically at 0.5 psi for 5.0 s and separated at 19.5 kV (505 V/cm) with a current of 19.5 µA.

The surfactant, SDS, frequently has been used in CE methods for separating ADP and ATP [49, 77, 130, 131], but removal of SDS from the separation buffer for ACC assays would reduce the mismatch of sample and separation buffers and avoid problems with SDS precipitation due to potassium in the reaction buffer. In an effort to eliminate SDS, a buffer containing 5.0 mM potassium phosphate, 5.0 mM $KHCO_3$, and 2.5 mM $MgCl_2$ at pH 7.50 was used as both separation and sample buffer for the

separation of Mg-ADP, Mg-ATP, acetyl-CoA, and malonyl-CoA as shown in Figure 3.5.

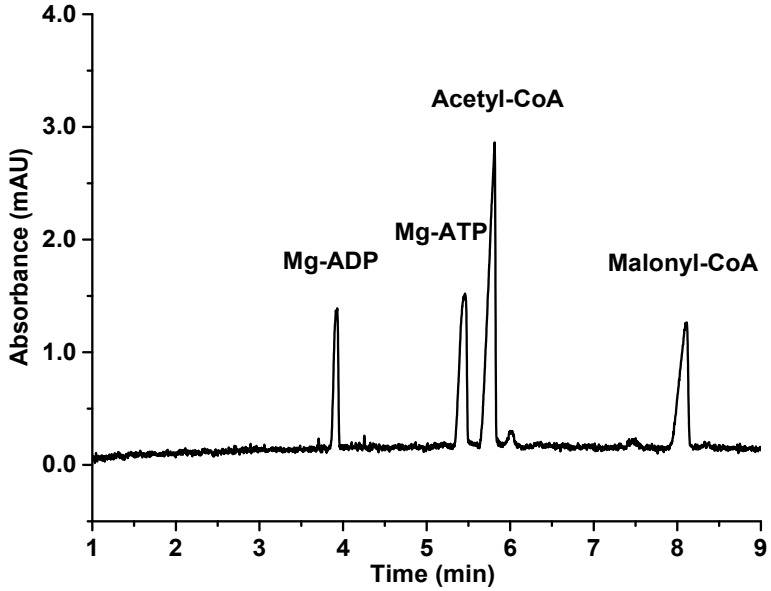

Figure 3.5. Electropherogram for the separation of ACC assay components without SDS. The sample solution contained 50.0 μM ADP, 50.0 μM ATP, 100.0 μM acetyl-CoA, 100.0 μM malonyl-CoA. The separation buffer and sample buffer both contained 5.0 mM potassium phosphate, 5.0 mM $KHCO_3$, and 2.5 mM $MgCl_2$ at pH 7.50. The sample was injected hydrodynamically at 0.5 psi for 5.0 s and then separated at 19.5 kV (505 V/cm) with a current of 19.8 μA.

The four compounds were baseline resolved, and the migration order of the four components did not change after eliminating SDS (Figure 3.5 vs Figure 3.4). SDS was not used in subsequent experiments.

3.3.2. Adaptation of the Separation for the Human ACC2 Assay

Bacterial holo-ACC and human ACC2 both catalyze the conversion of acetyl-CoA to malonyl-CoA as shown in Scheme 3.1. A CE-based assay for both enzymes requires the separation of Mg-ATP, Mg-ADP, acetyl-CoA, and malonyl-CoA; however, there are significant differences in the optimal reaction conditions for these two enzymes. Human ACC2 requires citrate as an enzyme activator with reported K_a values of 0.3-10.0 mM [30, 66, 136]. Therefore, the human ACC2 reaction solution

must contain ATP, acetyl-CoA, $KHCO_3$, $MgCl_2$, and citrate. Based on reported K_m values and concentrations of the substrates and cofactors used in previously reported human ACC assays, the concentrations used for the enzyme assay solution were 100.0 μM ATP, 50.0 μM acetyl-CoA, 3.0 mM $MgCl_2$, 2.5 mM $KHCO_3$, and 2.5 mM potassium citrate [30, 62, 65, 66, 136].

Solutions buffered with HEPES and Tris-HCl were evaluated for the separation of Mg-ADP, Mg-ATP, acetyl-CoA, and malonyl-CoA. Although phosphate buffer worked for the bacterial holo-ACC assay [49], the interaction of phosphate and Mg^{2+} has the potential to negatively impact assay reproducibility due to the low solubility products of Mg^{2+} with phosphate in aqueous solution [K_{sp} = 1.5×10^{-6} for $MgHPO_4\cdot3H_2O$, 2.0×10^{-24} for $Mg_3(PO_4)_2\cdot22H_2O$, and 5.2×10^{-24} for $Mg_3(PO_4)_2$] [137]. HEPES (pK_a 7.55) and Tris-HCl (pK_a 8.3) were tested as alternatives to phosphate for the ACC enzyme assay based on previous use [11, 30, 34, 62, 65, 66, 124, 136]. The buffering ranges of HEPES and Tris-HCl cover the pH values at which human ACC assays were performed (pH 7.5-8.0) [11, 30, 34, 62, 65, 66, 124]. Unlike phosphate, these two buffers do not bind to Mg^{2+} [138], which makes them ideal for the ACC assay.

The HEPES and Tris-HCl buffers contained 2.5 mM $KHCO_3$, 2.5 mM potassium citrate and 3.0 mM $MgCl_2$ at pH 7.50 with either 30.0 mM HEPES or 30.0 mM Tris-HCl. At a field strength of 505 V/cm, the electrophoretic currents in HEPES and Tris-HCl buffers were 27.4 μA and 49.6 μA, respectively, which makes HEPES-containing buffer less prone to deleterious Joule heating during electrophoresis.

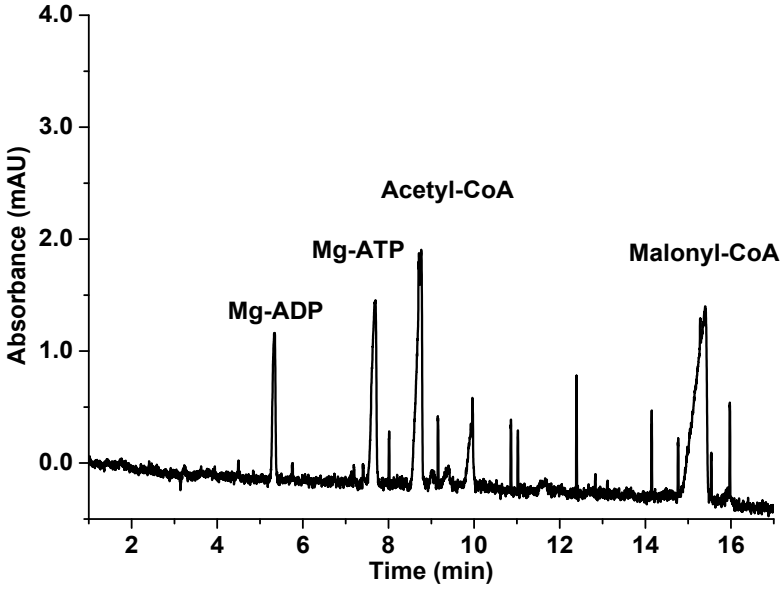

Figure 3.6. Electropherogram for the separation of human ACC2 assay components using a Tris buffer. The sample solution contained 50.0 µM ADP, 50.0 µM Mg-ATP, 100.0 µM acetyl-CoA, 100.0 µM malonyl-CoA. The separation buffer and sample buffer both contained 30.0 mM Tris-HCl, 3.0 mM $MgCl_2$, 2.5 mM $KHCO_3$, and 2.5 mM potassium citrate at pH 7.50. The sample was injected hydrodynamically at 0.5 psi for 5.0 s, then separated at 19.5 kV (505 V/cm) with a current of 49.6 µA.

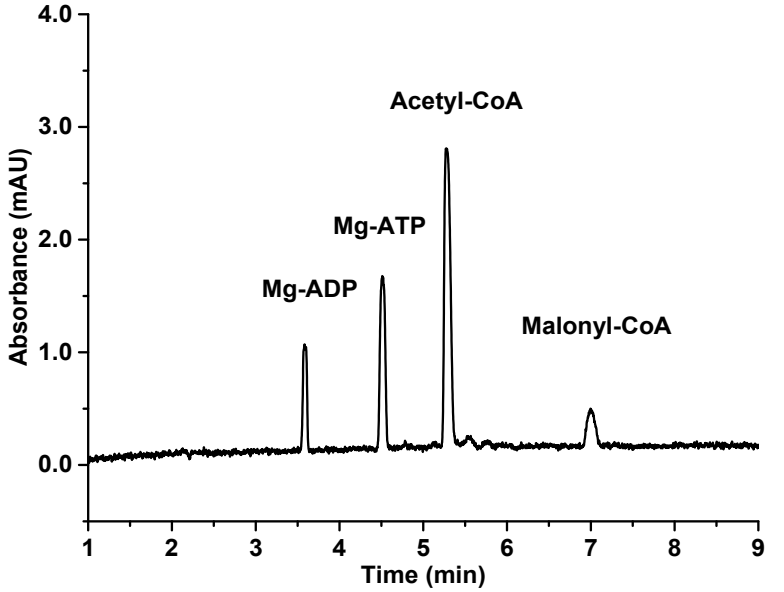

Figure 3.7**.** Electropherogram for the separation of human ACC2 assay components using a HEPES buffer. The sample solution contained 50.0 µM ADP, 50.0 µM Mg-ATP, 100.0 µM acetyl-CoA, 100.0 µM malonyl-CoA. The separation buffer and sample buffer both contained 30.0 mM HEPES, 3.0 mM $MgCl_2$, 2.5 mM $KHCO_3$, and 2.5 mM potassium citrate at pH 7.50. The sample was injected hydrodynamically at 0.5 psi for 5.0 s, then separated at 19.5 kV (505 V/cm) with a current of 27.4 µA.

Separation of assay components in both HEPES buffer and the Tris-HCl buffer resulted in well-separated peaks (Figure 3.7 and Figure 3.6), but the migration time of the last peak, malonyl-CoA, was more than twice as long for the Tris-HCl separation compared to the HEPES separation (15.2 min vs 7.0 min). The reproducibility of peak areas obtained using HEPES buffer is comparable to those obtained using phosphate buffers (Table 3.1). A buffer containing 30.0 mM HEPES, 2.5 mM $KHCO_3$, 2.5 mM potassium citrate, and 3.0 mM $MgCl_2$ at pH 7.50 was chosen as both the sample and separation buffer for further development and characterization of the human ACC2 assay.

Table 3.1. Relative standard deviation of Mg-ADP, Mg-ATP, acetyl-CoA, and malonyl-CoA peak areas with different separation buffers (N=3).

Separation Buffer (pH 7.50)	RSD (peak area), %			
	Mg-ADP	Mg-ATP	Acetyl-CoA	Malonyl-CoA
10.0 mM sodium phosphate, 20.0 mM SDS*	4.0	4.0	2.5	5.7
5.0 mM sodium phosphate, 10.0 mM SDS, 2.0 mM $MgCl_2$*	2.2	1.4	2.2	3.0
5.0 mM potassium phosphate, 5.0 mM $KHCO_3$, 2.5 mM $MgCl_2$	2.4	1.8	1.8	1.6
30.0 mM HEPES, 2.5 mM $KHCO_3$, 2.5 mM potassium citrate, 3.0 mM $MgCl_2$	1.3	1.8	1.3	2.2

*The sample buffers contained 5.0 mM potassium phosphate, 5.0 mM $KHCO_3$, and 2.5 mM $MgCl_2$ at pH 7.50. Otherwise, the separation and sample buffers were the same.

In addition to acetyl-CoA, ATP, Mg^{2+}, $KHCO_3$, citrate and HEPES, the reaction solution for the ACC2 assay will contain components from the enzyme storage solution. Testing the effect of these on the separation is essential. According to the product information provided by the manufacturer, human ACC2 is in a buffered aqueous solution containing Tris-HCl (pH 8.0), NaCl, 10-20% glycerol, and DTT, with

the possible presence of EDTA, KCl, imidazole, and TWEEN-20. The human ACC2 enzyme solution was added up to 10% v/v to the assay mixture.

A buffer solution consisting of 50 mM Tris-HCl, 275 mM NaCl, 10% glycerol, and 1.0 mM EDTA at pH 8.0 was prepared to mimic the ACC2 storage buffer and was used to test the effect of the enzyme storage buffer on the separation of human ACC2 assay components. The additional salts and glycerol in the enzyme storage buffer will result in a mismatch between the EOF of the separation buffer and the sample zone, which should reduce separation efficiency (broader peaks) [139]; however, with the simulated enzyme storage buffer added at 10% v/v to the assay solution to mimic assay conditions, the anionic assay components were still well resolved, and the separation efficiency was actually enhanced 1.2-3.2 fold (Table 3.2*).*

Table 3.2. Number of theoretical plates calculated for the separation of 50.0 µM ADP, 50.0 µM ATP, 40.0 µM acetyl-CoA, and 40.0 µM malonyl-CoA with and without simulated enzyme storage buffer added to the sample solution.

Analyte	Theoretical plates (x10^4 plates), N=3	
	0% simulated storage buffer	10% simulated storage buffer
ADP	2.20 ± 0.04	2.70 ± 0.15
ATP	1.80 ± 0.11	4.18 ± 0.05
Acetyl-CoA	1.96 ± 0.07	5.45 ± 0.03
Malonyl-CoA	1.76 ± 0.10	5.59 ± 0.50

Sample self-stacking or isotachophoresis could lead to the observed efficiency increases, but most examples of these in the literature include suppression of EOF or reversed polarity for CE [133, 140, 141]. Wei et al. reported increased separation efficiency for nucleic acids and FITC in presence of glycerol and high salt concentration without polarity reversal or EOF suppression, similar to our conditions with the enzyme storage buffer [142]. The authors did not provide a convincing explanation for their observations, but they are consistent with our results.

Quantification of the assay substrates and products was not significantly impacted by the enzyme storage buffer. Table 3.3 summarizes the calibration curves obtained for Mg-ADP, Mg-ATP, acetyl-CoA, and malonyl-CoA with and without 7% simulated enzyme storage buffer. In all cases, the R^2 values for a linear fit of the data were greater than 0.99. Analysis of the slopes confirmed (95% confidence) that the slopes were the same with and without the simulated enzyme storage buffer [143].

Table 3.3. Calibration curves of ADP, ATP, acetyl-CoA, and malonyl-CoA without and with 7% simulated enzyme storage buffer. The concentration range for the calibration curves is from 2.5 to 150.0 µM.

Compound	Without simulated storage buffer	With simulated 7% storage buffer
ADP	y = 69.6x - 148.4 R^2 = 0.9986	y = 71.2x - 165.9 R^2 = 0.9944
ATP	y = 156.5x - 153.4 R^2 = 0.9992	y = 153.5x - 176.8 R^2 = 0.9946
Acetyl-CoA	y = 132.1x - 191.5 R^2 = 0.9993	y = 128.7x - 340.4 R^2 = 0.9955
Malonyl-CoA	y = 19.1x - 60.1 R^2 = 0.9986	y = 20.0x - 175.5 R^2 = 0.9944

3.3.3. CE Assay for Human ACC2

Electropherograms for an assay of human ACC2 using the HEPES separation buffer are presented in Figure 3.8. Figure 3.8A is an electropherogram before the addition of enzyme, and peaks are observed for 100.0 µM of Mg-ATP and 50.0 µM acetyl-CoA. Figure 3.8B shows the separation of reaction components 18 min after adding 7.0 µL human ACC2 to the total volume of 100.0 µL (final human ACC2 concentration of 25 nM). As expected, two product peaks (Mg-ADP and malonyl-CoA) were observed while the peak areas of Mg-ATP and acetyl-CoA decreased.

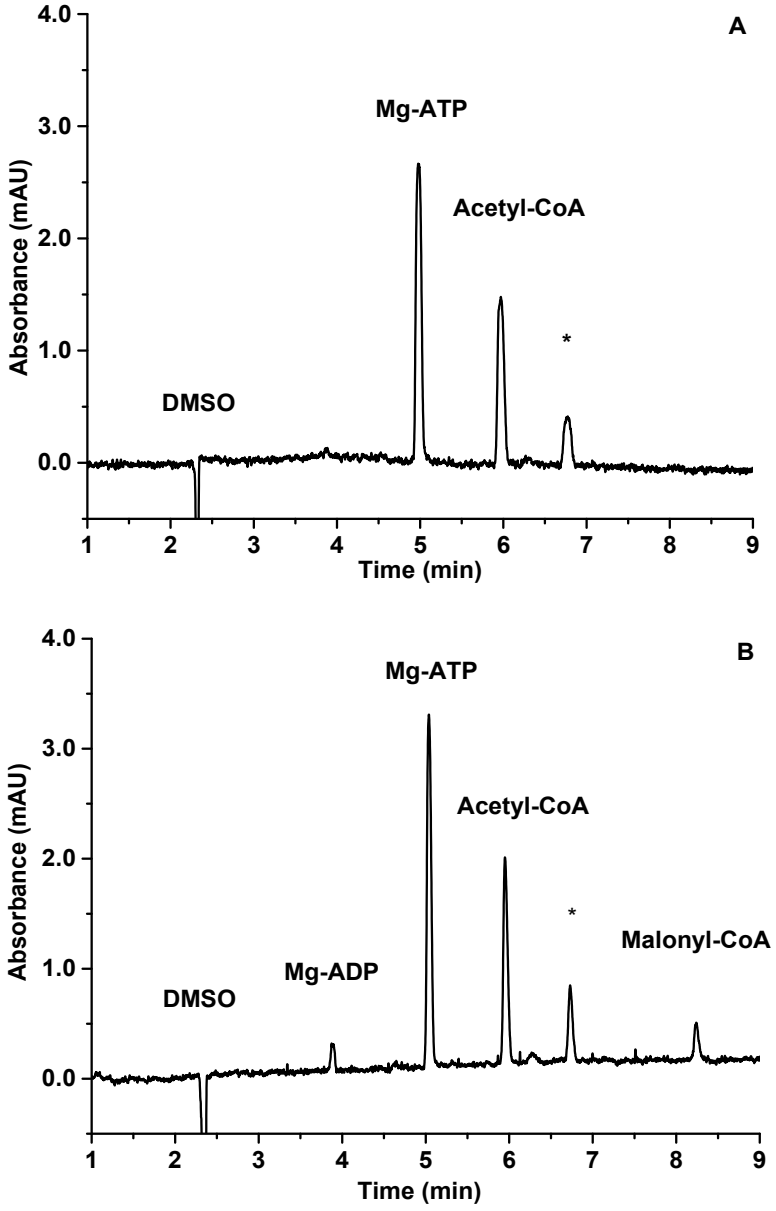

Figure 3.8. Electropherogram for human ACC2 assay.(A) The reaction mixture contained 100.0 μM ATP, 50.0 μM acetyl-CoA, and 1.0% DMSO prior to the addition of enzyme. (B) The reaction mixture at 18 min after the addition of 25 nM human ACC2. Other conditions are the same as in Figure 3.7.

It is interesting to note that the separation efficiency of Mg-ATP and acetyl-CoA in Figure 3.8B increased by 1.8 and 2.3 fold, respectively, relative to the separation in Figure 3.8A. This is consistent with our results with the simulated enzyme buffer (Table 3.2). The peak labeled with an asterisk at 6.9 min is an unidentified compound likely

associated with the decomposition of acetyl-CoA. A control experiment showed that this peak is not CoA, and more detail about our efforts to understand this peak are included in Figure 3.9. The unidentified peak could be minimized by freshly preparing acetyl-CoA solutions, and it did not interfere with the assay.

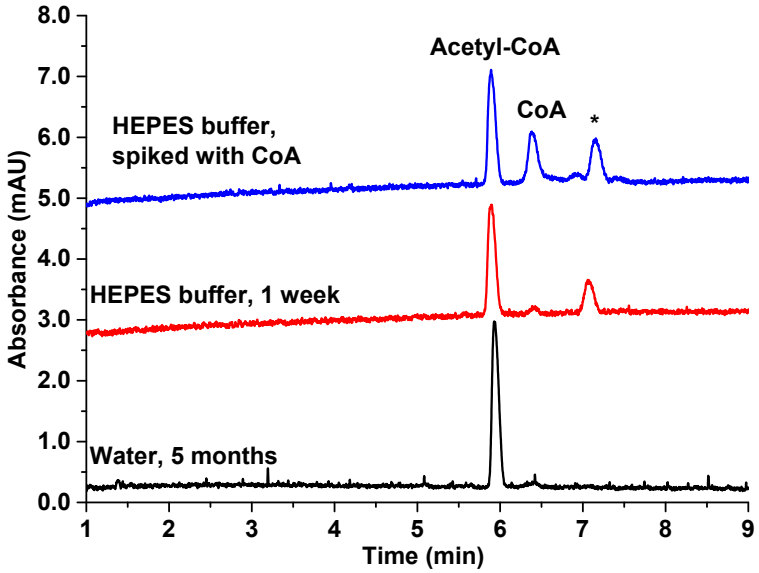

Figure 3.9. Electropherograms for separation of acetyl-CoA solutions prepared and stored in water for 5 months (blue line), in a buffer containing 30.0 mM HEPES, 3.0 mM $MgCl_2$, 2.5 mM $KHCO_3$, and 2.5 mM potassium citrate for 1 week (black line), and in HEPES-containing buffer for 1 week, spiked with 100.0 μM CoA (red line). The peak denoted with an asterisk (*) indicates the unidentified impurity or degradation product of acetyl-CoA.

DMSO is commonly used to solubilize enzyme inhibitors before dilution in aqueous solution, and it was important to understand the impact of DMSO on human ACC2 activity. Like other organic solvents, DMSO can alter enzymatic reactions by changing enzyme conformations or interacting with substrates, products, and co-enzymes [144]. The effect of DMSO on ACC2 activity was examined by adding DMSO to the reaction solution at final concentrations of 0.0-3.0%. Reaction progress curves for the human ACC2-catalyzed reaction at different DMSO concentrations are presented in Figure 3.10.

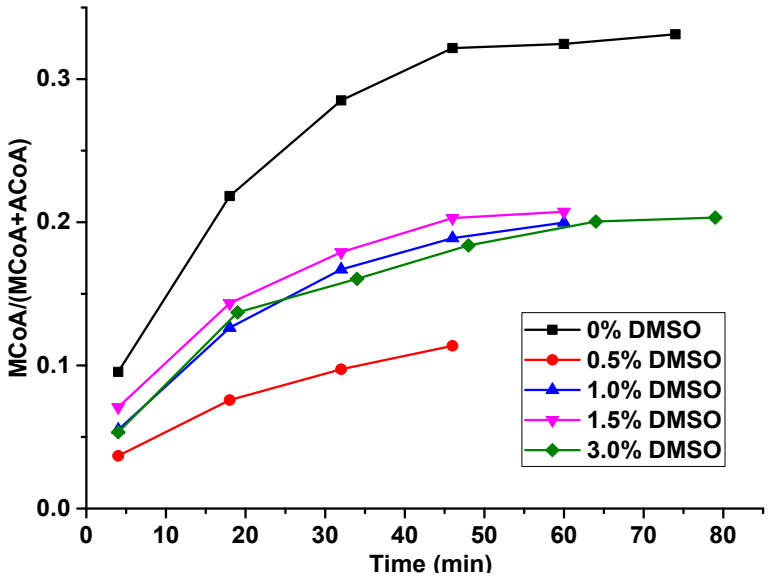

Figure 3.10. Progression curve showing the dependence of malonyl-CoA production on the concentration of DMSO at reaction time up to 79 min (0% DMSO, 3.0% DMSO), 60 min (1.0% DMSO, 1.5% DMSO), and 46 min (0.5% DMSO). The reaction mixtures contained 100 µM ATP, 50 µM acetyl-CoA, 25 nM human ACC2, and DMSO at concentrations from 0.0 - 3.0% v/v. The separation buffer and sample buffer both contained 30.0 mM HEPES, 3.0 mM $MgCl_2$, 2.5 mM $KHCO_3$, and 2.5 mM potassium citrate at pH 7.50. The samples were injected hydrodynamically at 0.5 psi for 5.0 s, then separated at 19.5 kV (505 $V.cm^{-1}$) with a current of 27.4 µA.

Enzyme activity was calculated as the ratio of malonyl-CoA concentration to the total concentration of malonyl-CoA and acetyl-CoA. This normalization enhances the precision of CE-based enzyme assay, reducing the effects of inconsistencies in sample injection and separation [77]. Human ACC2 exhibited the highest activity in the absence of DMSO. The enzyme activity dropped 3 fold at 0.5% DMSO but only 1.5 fold at 1.0-3.0% DMSO. A DMSO concentration of 1.0% was chosen for inhibition experiments to keep the organic solvent content as low as possible while obtaining adequate enzyme activity.

3.3.4. Inhibition of Human ACC2

A known inhibitor of human ACC2, CP-640186 (Figure 3.1), was used to evaluate the applicability of our CE assay to detect ACC2 inhibition. CP-640186 was

tested at 250 μM, well above its reported IC_{50} value of 61 nM [34]. Figure 3.11 shows an electropherogram for an injection 18 min after the addition of 25 nM human ACC2 to a reaction mixture containing 250 μM CP-640186, 100.0 μM Mg-ATP, and 50.0 μM acetyl-CoA.

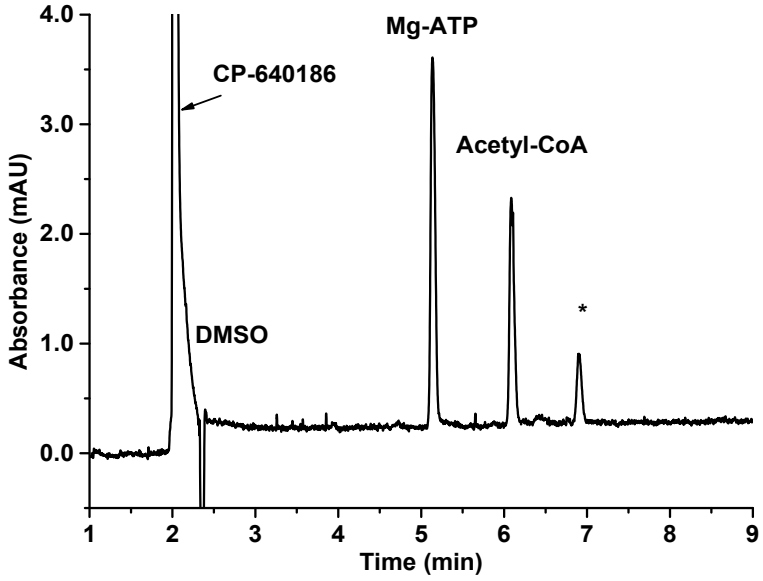

Figure 3.11. Electropherogram for inhibition of human ACC2. The sample solution contained 100.0 μM ATP, 50.0 μM acetyl-CoA, 1.0% DMSO, 250 μM CP-640186, and 25.2 nM human ACC2. Other conditions are the same as in Figure 3.7.

In the presence of the inhibitor, peaks for Mg-ADP and malonyl-CoA were not detected, indicating that CP-640186 fully inhibited human ACC2 at this concentration. It is important to note that CP-640186 strongly absorbs at 256 nm (Figure 3.2). As shown in Figure 3.11, an extra peak for CP-640186 was detected at 2.0 min in addition to peaks of DMSO (negative), Mg-ATP, and acetyl-CoA. In our CE assay, all the assay components were separated prior to UV detection at 256 nm, which eliminated spectral interference caused by the inhibitor, a problem common for spectrophotometric assays.

3.4. Conclusion

This paper demonstrated a simple, direct, off-column CE-based enzyme assay developed to study activity and inhibition of human ACC2. This CE-based assay enables the measurement of enzyme activity and screening of inhibitors by simultaneously monitoring the depletion of Mg-ATP and acetyl-CoA accompanying with the formation of Mg-ADP and malonyl-CoA. All the assay components and CP-640186 were separated in well-resolved peaks, making spectral interference, a common issue with spectrophotometric assays, unlikely when screening for inhibitors.

A previous assay for bacterial ACC served as the foundation for this work, and significant improvements were made for the ACC2 assay. Reproducibility problems associated with dissociation of Mg-ADP and Mg-ATP when migrating in separation buffer not containing Mg^{2+} were also addressed by adding Mg^{2+} to the separation buffer. SDS was eliminated from the separation buffer and the potential for problematic interactions of phosphate with the Mg^{2+} in the separation buffer was eliminated by switching to a HEPES buffer. These improvements to the separation are also applicable to the bacterial ACC assay and other CE enzyme assays based on the separation of nucleotides.

This optimized ACC2 assay will be useful for screening of potential inhibitors of human ACC2, which is a starting point to develop new anti-cancer or anti-obesity drugs. Because the two isoforms of human ACC catalyze the same reaction, we expect the CE assay for human ACC2 to be applicable for human ACC1 although further experiments will be required to confirm this.

CHAPTER 4. QUANTITATIVE COMPARISON OF A LIGHT-EMITTING DIODE AND LASER FOR FLUORESCENCE DETECTION WITH CAPILLARY ELECTROPHORESIS

4.1. Introduction

Capillary electrophoresis (CE) has developed into a powerful and versatile tool for bioanalytical separations. While the small scale of CE is critical to some of its main advantages relative to other analytical separation techniques (small sample volumes, high efficiency and speed), sensitive detection for CE has been a related challenge since the technique's emergence in the 1980's. Capillary electrophoretic separation performed in microchips, also known as microchip electrophoresis (ME), offers additional advantages compared to CE (smaller scale, speed, sample handling), but detection for ME is even more challenging than for CE due to small channel dimensions. Fluorescence detection is, to date, the second most common detection method for CE and the dominant detection method for ME [71, 145-147]. Although UV-Vis absorption detection is a more universal a detection method compared to fluorescence, for CE and ME, fluorescence detection is better able to overcome the associated short optical path lengths for detection at low concentrations, providing the LOD up to 1000 fold lower than absorbance [145-147]. Laser-induced fluorescence (LIF) detection was introduced early in the development of CE [148, 149] and was the first detection method used for ME [150]. Detection of just a few molecules and even single molecules was later demonstrated using CE-LIF and ME-LIF [72, 73, 151, 152].

Lasers have been used extensively as excitation sources for fluorescence detection with CE and ME because they are monochromatic, highly collimated, and powerful. However, drawbacks of lasers can include high cost, high power consumption, bulky cooling systems, and short lifetimes (depending on the type of laser and wavelength). Recently, the drive towards light sources of lower cost, lower

power consumption, longer lifetime, higher stability and easier operation has led scientists to light-emitting diodes (LEDs). Relative to lasers, commercially available LEDs are cheaper, easier to use, and consume less power while functioning without the need of bulky cooling systems. In addition, the LEDs generate continuous emission, commonly of 30 nm full width at half maximum (FWHM), which are advantageous for excitation at a wide range of wavelengths.

Since the 1990's, LEDs have been explored as alternative excitation sources to lasers for fluorescence detection in CE and ME with applications in pharmaceutical studies, including detection of amino acids or DNA analysis [74] [153-156]. The LODs for the fluorescence detection in CE have been enhanced by modification of the detectors or by using spectral filtering [153, 154, 157]. Bruno et al. [153] designed a pigtail detector coupled to a green LED (λ_{max} = 560 nm) for capillary electrophoretic separation with LED-induced fluorescence (LEDIF) detection of rhodamine B, resulting in an LOD of 10^{-7} M. In another study by Dasgupta et al. [154], a capillary was used as the liquid core waveguide detection cell, which was coupled with two blue LEDs (λ_{max} = 470 nm and λ_{max} = 495 nm) for the LEDIF detection of fluorescein with an estimated LOD of 8.0×10^{-9} M. In a study by Uchiyama et al., a blue LED (λ_{max} = 476 nm) was used as the excitation source for the LEDIF detection of FITC-labeled amino acids in microfluidic electrophoresis, resulting in LODs of 160 µM for valine and 90 µM for phenylalanine [156]. Alternatively, a miniaturized version of liquid core waveguide-capillary electrophoresis system was developed, using blue LEDs (λ_{max} = 478 nm) as the excitation source for fluorescence detection of FITC-labeled amino acids [155]. This set up allowed for the detection of FITC-labeled phenylalanine at the LOD of 1.9 µM, which was 47 fold lower compared to the study by Uchiyama et al. [155, 156]. In addition to the modified detector, the optimization of spectral filtering

also enhanced fluorescence detection in CE-LEDIF. According to de Jong et al., when using the 467 nm LED with a 470 nm band pass filter, the S/N for riboflavin was improved by a factor of 70. Although there has been success with LEDs for fluorescence detection, the low LODs obtained with CE and ME-LIF have not been matched.

LEDs have been referred to as the sources of high stability and low noise [158-160]. However, the data on stability and noise of LEDs is very limited. Previously, LEDs were compared to lasers as excitation sources for fluorescence detection of labeled amino acids and antibodies in CE [159, 160]. Rodat-Boutonnet et al. reported the separation of IgG labelled with three fluorophores (naphthalene-2,3-dialdehyde, 3-(2-furoyl)-quinoline-2-carboxaldehyde, and 5-carboxytetramethylrhodamine succinimidyl ester) using SDS capillary gel electrophoresis with fluorescence detection [159]. Different LEDs (450-nm, 480-nm, and 530-nm LEDs) and lasers (410-nm, 488-nm, and 532-nm laser diodes) served as excitation sources and were compared quantitatively based on the S/Ns. It was demonstrated that the LEDs resulted in the same or higher S/Ns than the lasers. However, the LEDs and lasers were not employed at the same output power, with the LED intensities at 2-6 times higher than that of the lasers. Also, because the output powers were not optimized, it was not clear how the S/Ns were affected by LED and laser output powers as photobleaching and ground-state depletion occur at high excitation intensity [161]. The baselines of SDS capillary gel electrophoresis with the 480-nm LED and 488-nm laser were also compared, and the LEDIF technique was indicated to provide slightly higher low-frequency noise and lower high-frequency noise than the LIF. However, while noise depends on the source power, it was not clear if the LED and laser were compared at the same output power. In another work by Enzonga and coworkers [160], the amino

acids labeled with FITC were separated by CE and detected by LIF and LEDIF, using a 488-nm diode laser and a 470-nm LED as excitation sources. The LEDIF detection resulted in higher S/Ns (1.7-2.5-fold) and lower LODs (1.9-2.5-fold) than the LIF. However, the LED output power was reported to be 150 mW while information on the diode laser output power was missing. Therefore, a quantitative study that clearly establishes the relative performance of LEDs and lasers as excitation sources is still lacking.

In this work, a 470-nm LED and a tunable argon ion laser were quantitatively compared as excitation sources for fluorescence detection of three common, visible fluorophores with a commercial CE instrument. The S/Ns and LODs were compared in order to evaluate the relative performance of the two sources. For the comparison of the LED and laser, all experimental conditions such as separation conditions, fluorophore concentrations, output power (measured at the output end of the optical fiber), and optical filters were identical. The LED and laser were coupled to a 400 μm optical fiber for excitation, so the lack of collimation of the LED source was not an issue for the comparison. The overall impact of source emission spectra, fluorophore excitation and emission spectra, and optical filters on fluorescence detection were all considered.

4.2. Materials and Methods

4.2.1. Chemicals

Boric acid and sodium hydroxide were purchased from Fisher (Fair Lawn, NJ, USA). 5-carboxyfluorescein (5-FAM) were obtained from Fluka (Steinheim, Slovakia). Fluorescein, rhodamine 123, and ethanol were purchased from Sigma (St. Louis, MO, USA). Borate buffer (50.0 mM, pH 9.00) was prepared from boric acid and sodium hydroxide in 18 MΩ deionized water (Barnstead Nanopure, ThermoFisher, Marietta,

Ohio, USA). Fluorescein and 5-FAM solutions were prepared in borate buffer. A stock solution of rhodamine 123 was prepared in ethanol and diluted in borate buffer. All solutions were filtered through 0.2-μm membranes (Whatman, Hilsboro, OR, USA) before use.

4.2.2. Instrumentation

All separations were performed using a P/ACE MDQ Molecular Characterization System (Beckman Coulter, Fullerton, CA, USA) equipped with a LIF detector module utilizing a 520/20 nm emission filter and a 488-nm notch filter. Data were acquired with 32 Karat software version 7.0 (Beckman Coulter, Brea, CA, USA) and analyzed using Microsoft Excel (Microsoft Corporation, Redmond, WA, USA). Capillary electrophoretic separations were performed in fused-silica capillaries (Polymicro Technologies, Phoenix, Arizona, USA) of 49 μm ID and 362 μm OD with a total length of 38.5 cm and an effective length of 28.5 cm. A blue fiber-coupled high-power LED (M470F1, Thorlabs, Newton, NJ, USA) with nominal wavelength of 470 nm and adjustable power output controlled by a T-cube LED driver (Thorlabs, Newton, NJ, USA) was used as an excitation source for CE-LEDIF. An air-cooled argon ion laser (43 series ion laser, Melles Griot, Carlsbad, CA, USA) with tunable wavelengths was used for CE-LIF detection. An optical fiber with a core diameter of 400 μm and a numerical aperture of 0.29 (Ocean Optics, Dunedin, FL, USA) was coupled to the 470-nm LED by an SMA-905 connector and to the laser by focusing laser beam directly to one end of the optical fiber. The output power of the LED and laser lines were measured at the other end of the optical fiber, which is coupled to the LIF detector module, using a broadband power/energy meter (13PEM001, Melles Griot, Carlsbad, CA, USA). LED emission spectral characterization at different output powers was performed using an Avantes-2408 spectrometer (Broomfield, CO, USA). A UV-Vis-

NIR scanning spectrophotometer (UV-3101PC, Shimadzu, Kyoto, Japan) was used to characterize the emission and notch filters. The excitation and emission spectra of the fluorophores were collected using a Varian Cary Eclipse fluorescence spectrophotometer (Victoria, Australia).

4.2.3. CE conditions

The capillary was conditioned daily by rinsing at 20.0 psi with 1.0 M NaOH for 10 min, deionized water for 10 min, and borate buffer for 10 min. Borate buffer (50.0 mM, pH 9.00) was used as both the sample buffer and separation buffer in this experiment. Between runs, the capillary was rinsed with borate buffer for 0.5 min at 20.0 psi. The samples were introduced into the capillary by hydrodynamic injection at 1.0 psi for 10.0 s and separated at 30.0 kV (779 V/cm).

4.3. Results and Discussion

4.3.1. Separation of Fluorophores

Three fluorophores were chosen for this study: rhodamine 123, fluorescein, and 5-FAM. The structures of three fluorophores are shown in Figure 4.1.

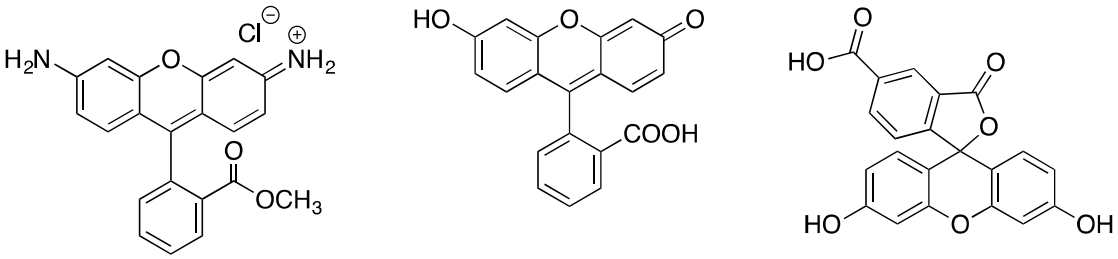

Rhodamine 123 Fluorescein 5-FAM

Figure 4.1. Structures of rhodamine 123, fluorescein, and 5-FAM

Normalized excitation and emission spectra collected for 1.0 μM rhodamine 123, fluorescein, and 5-FAM in 50.0 mM borate buffer (pH 9.00) are presented in Figure 4.2.

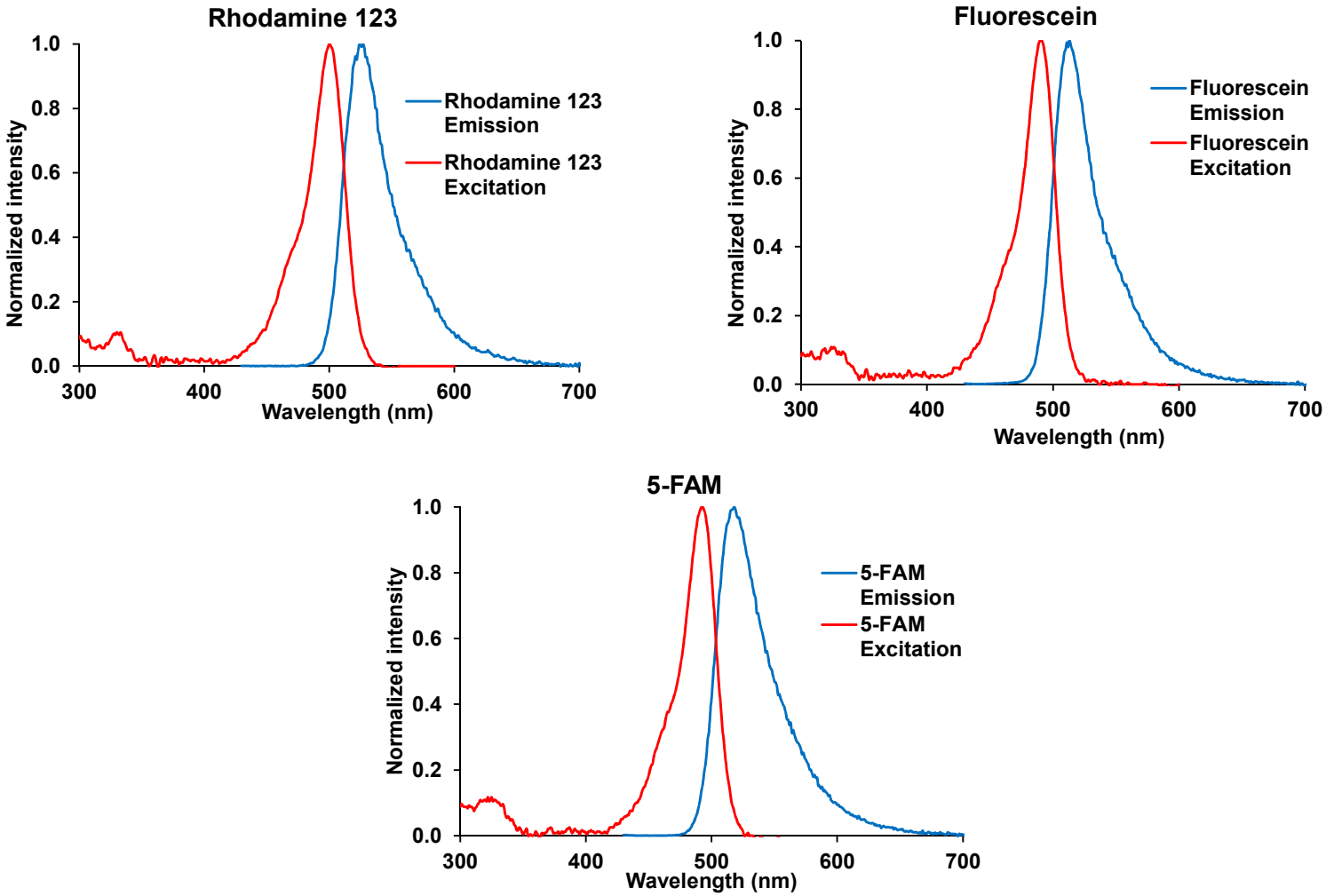

Figure 4.2. Excitation and emission spectra of rhodamine 123, fluorescein, and 5-FAM

The LED emission spectra and the laser lines at 457 nm, 465 nm, 472 nm, 476 nm, and 488 nm all overlap with the excitation spectra of the fluorophores, which enables the comparison of the LED and laser as the excitation sources for fluorescence detection of the rhodamine 123, fluorescein, and 5-FAM.

Rhodamine 123, a fluorescent cationic dye, has been used for biomedical applications including *in vitro* drug transport assays, and is a product of the reaction between dihydrorhodamine-123 and reactive oxygen species [162, 163]. Fluorescein, an anionic fluorophore, and its derivatives have been widely used to label amino acids, proteins and peptides [72, 146, 164-166]. A derivative of fluorescein, 5-FAM, which has one carboxyl group attached to fluorescein, can be used to label proteins, peptides, and nucleotides through the reaction of the carboxyl group with the primary amines [164]. In aqueous solution pH 9.00, the phenol and carboxylic acid functional groups in fluorescein and 5-FAM are ionized, and these compounds exist as anions.

Electropherograms showing the separation of the three fluorophores are presented in Figure 4.3. In this study, a buffer solution of 50.0 mM borate at pH 9.00 was used as both the sample and separation buffer. When the sample was introduced to the capillary in a longer hydrodynamic injection (1.0 psi for 10.0 s), wide, flat-topped peaks were obtained (Figure 4.3 A). The precision of the S/N ratio measured for these peaks is therefore improved without significantly compromising the separation. A short injection of the sample (0.5 psi for 5.0 s) resulted in sharp peaks of the fluorophores, as shown in Figure 4.3 B. Hydrodynamic injections at 1.0 psi for 10.0 s were used for all subsequent experiments.

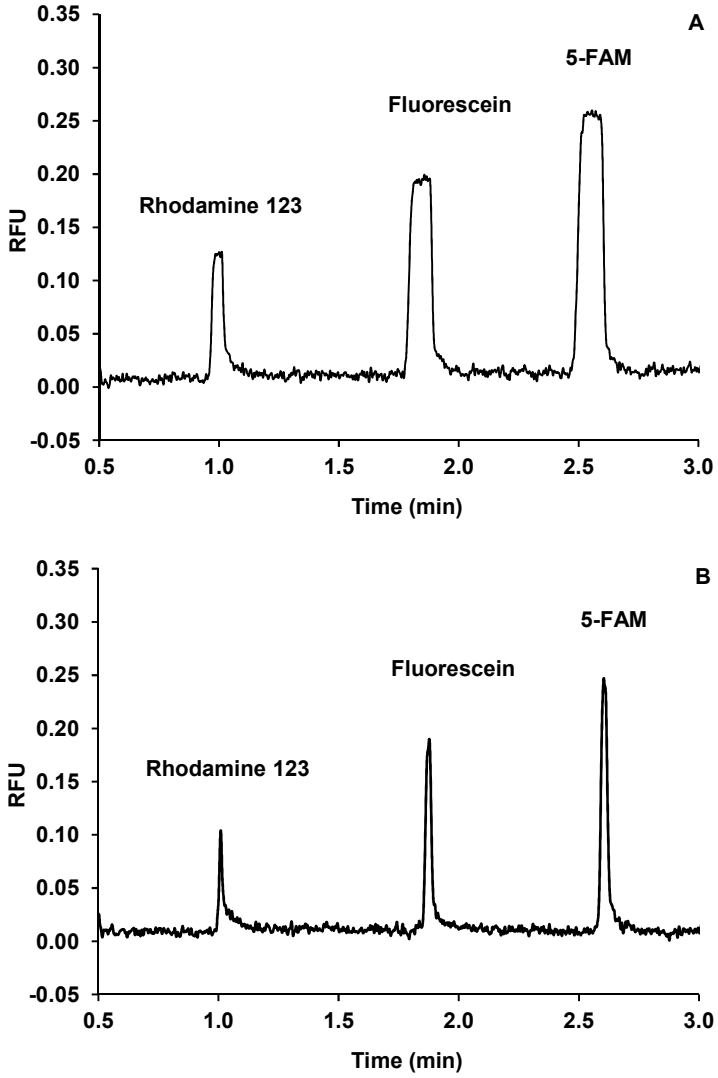

Figure 4.3. Electropherograms of 50 nM rhodamine 123, 50 nM fluorescein, and 50 nM 5-FAM with excitation by the LED at 5.5 mW. Injection conditions: A) 1.0 psi, 10.0 s, and B) 0.5 psi, 5.0 s.

4.3.2. Comparison of S/N for Different Light Sources

The S/N values for detection of the three fluorophores were compared using the LED and laser excitation at the same output power with identical separation conditions, the same commercial CE instrument, and the same fluorescence detection module. Figure 4.4 shows the S/N calculated for the three fluorophores using the 470-nm LED as well as the 465-nm, 472-nm and 488-nm lines from a tunable air-cooled argon ion laser as the excitation sources.

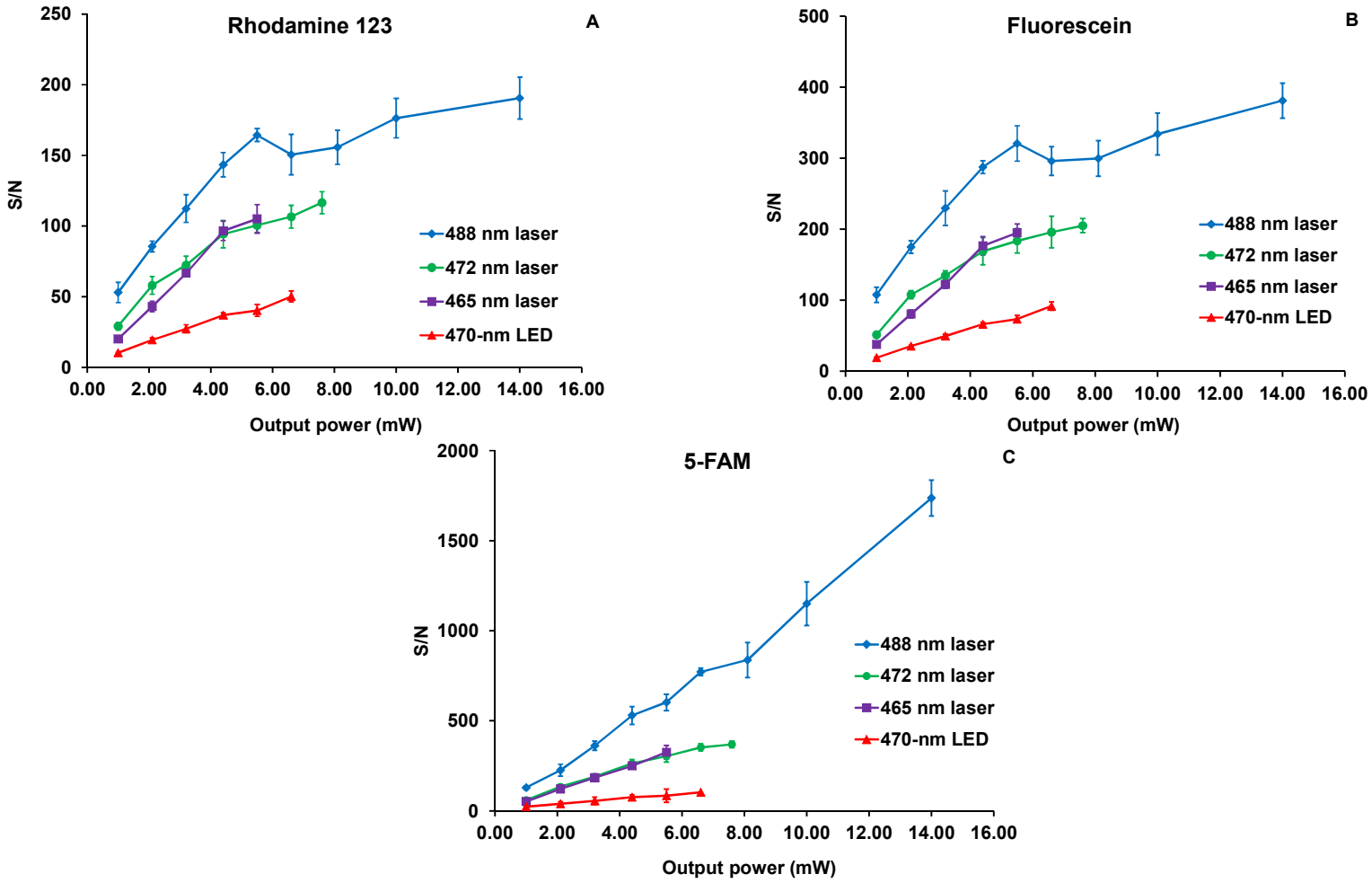

Figure 4.4. S/N for detection of 50.0 nM rhodamine 123, 50.0 nM fluorescein, and 50.0 nM 5-FAM using the 470-nm LED, 465-nm, 472-nm and 488-nm laser lines as excitation sources. The error bars present the standard deviations of the S/Ns, each measured in triplicates.

The excitation output power was increased from 1.0 mW in 1-mW increments up to the maximum output available for each source, except for the 488-nm laser line, which was increased up to 14.0 mW. Generally, the S/N increased as the output power of each source increased. The plots for rhodamine 123 and fluorescein 123 show evidence of reaching plateaus starting at 5-6 mW, which is likely due to a combination of singlet saturation and photobleaching [161].

For all three compounds excited by the LED and laser lines with the same output power at the fluorescence detector, the raw S/N values were the highest for the 488-nm laser line, followed by the 472-nm and 465-nm laser lines, and the lowest S/N values were obtained with the 470-nm LED. Although this simple comparison was performed with the same fluorophores, instrument and source intensities, it does not account for differences in the emission spectra of the 470-nm LED and laser lines relative to the excitation spectra of the three fluorophores and the optical filters used in the fluorescence detector. Consideration of these issues will provide a more complete view of the relative performance of these sources [71, 149, 157, 161].

4.3.3. Characterization of the LED

Unlike lasers, commercial LED sources of the same type do not have identical emission wavelengths, and their emission spectra will shift as the output power is changed by adjusting the forward current [167]. Typically LEDs are sold with only a nominal peak emission wavelength listed as was the case with the LED used in this work. In order to investigate the potential impact of the LED output power on CE detection, emission spectra of the LED (nominally 470 nm) were collected at different LED output intensities. The output power of the 470-nm LED was measured at the outlet of the optical fiber as in the CE experiments. Figure 4.5 presents the output spectra for the LED as the power was increased. In Figure 4.5A, the spectra were

normalized by total output power from 300 to 600 nm (areas under each spectrum are identical). Alternatively, the spectra can be normalized by peak output power (Figure 4.5B). As the current was increased from 150 mA up to 1000 mA, the corresponding LED output power increased from 1.0 mW up to 6.6 mW and the peak wavelength shifted from 468 nm to 465 nm, with the full width at half maximum (FWHM) increasing from 19 to 25 nm. The blue shift and spectral broadening of the LED emission due to increasing forward current was previously reported and attributed to the band-filling effect of the localized energy states and the screening of the piezoelectric field in the strained multiple quantum well region [167].

Although broad-band emissions of LEDs are advantageous for excitation of fluorophores at a wide range of wavelengths, polychromaticity is a pernicious factor in fluorescence detection. The commercial LED used in this study has 19-25 nm FWHM while the Stokes' shifts for rhodamine 123, fluorescein, and 5-FAM are 21 nm, 21 nm, and 25 nm, respectively. Since the LED bandwidth is comparable to the Stokes' shift for the fluorophores, it is feasible for the LED emission to overlap with the emission filter [157], which scarcely occurs when a laser is used as an excitation source.

The long wavelength component of the LED, that may coincide with the fluorescence emission contributes to the background signal, and consequently degrades the signal-to-noise ratio (S/N) or limit of detection (LOD) measurements [157]. Emission and notch filters have been used simultaneously to address this issue by removing unwanted scattered light at the detection wavelength from the LEDs and allowing the emitted signal to go through. According to de Jong et al., when using proper spectral filters, the S/N for riboflavin was improved by 70 times [157].

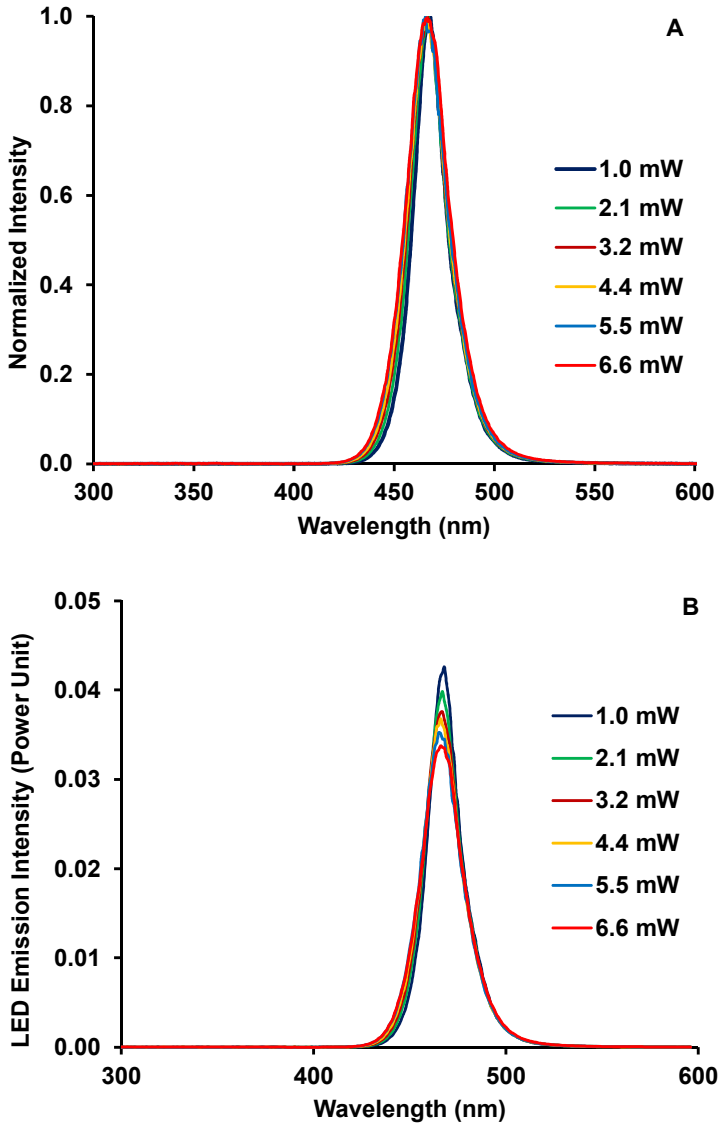

Figure 4.5. Normalized emission spectra of the 470-nm LED at output power from 1.0 mW to 6.6 mW. The spectra were normalized by peak output power (A) and total output power (B).

Figure 4.6 presents the transmission spectra of the 488 nm notch filter and the 520/20 nm notch filter in this study. In this study, as the power of the LED was increased from 1.0 mW to 6.6 mW, the tail of the LED (from 500 nm to 596 nm) increased from 2.5% to 2.9% of the total LED power. Even with the use of the filters, 8.8%-9.4% of the tail (0.22%-0.26% of the total LED power) that coincides with the fluorescence detection wavelength still passed through these filters, giving rise to

significant background signal. Such an issue does not apply for the laser lines which are effectively blocked by the filters. As a consequence, the S/N values for the fluorescence detection of the fluorophores was lower when using the LED as the excitation source. Figure 4.7 shows the emission spectra of the LED and laser lines along with transmission profiles of the 488-nm notch filter and 520/20 nm emission filter.

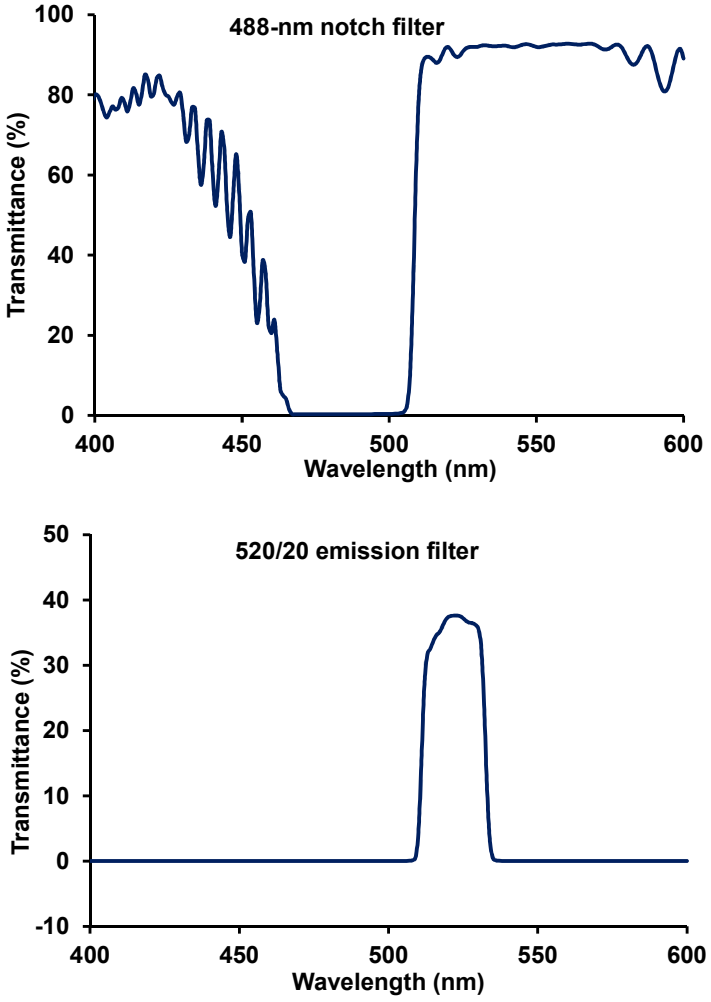

Figure 4.6. Spectra of a 488-nm notch filter and a 520/20 emission filter

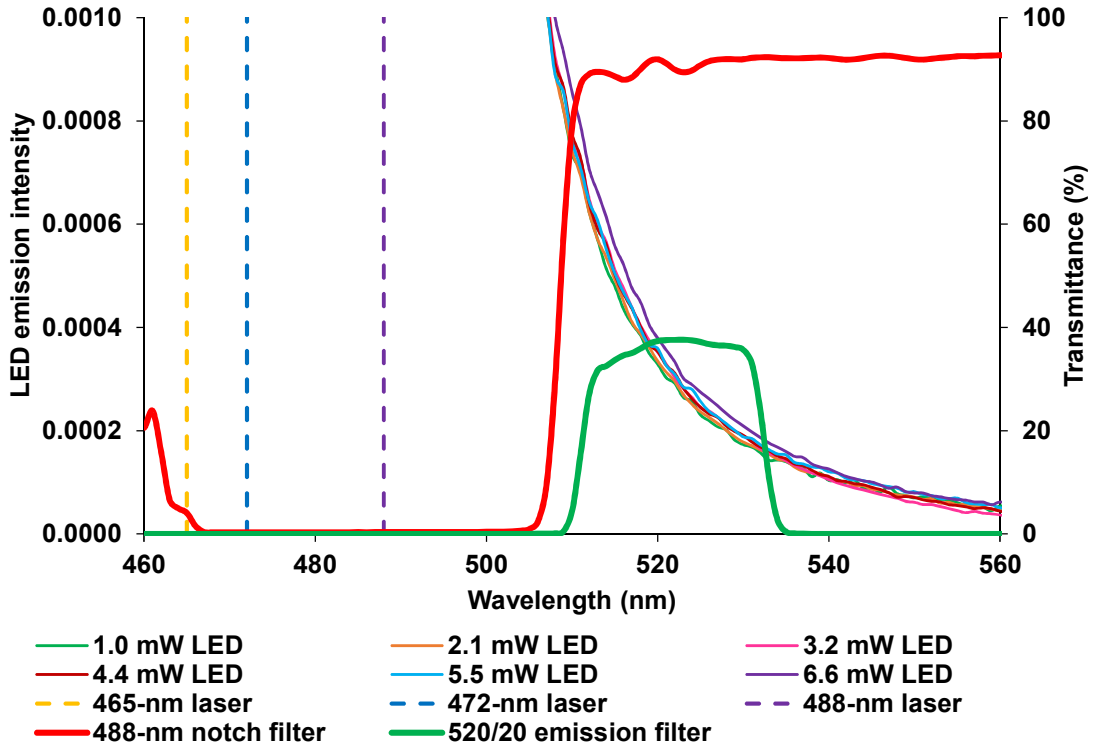

Figure 4.7. Emission spectra of the LED and laser lines, and transmittance profiles of a 488-nm notch filter and a 520/20 nm emission filter.

4.3.4. Comparison of S/N Adjusted for Light Source-Fluorophore Spectral Overlap

The aim of the experiments presented in Figure 4.4 was to directly compare the S/N values that could be obtained with LEDIF and LIF under separation and detection conditions that were as experimentally similar as possible. Differences in spectral overlap between the emission spectra of the sources and the excitation spectra of the fluorophores can have a significant impact on the S/N. This is particularly true for the LED which has a very broad spectral output (Figure 4.5) compared to the laser lines. To quantitatively evaluate this effect, an adjusted excitation intensity, $I_{adj,ex}$, was calculated for each source-fluorophore combination. Herein, $I_{adj,ex}$, represents the total light intensity that a fluorophore absorbed from an excitation source whose spectra were normalized by the total output power. The adjusted excitation intensity

of the fluorophores using the LED as an excitation source was calculated using the following equation:

$$\mathrm{I}_{adj,ex} = \sum_{\lambda_i=300}^{600} (\mathrm{E}m_{(\lambda_i,\lambda_i+1)} \times \mathrm{E}x_{\lambda_i}) \quad 4.1$$

where $\mathrm{E}m_{(\lambda_i,\lambda_i+1)}$ is the emission intensity of the LED over a 1 nm increment from λ_i to $\lambda_i + 1$ as presented in Figure 4.5 B, and $\mathrm{E}x_{\lambda_i}$ is the normalized excitation intensity of the fluorophore at wavelength λ_i as presented in Figure 4.2.

The output power of the LED was spread over a broad range of wavelengths relative to the laser lines. The range from 300 nm to 600 nm was selected for these calculations because outside this range, the light intensity is negligibly low (10^{-4}-10^{-3}% the total output power). Table 4.1 presents the adjusted excitation intensities of the fluorophores at different LED output powers. The adjusted excitation intensities of the fluorophores decreased by 5.1%-5.4% when the LED output power increased from 1.0 mW to 6.6 mW due to the blue shift in LED peak emission and broadening of the LED output spectrum (Figure 4.5).

Since laser lines are effectively monochromatic with typical 0.0004 nm FWHM [168], their adjusted excitation intensities for each fluorophore were calculated using the following equation:

$$\mathrm{I}_{adj,ex} = \mathrm{E}m_{\lambda_i} \times \mathrm{E}x_{\lambda_i} \quad 4.2$$

where $\mathrm{I}_{adj,ex}$ is the adjusted excitation intensity of the fluorophore, $\mathrm{E}m_{\lambda_i}$ is the emission intensity of the laser line at wavelength λ_i, and $\mathrm{E}x_{\lambda_i}$ is the normalized excitation intensity of the fluorophore at wavelength λ_i as presented in Figure 4.2.

The adjusted excitation intensities of rhodamine 123, fluorescein, and 5-FAM at the five laser lines are presented in Table 4.2. Because the output wavelength and FWHM for the output spectrum will not vary significantly with output power, a single value is presented for each source. A 1-nm width for the laser centered at the emission line was used so that the adjusted excitation intensities calculated by Equation 4.2 can be compared to the value calculated in Equation 4.1. The differences observed between sources are due to the difference in the line wavelength and fluorophore excitation spectra.

Table 4.1. Adjusted excitation intensity of rhodamine 123, fluorescein, and 5-FAM at different LED output powers

LED power (mW)	Adjusted excitation intensity		
	Rhodamine 123 (λ_{ex}=498 nm)	Fluorescein (λ_{ex}=491 nm)	5-FAM (λ_{ex}=493 nm)
1.0	0.466	0.495	0.477
2.1	0.455	0.484	0.466
3.2	0.451	0.480	0.462
4.4	0.446	0.474	0.456
5.5	0.441	0.470	0.452
6.6	0.445	0.474	0.456

Table 4.2. Adjusted excitation intensity of rhodamine 123, fluorescein, and 5-FAM at different laser lines

laser line (mW)	Adjusted excitation intensity		
	Rhodamine 123 (λ_{ex}=498 nm)	Fluorescein (λ_{ex}=491 nm)	5-FAM (λ_{ex}=493 nm)
457	0.302	0.331	0.318
465	0.397	0.410	0.398
472	0.473	0.496	0.471
476	0.528	0.588	0.550
488	0.832	0.962	0.921

Comparison of Table 4.1 and Table 4.2 shows that the 488-nm laser line exhibits the best overlap with all three fluorophores. The 465-nm laser line was closest to the LED emission peak wavelength (465-468 nm) while the 472-nm laser line

exhibited the adjusted excitation intensities closest to those of the LED for all three fluorophores. Therefore, the 472 nm, and 465 nm were chosen for further comparison with the LED. The 488-nm line was also considered because it is the most commonly used laser line for CE-LIF and ME-LIF.

Figure 4.8 presents the $S/N_{corrected}$ for the three fluorophores using the LED and 488-nm, 472-nm, and 465-nm laser lines for excitation. The corrected signal-to-noise ratios were calculated using Equation 4.3:

$$S/N_{corrected} = \frac{S/N}{I_{adj,ex}} \qquad 4.3$$

where $S/N_{corrected}$ is the corrected signal-to-noise ratio, S/N is the raw signal-to-noise ratio (Figure 4.4), and $I_{adj,ex}$ is the adjusted excitation intensity calculated using either Equation 4.1 or Equation 4.2. Correcting these plots to account for source-fluorophore spectral overlap results in the S/N ratios for the three laser lines being almost identical, but the S/N obtained with the LED is significantly lower in all cases (2-4 times lower). The difference in $S/N_{corrected}$ is likely due to the tail of the LED that was ineffectively blocked by the optical filters, as discussed in Section 0. The $S/N_{corrected}$ in CE-LEDIF can be improved by optimizing the spectral filter to reduce the optical noise associated with the LED [157, 169].

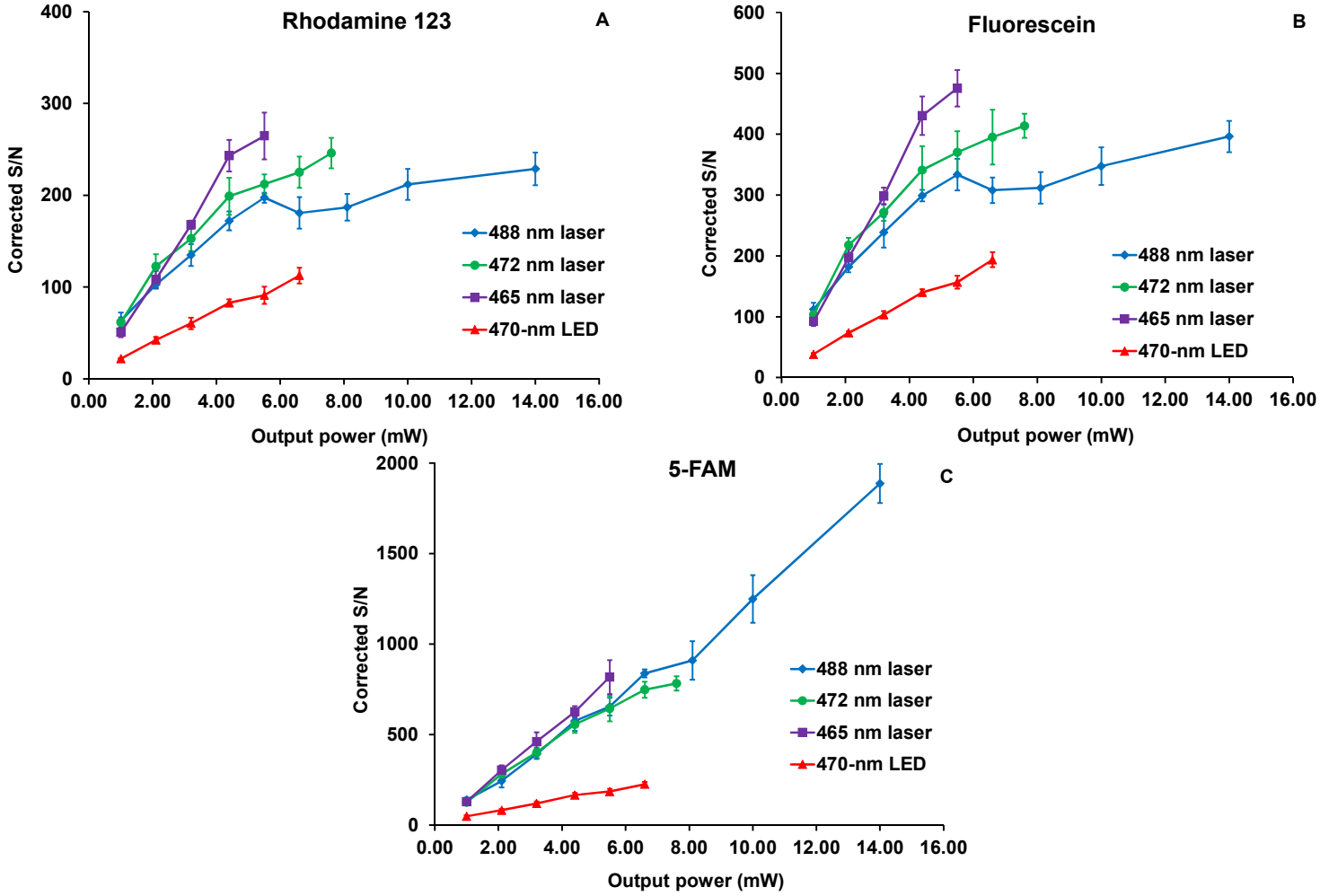

Figure 4.8. Corrected S/N ratios comparing the LED and laser lines. The error bars present the standard deviations of corrected S/Ns, each measured in triplicates.

4.3.5. Limits of detection

The LODs of rhodamine 123, fluorescein, and 5-FAM obtained using the LED and laser lines as excitation sources are summarized in Table 4.3. The power of 5.5 mW was selected for the comparison because it was the highest power output that could be generated by all sources used in the study (Figure 4.4). These LOD values were not adjusted for source-fluorophore spectral overlap (Section 4.3.4). For all three fluorophores, the lowest LODs were obtained with the 488-nm laser line, followed by the 465-nm and 472-nm laser lines. The LODs obtained with the 470-nm LED were 4-20 times higher than those obtained with the 488-nm laser line. The spectral overlap data (Table 4.1 and Table 4.2) would only account for 2-fold difference. Taking this into account, the LOD's obtained with the 488-nm laser line would still be 2-10 times lower and the ineffective blocking of unwanted scattered emission from the LED by the spectral filters.

Table 4.3. LODs obtained for the fluorophores with the 470-nm LED and laser lines (output power = 5.5 mW) as excitation sources

Excitation source	Limit of detection (nM)		
	Rhodamine 123	Fluorescein	5-FAM
470-nm LED	4	3	2
465-nm laser line	1	0.6	0.2
472-nm laser line	2	0.7	0.7
488-nm laser line	1	0.3	0.6

4.4. Conclusion

The LEDs are promising alternatives to the lasers for fluorescence detection due to their small size, low cost, and simple operation. However, spectral overlap of the LED emission spectrum with the fluorophore excitation spectrum as well as the optical filter transmittance spectrum should be taken into account. We have demonstrated that the 470-nm LED used for the detection of three fluorophores including rhodamine 123, fluorescence, and 5-FAM yielded the S/N values 2-4 times

lower than the 465-nm, 472-nm, and 488-nm laser lines, even when the overlap of fluorophore-source was taken into account. In addition, the limits of detection for the fluorophores were 3-20 times lower with the laser lines compared to the 470-nm LED. The underperformance of the LED compared to the laser lines is due to the ineffective filtering of the LED emission at long wavelengths. With the use of the 488 nm notch filter and 520/20 nm emission filter, a portion of the LED tail at long wavelengths (500 nm - 596 nm), which accounted for 0.22%-0.26% the total output of the LED, still reached the detector due to the overlap of LED emission with the fluorophore emission spectra. This attributed to the higher noise and lower S/N values obtained with the LED compared to the laser lines. Therefore, optimizing the spectral filter is important in order to improve the S/N and LOD in CE-LEDIF.

CHAPTER 5. CONCLUSION AND FUTURE DIRECTIONS

5.1. Conclusion

In this dissertation, capillary electrophoresis-based assays were developed to address limitations of coupled enzyme assays. The first approach was to develop and apply direct off-line enzyme assays to separate assay components (substrates, products and inhibitors). The second approach was to use coupling enzymes in combination with CE to reduce spectral and inhibition interferences associated with the coupling reactions.

Chapter 2 presents first the application of CE assays to determine the IC_{50} values for inhibitors of bacterial holo-ACC, BC, and CT. The inhibition study of bacterial holo-ACC, BC, and CT by five flavonols (myricetin, quercetin, anrantine osage orange, galangin and 3,6-dihydroxyflavone) was performed using the CE off-line assays. These compounds were selected previously based on CE screening and computational studies. Out of the five flavonols, myricetin, quercetin, and anrantine osage orange all strongly inhibited the three enzymes. DHF inhibited BC and CT but its solubility ($<1.0 \times 10^{-4}$ M) was too low for IC_{50} quantification whereas galagin exhibited insignificant inhibition towards the three enzymes. The IC_{50} values for myricetin, quercetin, and anrantine osage orange were determined and compared to explore the structure-activity relation of the flavonols towards inhibition of bacterial holo-ACC, BC, and CT. The IC_{50} values of the flavonols depend on the position of hydroxyl groups. The 5,7-dihydroxylation of the A ring is insufficient for inhibition of holo-ACC, BC, and CT. In addition, the hydroxyl groups C-4' and C-2' are likely to enhance the inhibition of bacterial ACC by flavonols whereas the hydroxyl groups at the C-3' and C-5' decrease the potency of flavonols. The IC_{50} values determined in the holo-ACC and BC assays are comparable, but are 2 order of magnitude higher

than the IC_{50} values in the CT assay. Chapter 2 shows that simple CE-based assays can be applied to study bacterial holo-ACC, BC, and CT inhibition without the need of coupling enzymes.

Chapter 3 presents the first CE assay developed for human ACC2. The separation conditions were based on a previously developed CE offline assay for bacterial ACC, which was successfully applied for inhibition study but occasionally suffered from reproducibility issues and peak splitting of ADP and ATP. First, Mg^{2+} was added to both the sample and separation buffers to improve the separation reproducibility. Second, citrate was added to the buffer to activate the enzyme. Third, SDS was removed from the separation buffer to avoid the mismatch of sample and separation buffers while avoiding problems with SDS precipitation due to potassium in the reaction buffer. Finally, phosphate was replaced by HEPES to eliminate the potential problematic interaction of Mg^{2+} with phosphate. The assay was then demonstrated to detect the inhibition of human ACC2 by CP-640186, a known inhibitor. The CE assay of human ACC2, which was developed without coupling enzymes, is applicable to inhibition study with minimal spectral interference.

For the second approach to address limitations of coupled enzyme assays, a CE online coupled assay will be monitored by measuring the fluorescence of NADH using a LED as the excitation source. Chapter 4 presents the quantitative comparison of a 470-nm LED to argon laser lines at 457, 465, 472 and 488 nm as the excitation sources for fluorescence detection of rhodamine 123, fluorescein, and 5-carboxyfluorescein with CE separation. The S/Ns obtained using the LED were 2-7 times lower compared to the laser lines at the same output power. When corrected for the difference in fluorophore excitation, which is presented as the spectral overlap of the fluorophore excitation and light source emission spectra, the corrected S/Ns

obtained for the fluorophores using the LED were still 2-4 times lower than using the laser lines. The underperformance of the LED compared to the laser lines might be due to a portion of the LED emission at long wavelength (or the LED “tail”) that was not effectively blocked by the optical filters used for isolating fluorescence emission. Even with the use of a 488-nm notch filter (57 nm FWHM) and the 520/20 nm emission filter, 0.22%-0.26% the total output of the LED, which corresponds to the unfiltered portion of the LED tail, still reached the detector and contributed to the higher noise and lower S/N values obtained with the LED compared to the laser lines.

Appendix 1 presents preliminary results in the development of a CE online coupled assay on a liquid coolant-based CE system. A portion of the coolant tubing was modified with smaller tubing dimension to decrease the magnet-magnet and magnet-capillary distances while not obstructing the coolant flow. The coupling enzyme lactate dehydrogenase was immobilized onto magnetic beads, which were held inside the capillary by the magnetic field generated by a pair of rare earth magnets. In the CE online assay of the second coupling enzyme (lactate dehydrogenase), the negative peak corresponding to the consumed NADH was detected by fluorescence, using a 365-nm LED as the excitation source. The magnetic bead injection time and pyruvate concentration were demonstrated to impact the NADH consumption in the online assay.

5.2. Future Directions

In this dissertation, only five flavonols (myricetin, quercetin, anrantine osage orange, galangin, and DHF) were tested. Other flavonoids including flavanols, flavones, flavanones can also be tested using the developed assays to identify potential inhibitors of bacterial holo-ACC, BC, and CT. Similar to flavonols, these are the phenolic compounds that can be found in botanical extracts. The potency of the

inhibitors can also be evaluated based on the calculated IC_{50} values. In addition, the comparison of the IC_{50} values for the compounds tested will enable for further understanding of the structure-activity relation of flavonoids towards inhibition of bacterial holo-ACC, BC, and CT, which helps accelerate the search for potent inhibitors of these enzymes.

The offline assay of human ACC2 can be applied to quantify the IC_{50} values of myricetin, quercetin, and anrantine osage orange. The inhibition study can be expanded to other flavonoids to screen for structural leads. In addition, the offline CE assay of human ACC2 can be extended to study human ACC1, which is an isozyme of ACC2.

The CE coupled assay will be further developed for assays with lactate dehydrogenase and pyruvate kinase as the coupling enzymes. These coupled assays will then be applied to study ACC and PFK-1, which catalyze enzymatic reactions that involve the consumption or production of ADP. These are two enzymes that have been previously extensively researched in our lab. These CE-based coupled assays will be subsequently applied to study inhibition of ACC and PFK-1 to avoid the spectral and inhibitor interferences of coupled enzyme assays.

REFERENCES

[1] G.J. Narlikar, D. Herschlag, Mechanistic Aspects of Enzymatic Catalysis: Lessons from Comparison of RNA and Protein Enzymes, Annu. Rev. Biochem, 66 (1997) 19.

[2] J.A. Doudna, T.R. Cech, The chemical repertoire of natural ribozymes, Nature, 418 (2002) 222.

[3] R. Wolfenden, M.J. Snider, The Depth of Chemical Time and the Power of Enzymes as Catalysts, Acc. Chem. Res., 34 (2001) 938-945.

[4] A. Radzicka, R. Wolfenden, A proficient enzyme, Science, 267 (1995) 90-93.

[5] M.J. Snider, R. Wolfenden, The Rate of Spontaneous Decarboxylation of Amino Acids, JACS, 122 (2000) 11507-11508.

[6] R.A. Copeland, Evaluation of enzyme inhibitors in drug discovery: a guide for medicinal chemists and pharmacologists, John Wiley & Sons, Inc., Hoboken, New Jersey, 2013.

[7] G.L. Waldrop, H.M. Holden, M.S. Maurice, The Enzymes of Biotin Dependent CO_2 Metabolism: What Structures Reveal about Their Reaction Mechanisms, Protein Sci., 21 (2012) 1597-1619.

[8] J.R. Knowles, The Mechanism of Biotin-Dependent Enzymes, Annu. Rev. Biochem, 58 (1989) 195-221.

[9] D.L. Nelson, M.M. Cox, Lehninger principles of biochemistry, Fifth edition ed., W.H. Freeman and Company, New York, 2008.

[10] A.L. Hopkins, C.R. Groom, The druggable genome, Nature Reviews Drug Discovery, 1 (2002) 727-730.

[11] T. Tanabe, S. Nakanishi, T. Hashimoto, H. Ogiwara, J. Nikawa, S. Numa, Acetyl-CoA carboxylase from rat liver, Methods Enzymol., 71 Pt C (1981) 5-16.

[12] R.B. Guchhait, S.E. Polakis, P. Dimroth, E. Stoll, J. Moss, M.D. Lane, Acetyl Coenzyme A Carboxylase System of Escherichia coli : Purification and Properties of the Biotin Carboxylase, Carboxyltransferase, and Carboxyl Carrier Protein Components, J. Biol. Chem., 249 (1974) 6633-6645.

[13] J.K. Hayre, G. Xu, L. Borgianni, G.L. Taylor, P.W. Andrew, J.-D. Docquier, M.R. Oggioni, Optimization of a direct spectrophotometric method to investigate the kinetics and inhibition of sialidases, BMC Biochemistry, 13 (2012) 19.

[14] B. Holmquist, P. Bünning, J.F. Riordan, A continuous spectrophotometric assay for angiotensin converting enzyme, Anal. Biochem., 95 (1979) 540-548.

[15] S. Ronca-Testoni, Direct spectrophotometric assay for angiotensin-converting enzyme in serum, Clin. Chem., 29 (1983) 1093-1096.

[16] V. Vermeirssen, J. Van Camp, W. Verstraete, Optimisation and validation of an angiotensin-converting enzyme inhibition assay for the screening of bioactive peptides, J. Biochem. Bioph. Methods, 51 (2002) 75-87.

[17] D.O. Lambeth, W.W. Muhonen, High-performance liquid chromatography-based assays of enzyme activities, Journal of Chromatography B: Biomedical Sciences and Applications, 656 (1994) 143-157.

[18] G.K.E. Scriba, F. Belal, Advances in Capillary Electrophoresis-Based Enzyme Assays, Chromatographia, 78 (2015) 947-970.

[19] L. Tong, Acetyl-coenzyme A carboxylase: crucial metabolic enzyme and attractive target for drug discovery, Cellular and Molecular Life Sciences CMLS, 62 (2005) 1784-1803.

[20] S.J. Wakil, E.B. Titchener, D.M. Gibson, Evidence for the participation of biotin in the enzymic synthesis of fatty acids, Biochim. Biophys. Acta, 29 (1958) 225-226.

[21] K.-H. Kim, Regulation of Mammalian Acetyl-coenzyme A Carboxylase, Annual Review of Nutrition, 17 (1997) 77-99.

[22] M. Hunkeler, A. Hagmann, E. Stuttfeld, M. Chami, Y. Guri, H. Stahlberg, T. Maier, Structural basis for regulation of human acetyl-CoA carboxylase, Nature, 558 (2018) 470-474.

[23] E. Choi-Rhee, J.E. Cronan, The Biotin Carboxylase-Biotin Carboxyl Carrier Protein Complex of Escherichia coli Acetyl-CoA Carboxylase, J. Biol. Chem., 278 (2003) 30806-30812.

[24] N. Santoro, T. Brtva, S.V. Roest, K. Siegel, G.L. Waldrop, A high-throughput screening assay for the carboxyltransferase subunit of acetyl-CoA carboxylase, Anal. Biochem., 354 (2006) 70-77.

[25] L. Abu-Elheiga, D.B. Almarza-Ortega, A. Baldini, S.J. Wakil, Human Acetyl-CoA Carboxylase 2: Molecular Cloning, Characterization, Chromosomal Mapping, and Evidence for Two Isoforms, J. Biol. Chem., 272 (1997) 10669-10677.

[26] L. Abu-Elheiga, W.R. Brinkley, L. Zhong, S.S. Chirala, G. Woldegiorgis, S.J. Wakil, The subcellular localization of acetyl-CoA carboxylase 2, Proceedings of the National Academy of Sciences, 97 (2000) 1444-1449.

[27] J.D. McGarry, G.F. Leatherman, D.W. Foster, Carnitine palmitoyltransferase I. The site of inhibition of hepatic fatty acid oxidation by malonyl-CoA, J. Biol. Chem., 253 (1978) 4128-4136.

[28] S.J. Wakil, J.K. Stoops, V.C. Joshi, Fatty Acid Synthesis and Its Regulation, Annu. Rev. Biochem, 52 (1983) 537-579.

[29] T. Hashimoto, S. Numa, Kinetic studies on the reaction mechanism and the citrate activation of liver acetyl coenzyme A carboxylase, Eur. J. Biochem., 18 (1971) 319-331.

[30] G.A. Locke, D. Cheng, M.R. Witmer, J.K. Tamura, T. Haque, R.F. Carney, A.R. Rendina, J. Marcinkeviciene, Differential activation of recombinant human acetyl-CoA carboxylases 1 and 2 by citrate, Arch. Biochem. Biophys., 475 (2008) 72-79.

[31] S.J. Kwon, Y.S. Cho, Y.-S. Heo, Structural Insights into the Regulation of ACC2 by Citrate, Bull. Korean Chem. Soc, 34 (2013) 565-568.

[32] L. Abu-Elheiga, M.M. Matzuk, K.A. Abo-Hashema, S.J. Wakil, Continuous fatty acid oxidation and reduced fat storage in mice lacking acetyl-CoA carboxylase 2, Science, 291 (2001) 2613-2616.

[33] L. Abu-Elheiga, W. Oh, P. Kordari, S.J. Wakil, Acetyl-CoA carboxylase 2 mutant mice are protected against obesity and diabetes induced by high-fat/high-carbohydrate diets, Proc. Natl. Acad. Sci. U. S. A., 100 (2003) 10207-10212.

[34] H.J. Harwood, Jr., S.F. Petras, L.D. Shelly, L.M. Zaccaro, D.A. Perry, M.R. Makowski, D.M. Hargrove, K.A. Martin, W.R. Tracey, J.G. Chapman, W.P. Magee, D.K. Dalvie, V.F. Soliman, W.H. Martin, C.J. Mularski, S.A. Eisenbeis, Isozyme-nonselective N-substituted bipiperidylcarboxamide acetyl-CoA carboxylase inhibitors reduce tissue malonyl-CoA concentrations, inhibit fatty acid synthesis, and increase fatty acid oxidation in cultured cells and in experimental animals, J. Biol. Chem., 278 (2003) 37099-37111.

[35] D.W. Kung, D.A. Griffith, W.P. Esler, F.F. Vajdos, A.M. Mathiowetz, S.D. Doran, P.A. Amor, S.W. Bagley, T. Banks, S. Cabral, K. Ford, C.N. Garcia-Irizarry, M.S. Landis, K. Loomis, K. McPherson, M. Niosi, K.L. Rockwell, C. Rose, A.C. Smith, J.A. Southers, S. Tapley, M. Tu, J.J. Valentine, Discovery of spirocyclic-diamine inhibitors of mammalian acetyl CoA-carboxylase, Biorg. Med. Chem. Lett., 25 (2015) 5352-5356.

[36] C.-W. Kim, C. Addy, J. Kusunoki, N.N. Anderson, S. Deja, X. Fu, S.C. Burgess, C. Li, M. Ruddy, M. Chakravarthy, S. Previs, S. Milstein, K. Fitzgerald, D.E. Kelley, J.D. Horton, Acetyl CoA Carboxylase Inhibition Reduces Hepatic Steatosis but Elevates Plasma Triglycerides in Mice and Humans: A Bedside to Bench Investigation, Cell Metabolism, 26 (2017) 394-406.e396.

[37] G. Harriman, J. Greenwood, S. Bhat, X. Huang, R. Wang, D. Paul, L. Tong, A.K. Saha, W.F. Westlin, R. Kapeller, H.J. Harwood, Jr., Acetyl-CoA carboxylase inhibition by ND-630 reduces hepatic steatosis, improves insulin sensitivity, and modulates dyslipidemia in rats, Proc Natl Acad Sci U S A, 113 (2016) E1796-1805.

[38] L. Tong, Structure and function of biotin-dependent carboxylases, Cellular and Molecular Life Sciences, 70 (2013) 863-891.

[39] T. Chen, H. Li, Fatty acid metabolism and prospects for targeted therapy of cancer, Eur. J. Lipid Sci. Technol., 119 (2017) 1600366.

[40] V. Chajès, M. Cambot, K. Moreau, G.M. Lenoir, V. Joulin, Acetyl-CoA Carboxylase α Is Essential to Breast Cancer Cell Survival, Cancer Research, 66 (2006) 5287-5294.

[41] W. Fang, H. Cui, D. Yu, Y. Chen, J. Wang, G. Yu, Increased expression of phospho-acetyl-CoA carboxylase protein is an independent prognostic factor for human gastric cancer without lymph node metastasis, Medical Oncology, 31 (2014) 15.

[42] R.U. Svensson, S.J. Parker, L.J. Eichner, M.J. Kolar, M. Wallace, S.N. Brun, P.S. Lombardo, J.L. Van Nostrand, A. Hutchins, L. Vera, L. Gerken, J. Greenwood, S. Bhat, G. Harriman, W.F. Westlin, H.J. Harwood Jr, A. Saghatelian, R. Kapeller, C.M. Metallo, R.J. Shaw, Inhibition of acetyl-CoA carboxylase suppresses fatty acid synthesis and tumor growth of non-small-cell lung cancer in preclinical models, Nature Medicine, 22 (2016) 1108.

[43] A. Beckers, S. Organe, L. Timmermans, K. Scheys, A. Peeters, K. Brusselmans, G. Verhoeven, J.V. Swinnen, Chemical Inhibition of Acetyl-CoA Carboxylase Induces Growth Arrest and Cytotoxicity Selectively in Cancer Cells, Cancer Res., 67 (2007) 8180-8187.

[44] J.W. Corbett, H.J. Harwood, Jr., Inhibitors of Mammalian Acetyl-CoA Carboxylase, Recent Patents on Cardiovascular Drug Discovery, 2 (2007) 162-180.

[45] L. Tong, H.J. Harwood, Jr., Acetyl-coenzyme A carboxylases: versatile targets for drug discovery, J. Cell. Biochem., 99 (2006) 1476-1488.

[46] M.P. Bourbeau, M.D. Bartberger, Recent Advances in the Development of Acetyl-CoA Carboxylase (ACC) Inhibitors for the Treatment of Metabolic Disease, J. Med. Chem., 58 (2015) 525-536.

[47] T.C. Broussard, A.E. Price, S.M. Laborde, G.L. Waldrop, Complex Formation and Regulation of Escherichia coli Acetyl-CoA Carboxylase, Biochemistry, 52 (2013) 3346-3357.

[48] C. Freiberg, N.A. Brunner, G. Schiffer, T. Lampe, J. Pohlmann, M. Brands, M. Raabe, D. Haebich, K. Ziegelbauer, Identification and Characterization of the First Class of Potent Bacterial Acetyl-CoA Carboxylase Inhibitors with Antibacterial Activity, J. Biol. Chem., 279 (2004) 26066-26073.

[49] S.K. Bryant, G.L. Waldrop, S.D. Gilman, A capillary electrophoretic assay for acetyl coenzyme A carboxylase, Anal. Biochem., 437 (2013) 32-38.

[50] C.Z. Blanchard, G.L. Waldrop, Overexpression and Kinetic Characterization of the Carboxyltransferase Component of Acetyl-CoA Carboxylase, J. Biol. Chem., 273 (1998) 19140-19145.

[51] M.S. Davis, J. Solbiati, J.E. Cronan, Overproduction of Acetyl-CoA Carboxylase Activity Increases the Rate of Fatty Acid Biosynthesis in Escherichia coli, J. Biol. Chem., 275 (2000) 28593-28598.

[52] G. Meades, Jr., R.L. Henken, G.L. Waldrop, M.M. Rahman, S.D. Gilman, G.P. Kamatou, A.M. Viljoen, S. Gibbons, Constituents of cinnamon inhibit bacterial acetyl CoA carboxylase, Planta Med., 76 (2010) 1570-1575.

[53] M.A. Silvers, S. Pakhomova, D.B. Neau, W.C. Silvers, N. Anzalone, C.M. Taylor, G.L. Waldrop, Crystal Structure of Carboxyltransferase from Staphylococcus aureus Bound to the Antibacterial Agent Moiramide B, Biochemistry, 55 (2016) 4666-4674.

[54] J.K. Kroeger, J. Zarzycki, G. Fuchs, A spectrophotometric assay for measuring acetyl-coenzyme A carboxylase, Anal. Biochem., 411 (2011) 100-105.

[55] L.B. Willis, W.S.W. Omar, R. Sambanthamurthi, A.J. Sinskey, Non-radioactive assay for acetyl-CoA carboxylase activity, J Oil Palm Res, 2 (2008) 30-36.

[56] M.A. Silvers, G.T. Robertson, C.M. Taylor, G.L. Waldrop, Design, Synthesis, and Antibacterial Properties of Dual-Ligand Inhibitors of Acetyl-CoA Carboxylase, J. Med. Chem., 57 (2014) 8947-8959.

[57] C. Gregolin, E. Ryder, R.C. Warner, A.K. Kleinschmidt, M.D. Lane, Liver Acetyl CoA Carboxylase: The Dissociation-Reassociation Process and Its Relation to Catalytic Activity, Proc. Natl. Acad. Sci. U.S.A., 56 (1966) 1751-1758.

[58] N.B. Beaty, M.D. Lane, Acetyl coenzyme A carboxylase. Rapid purification of the chick liver enzyme and steady state kinetic analysis of the carboxylase-catalyzed reaction, J. Biol. Chem., 257 (1982) 924-929.

[59] K.G. Thampy, Formation of malonyl coenzyme A in rat heart. Identification and purification of an isozyme of acetyl-coenzyme A carboxylase from rat heart, J. Biol. Chem., 264 (1989) 17631-17634.

[60] A. Bianchi, J.L. Evans, A.J. Iverson, A.C. Nordlund, T.D. Watts, L.A. Witters, Identification of an isozymic form of acetyl-CoA carboxylase, J. Biol. Chem., 265 (1990) 1502-1509.

[61] J.R. Miller, S. Dunham, I. Mochalkin, C. Banotai, M. Bowman, S. Buist, B. Dunkle, D. Hanna, H.J. Harwood, M.D. Huband, A. Karnovsky, M. Kuhn, C. Limberakis, J.Y. Liu, S. Mehrens, W.T. Mueller, L. Narasimhan, A. Ogden, J. Ohren, J.V. Prasad, J.A. Shelly, L. Skerlos, M. Sulavik, V.H. Thomas, S. VanderRoest, L. Wang, Z. Wang, A. Whitton, T. Zhu, C.K. Stover, A class of selective antibacterials derived from a protein kinase inhibitor pharmacophore, Proc Natl Acad Sci U S A, 106 (2009) 1737-1742.

[62] Y. Liu, L. Zalameda, K.W. Kim, M. Wang, J.D. McCarter, Discovery of Acetyl-Coenzyme A Carboxylase 2 Inhibitors: Comparison of a Fluorescence Intensity-Based Phosphate Assay and a Fluorescence Polarization-Based ADP Assay for High-Throughput Screening, Assay Drug Dev. Technol., 5 (2007) 225-236.

[63] C.C. Chung, K. Ohwaki, J.E. Schneeweis, E. Stec, J.P. Varnerin, P.N. Goudreau, A. Chang, J. Cassaday, L. Yang, T. Yamakawa, A fluorescence-based thiol quantification assay for ultra-high-throughput screening for inhibitors of coenzyme A production, Assay and drug development technologies, 6 (2008) 361-374.

[64] B. De Spiegeleer, G. Mannens, G. Slegers, W.V.D. Bossche, A. Claeys, Direct assay for phosphotransacetylase and acetyl-coenzyme a carboxylase by high-performance liquid chromatography, Anal. Biochem., 158 (1986) 195-200.

[65] K.W. Kim, H. Yamane, J. Zondlo, J. Busby, M. Wang, Expression, purification, and characterization of human acetyl-CoA carboxylase 2, Protein Expr Purif, 53 (2007) 16-23.

[66] V.K. Kaushik, M. Kavana, J.M. Volz, S.C. Weldon, S. Hanrahan, J. Xu, S.L. Caplan, B.K. Hubbard, Characterization of recombinant human acetyl-CoA carboxylase-2 steady-state kinetics, Biochim. Biophys. Acta, 1794 (2009) 961-967.

[67] J.W. Jorgenson, K.D. Lukacs, Zone electrophoresis in open-tubular glass capillaries, Anal. Chem., 53 (1981) 1298-1302.

[68] N. Banke, K. Hansen, I. Diers, Detection of enzyme activity in fractions collected from free solution capillary electrophoresis of complex samples, J. Chromatogr. A, 559 (1991) 325-335.

[69] M.G. Khaledi, Micelles as separation media in high-performance liquid chromatography and high-performance capillary electrophoresis: overview and perspective, J. Chromatogr. A, 780 (1997) 3-40.

[70] B.M. Simonet, A. Ríos, M. Valcárcel, Enhancing Sensitivity in Capillary Electrophoresis, TrAC, Trends Anal. Chem., 22 (2003) 605-614.

[71] M.E. Johnson, J.P. Landers, Fundamentals and practice for ultrasensitive laser-induced fluorescence detection in microanalytical systems, Electrophoresis, 25 (2004) 3513-3527.

[72] P.G. Schiro, C.L. Kuyper, D.T. Chiu, Continuous-flow Single-molecule CE with High Detection Efficiency, Electrophoresis, 28 (2007) 2430-2438.

[73] S. Nie, R.N. Zare, Optical detection of single moecules, Annu. Rev. Biophys. Biomol. Struct., 26 (1997) 567-596.

[74] D. Xiao, L. Yan, H. Yuan, S. Zhao, X. Yang, M.M.F. Choi, CE with LED-based Detection: An Update, Electrophoresis, 30 (2009) 189-202.

[75] D.A. Bui, P.C. Hauser, Analytical devices based on light-emitting diodes--a review of the state-of-the-art, Anal. Chim. Acta, 853 (2015) 46-58.

[76] Z. Glatz, Determination of enzymatic activity by capillary electrophoresis, J. Chromatogr. B: Anal. Technol. Biomed. Life Sci., 841 (2006) 23-37.

[77] A. Malina, S.K. Bryant, S.H. Chang, G.L. Waldrop, S.D. Gilman, Capillary electrophoresis-based assay of phosphofructokinase-1, Anal. Biochem., 447 (2014) 1-5.

[78] J. Bao, F.E. Regnier, Ultramicro enzyme assays in a capillary electrophoretic system, J. Chromatogr. A, 608 (1992) 217-224.

[79] J. Iqbal, S. Iqbal, C.E. Muller, Advances in immobilized enzyme microbioreactors in capillary electrophoresis, Analyst, 138 (2013) 3104-3116.

[80] P. Nowak, M. Woźniakiewicz, P. Kościelniak, An overview of on-line systems using drug metabolizing enzymes integrated into capillary electrophoresis, Electrophoresis, 34 (2013) 2604-2614.

[81] S. Van Dyck, E. Kaale, S. Nováková, Z. Glatz, J. Hoogmartens, A. Van Schepdael, Advances in capillary electrophoretically mediated microanalysis, Electrophoresis, 24 (2003) 3868-3878.

[82] S. Huang, P. Paul, P. Ramana, E. Adams, P. Augustijns, A. Schepdael, Advances in Capillary Electrophoretically Mediated Microanalysis for On-line Enzymatic and Derivatization Reactions, Electrophoresis, 39 (2017) 97-110.

[83] S. Nováková, S. Van Dyck, A. Van Schepdael, J. Hoogmartens, Z. Glatz, Electrophoretically mediated microanalysis, J. Chromatogr. A, 1032 (2004) 173-184.

[84] B.J. Harmon, I. Leesong, F.E. Regnier, Moving boundary electrophoretically mediated microanalysis, J. Chromatogr. A, 726 (1996) 193-204.

[85] W. Xie, A. Xu, E.S. Yeung, Determination of NAD+ and NADH in a Single Cell under Hydrogen Peroxide Stress by Capillary Electrophoresis, Anal. Chem., 81 (2009) 1280-1284.

[86] J. Schejbal, Z. Glatz, Immobilized-enzyme reactors integrated with capillary electrophoresis for pharmaceutical research, J. Sep. Sci., 41 (2018) 323-335.

[87] R.A. Sheldon, S. van Pelt, Enzyme immobilisation in biocatalysis: why, what and how, Chem. Soc. Rev., 42 (2013) 6223-6235.

[88] L.G. Rashkovetsky, Y.V. Lyubarskaya, F. Foret, D.E. Hughes, B.L. Karger, Automated microanalysis using magnetic beads with commercial capillary electrophoretic instrumentation, J. Chromatogr. A, 781 (1997) 197-204.

[89] S. Bronzeau, N. Pamme, Simultaneous bioassays in a microfluidic channel on plugs of different magnetic particles, Anal. Chim. Acta, 609 (2008) 105-112.

[90] A.-L. Gassner, G. Proczek, H.H. Girault, Bubble cell for magnetic bead trapping in capillary electrophoresis, Analytical and Bioanalytical Chemistry, 401 (2011) 3239-3248.

[91] M. Slovakova, N. Minc, Z. Bilkova, C. Smadja, W. Faigle, C. Fütterer, M. Taverna, J.-L. Viovy, Use of self assembled magnetic beads for on-chip protein digestion, Lab on a Chip, 5 (2005) 935-942.

[92] M.D. Tarn, S.A. Peyman, N. Pamme, Simultaneous trapping of magnetic and diamagnetic particle plugs for separations and bioassays, RSC Advances, 3 (2013) 7209-7214.

[93] A.-L. Gassner, M. Abonnenc, H.-X. Chen, J. Morandini, J. Josserand, J.S. Rossier, J.-M. Busnel, H.H. Girault, Magnetic forces produced by rectangular permanent magnets in static microsystems, Lab on a Chip, 9 (2009) 2356-2363.

[94] X. Yan, S.D. Gilman, Improved peak capacity for CE separations of enzyme inhibitors with activity-based detection using magnetic bead microreactors, Electrophoresis, 31 (2010) 346-352.

[95] R.L. Henken, R. Chantiwas, S.D. Gilman, Influence of immobilized biomolecules on magnetic bead plug formation and retention in capillary electrophoresis, Electrophoresis, 33 (2012) 827-833.

[96] J. Schejbal, R. Řemínek, L. Zeman, A. Mádr, Z. Glatz, On-line coupling of immobilized cytochrome P450 microreactor and capillary electrophoresis: A promising tool for drug development, J. Chromatogr. A, 1437 (2016) 234-240.

[97] P. Ramana, E. Adams, P. Augustijns, A. Van Schepdael, Trapping magnetic nanoparticles for in-line capillary electrophoresis in a liquid based capillary coolant system, Talanta, 164 (2017) 148-153.

[98] P. Ramana, J. Schejbal, K. Houthoofd, J. Martens, E. Adams, P. Augustijns, Z. Glatz, A. Schepdael, An improved design to capture magnetic microparticles for capillary electrophoresis based immobilized microenzyme reactors, Electrophoresis, 39 (2018) 981-988.

[99] C.L. Ventola, The Antibiotic Resistance Crisis, Part 1: Causes And Threats, P&T 40 (2015) 277-283.

[100] J.M. Munita, C.A. Arias, Mechanisms of Antibiotic Resistance, Virulence Mechanisms of Bacterial Pathogens, Fifth Edition, American Society of Microbiology2016.

[101] H. Chandra, P. Bishnoi, A. Yadav, B. Patni, A.P. Mishra, A.R. Nautiyal, Antimicrobial Resistance and the Alternative Resources with Special Emphasis on Plant-Based Antimicrobials - A Review, Plants, 6 (2017) 16.

[102] M.S. Butler, M.A.T. Blaskovich, M.A. Cooper, Antibiotics In The Clinical Pipeline At The End Of 2015, J. Antibiot., 70 (2017) 3-24.

[103] G.D. Wright, Something Old, Something New: Revisiting Natural Products In Antibiotic Drug Discovery, Can. J. Microbiol., 60 (2014) 147-154.

[104] J.W. Campbell, J. John E. Cronan, Bacterial Fatty Acid Biosynthesis: Targets for Antibacterial Drug Discovery, Annual Review of Microbiology, 55 (2001) 305-332.

[105] R.J. Heath, S.W. White, C.O. Rock, Lipid biosynthesis as a target for antibacterial agents, Prog. Lipid Res., 40 (2001) 467-497.

[106] I. Górniak, R. Bartoszewski, J. Króliczewski, Comprehensive review of antimicrobial activities of plant flavonoids, Phytochem Rev, (2018).

[107] R. Puupponen-Pimiä, L. Nohynek, C. Meier, M. Kähkönen, M. Heinonen, A. Hopia, K.-M. Oksman-Caldentey, Antimicrobial Properties Of Phenolic Compounds From Berries, J. Appl. Microbiol., 90 (2001) 494-507.

[108] M. Samsonowicz, E. Regulska, Spectroscopic study of molecular structure, antioxidant activity and biological effects of metal hydroxyflavonol complexes, Spectrochim. Acta A, 173 (2017) 757-771.

[109] T. Wu, X. Zang, M. He, S. Pan, X. Xu, Structure–Activity Relationship of Flavonoids on Their Anti-Escherichia coli Activity and Inhibition of DNA Gyrase, J. Agric. Food. Chem., 61 (2013) 8185-8190.

[110] G. Eumkeb, S. Siriwong, S. Phitaktim, N. Rojtinnakorn, S. Sakdarat, Synergistic Activity And Mode Of Action Of Flavonoids Isolated From Smaller Galangal And Amoxicillin Combinations Against Amoxicillin-Resistant Escherichia Coli, J. Appl. Microbiol., 112 (2012) 55-64.

[111] G.K.E. Scriba, F. Belal, Advances in Capillary Electrophoresis-Based Enzyme Assays, Chromatographia, 78 (2015) 947-970.

[112] S.K. Bryant, The Development of Capillary Electrophoresis Assays to Study Enzyme Inhibition, Louisiana State University, 2013.

[113] S. Häkkinen, M. Heinonen, S. Kärenlampi, H. Mykkänen, J. Ruuskanen, R. Törrönen, Screening of selected flavonoids and phenolic acids in 19 berries, Food Research International, 32 (1999) 345-353.

[114] S.H. Häkkinen, S.O. Kärenlampi, I.M. Heinonen, H.M. Mykkänen, A.R. Törrönen, Content of the Flavonols Quercetin, Myricetin, and Kaempferol in 25 Edible Berries, J. Agric. Food. Chem., 47 (1999) 2274-2279.

[115] H. Chen, Y. Zuo, Y. Deng, Separation and determination of flavonoids and other phenolic compounds in cranberry juice by high-performance liquid chromatography, J. Chromatogr. A, 913 (2001) 387-395.

[116] J.M. Harnly, R.F. Doherty, G.R. Beecher, J.M. Holden, D.B. Haytowitz, S. Bhagwat, S. Gebhardt, Flavonoid Content of U.S. Fruits, Vegetables, and Nuts, J. Agric. Food. Chem., 54 (2006) 9966-9977.

[117] H. Tsuchiya, M. Sato, T. Miyazaki, S. Fujiwara, S. Tanigaki, M. Ohyama, T. Tanaka, M. Iinuma, Comparative study on the antibacterial activity of phytochemical flavanones against methicillin-resistant Staphylococcus aureus, J. Ethnopharmacol., 50 (1996) 27-34.

[118] A.-L. Liu, H.-D. Wang, S.M. Lee, Y.-T. Wang, G.-H. Du, Structure–Activity Relationship Of Flavonoids As Influenza Virus Neuraminidase Inhibitors And Their In Vitro Anti-Viral Activities, Biorg. Med. Chem., 16 (2008) 7141-7147.

[119] H.P. Ávila, E.d.F.A. Smânia, F.D. Monache, A. Smânia, Structure–Activity Relationship Of Antibacterial Chalcones, Biorg. Med. Chem., 16 (2008) 9790-9794.

[120] I. Climent, V. Rubio, ATPase activity of biotin carboxylase provides evidence for initial activation of HCO_3^- by ATP in the carboxylation of biotin, Arch. Biochem. Biophys., 251 (1986) 465-470.

[121] I. Mochalkin, J.R. Miller, A. Evdokimov, S. Lightle, C. Yan, C.K. Stover, G.L. Waldrop, Structural evidence for substrate-induced synergism and half-sites reactivity in biotin carboxylase, Protein Sci., 17 (2008) 1706-1718.

[122] J.E. Cronan, Jr., G.L. Waldrop, Multi-subunit acetyl-CoA carboxylases, Prog. Lipid Res., 41 (2002) 407-435.

[123] T. Tanabe, K. Wada, T. Okazaki, S. Numa, Acetyl-coenzyme-A carboxylase from rat liver. Subunit structure and proteolytic modification, Eur. J. Biochem., 57 (1975) 15-24.

[124] J.C. Castle, Y. Hara, C.K. Raymond, P. Garrett-Engele, K. Ohwaki, Z. Kan, J. Kusunoki, J.M. Johnson, ACC2 is expressed at high levels in human white adipose and has an isoform with a novel N-terminus PLoS One, 4 (2009) e4369.

[125] F. López-Casillas, D.H. Bai, X.C. Luo, I.S. Kong, M.A. Hermodson, K.H. Kim, Structure of the coding sequence and primary amino acid sequence of acetyl-coenzyme A carboxylase, Proc. Natl. Acad. Sci. U.S.A., 85 (1988) 5784-5788.

[126] K. Stiede, W. Miao, H.S. Blanchette, C. Beysen, G. Harriman, H.J. Harwood, H. Kelley, R. Kapeller, T. Schmalbach, W.F. Westlin, Acetyl-coenzyme A carboxylase inhibition reduces de novo lipogenesis in overweight male subjects: A randomized, double-blind, crossover study, Hepatology, 66 (2017) 324-334.

[127] R. Nehme, P. Morin, Advances in capillary electrophoresis for miniaturizing assays on kinase enzymes for drug discovery, Electrophoresis, 36 (2015) 2768-2797.

[128] S. Huang, P. Paul, P. Ramana, E. Adams, P. Augustijns, A. Schepdael, Advances in Capillary Electrophoretically Mediated Microanalysis for On-line Enzymatic and Derivatization Reactions, Electrophoresis, 39 (2018) 97-110.

[129] J. Moss, M.D. Lane, The Biotin-Dependent Enzymes, Adv. Enzymol. Relat. Areas Mol. Biol., John Wiley & Sons, Inc.2006, pp. 321-442.

[130] P. Elisabeth, M. Yoshioka, T. Sasaki, M. Senda, Separation of nucleotides using micellar electrokinetic capillary chromatography, J. Chromatogr. A, 806 (1998) 199-207.

[131] S.E. Geldart, P.R. Brown, Analysis of nucleotides by capillary electrophoresis, J. Chromatogr. A, 828 (1998) 317-336.

[132] A.L. Revilla, J. Havel, P. Jandik, Peak splitting observed during capillary electrophoresis of α- and β-naphthols in borate buffer, J. Chromatogr. A, 745 (1996) 225-232.

[133] R.-L. Chien, Sample stacking revisited: A personal perspective, Electrophoresis, 24 (2003) 486-497.

[134] B. Gaš, V. Hruška, M. Dittmann, F. Bek, K. Witt, Prediction and understanding system peaks in capillary zone electrophoresis, J. Sep. Sci., 30 (2007) 1435-1445.

[135] I.A. Rose, The state of magnesium in cells as estimated from the adenylate kinase equilibrium, Proc. Natl. Acad. Sci. U.S.A., 61 (1968) 1079-1086.

[136] D. Cheng, C.H. Chu, L. Chen, J.N. Feder, G.A. Mintier, Y. Wu, J.W. Cook, M.R. Harpel, G.A. Locke, Y. An, J.K. Tamura, Expression, purification, and characterization of human and rat acetyl coenzyme A carboxylase (ACC) isozymes, Protein Expr Purif, 51 (2007) 11-21.

[137] G.J. Racz, R.J. Soper, Solubility of Dimagnesium Phosphate Trihydrate and Trimagnesium Phosphate, Can J Soil Sci, 48 (1968) 265-269.

[138] N.E. Good, S. Izawa, Hydrogen ion buffers, Methods Enzymol., 24 (1972) 53-68.

[139] B. Gaš, M. Štědrý, E. Kenndler, Peak broadening in capillary zone electrophoresis, Electrophoresis, 18 (1997) 2123-2133.

[140] J.L. Beckers, P. Boček, Sample stacking in capillary zone electrophoresis: Principles, advantages and limitations, Electrophoresis, 21 (2000) 2747-2767.

[141] S.S. Bahga, J.G. Santiago, Coupling isotachophoresis and capillary electrophoresis: a review and comparison of methods, Analyst, 138 (2013) 735-754.

[142] H. Wei, C. Qi, X. Xu, Z. Zhang, Y. Zhou, Z. Cui, X.-E. Zhang, C. Zhang, Glycerol-salt Mediated Stacking of Nucleic Acids in CZE, Chromatographia, 67 (2008) 491-494.

[143] J.M. Andrade, M.G. Estévez-Pérez, Statistical comparison of the slopes of two regression lines: A tutorial, Anal. Chim. Acta, 838 (2014) 1-12.

[144] D.H. Rammler, The effect of DMSO on several enzyme systems, Ann. N.Y. Acad. Sci., 141 (1967) 291-299.

[145] K. Swinney, D.J. Bornhop, Detection in capillary electrophoresis, Electrophoresis, 21 (2000) 1239-1250.

[146] A.M. Garcia-Campana, M. Taverna, H. Fabre, LIF detection of peptides and proteins in CE, Electrophoresis, 28 (2007) 208-232.

[147] N. Nuchtavorn, W. Suntornsuk, S.M. Lunte, L. Suntornsuk, Recent applications of microchip electrophoresis to biomedical analysis, J. Pharm. Biomed. Anal., 113 (2015) 72-96.

[148] E. Gassmann, J.E. Kuo, R.N. Zare, Electrokinetic separation of chiral compounds, Science, 230 (1985) 813-814.

[149] S. Wu, N.J. Dovichi, High-sensitivity fluorescence detector fluorescein isothiocyanate derivatives of amino acids separated by capillary zone electrophoresis, J. Chromatogr., 480 (1989) 141-155.

[150] A. Manz, D.J. Harrison, E.M.J. Verpoorte, J.C. Fettinger, A. Paulus, H. Lüdi, H.M. Widmer, Planar chips technology for miniaturization and integration of separation techniques into monitoring systems, J. Chromatogr. A, 593 (1992) 253-258.

[151] N.J. Dovichi, D.D. Chen, Single-Molecule Detection in Analytical Chemistry, Single-Molecule Optical Detection, Imaging and Spectroscopy, VCH Verlagsgesellschaft mbH2007, pp. 223-243.

[152] Y.-H. Lee, R.G. Maus, B.W. Smith, J.D. Winefordner, Laser-Induced Fluorescence Detection of a Single Molecule in a Capillary, Anal. Chem., 66 (1994) 4142-4149.

[153] A.E. Bruno, F. Maystre, B. Krattiger, P. Nussbaum, E. Gassmann, The pigtailing approach to optical detection in capillary electrophoresis, TrAC, Trends Anal. Chem., 13 (1994) 190-198.

[154] P.K. Dasgupta, Z. Genfa, J. Li, C.B. Boring, S. Jambunathan, R. Al-Horr, Luminescence Detection with a Liquid Core Waveguide, Anal. Chem., 71 (1999) 1400-1407.

[155] S.-L. Wang, X.-J. Huang, Z.-L. Fang, P.K. Dasgupta, A miniaturized liquid core waveguide-capillary electrophoresis system with flow injection sample introduction and fluorometric detection using light-emitting diodes, Anal. Chem., 73 (2001) 4545-4549.

[156] K. Uchiyama, W. Xu, J. Qiu, T. Hobo, Polyester microchannel chip for electrophoresis – incorporation of a blue LED as light source, Fresenius' Journal of Analytical Chemistry, 371 (2001) 209-211.

[157] E.P. de Jong, C.A. Lucy, Spectral filtering of light-emitting diodes for fluorescence detection, Anal. Chim. Acta, 546 (2005) 37-45.

[158] M. Macka, T. Piasecki, P.K. Dasgupta, Light-emitting diodes for analytical chemistry, Annu. Rev. Anal. Chem., 2014, pp. 183-207.

[159] A. Rodat-Boutonnet, P. Naccache, A. Morin, J. Fabre, B. Feurer, F. Couderc, A comparative study of LED-induced fluorescence and laser-induced fluorescence in SDS-CGE: Application to the analysis of antibodies, ELECTROPHORESIS, 33 (2012) 1709-1714.

[160] J. Enzonga, V. Ong-Meang, F. Couderc, A. Boutonnet, V. Poinsot, M.M. Tsieri, T. Silou, J. Bouajila, Determination of free amino acids in African gourd seed milks by capillary electrophoresis with light-emitting diode induced fluorescence and laser-induced fluorescence detection, Electrophoresis, 34 (2013) 2632-2638.

[161] R.A. Mathies, K. Peck, L. Stryer, Optimization of high-sensitivity fluorescence detection, Anal. Chem., 62 (1990) 1786-1791.

[162] S. Forster, A.E. Thumser, S.R. Hood, N. Plant, Characterization of Rhodamine-123 as a Tracer Dye for Use In *In vitro* Drug Transport Assays, PLoS ONE, 7 (2012) e33253.

[163] C. Parmentier, M. Wellman, A. Nicolas, G. Siest, P. Leroy, Simultaneous measurement of reactive oxygen species and reduced glutathione using capillary electrophoresis and laser-induced fluorescence detection in cultured cell lines, Electrophoresis, 20 (1999) 2938-2944.

[164] T. Killelea, C. Saint-Pierre, C. Ralec, D. Gasparutto, G. Henneke, Anomalous electrophoretic migration of short oligodeoxynucleotides labelled with 5′-terminal Cy5 dyes, Electrophoresis, 35 (2014) 1938-1946.

[165] S. Zhao, H. Yuan, D. Xiao, Optical fiber light-emitting diode-induced fluorescence detection for capillary electrophoresis, Electrophoresis, 27 (2006) 461-467.

[166] F.-B. Yang, J.-Z. Pan, T. Zhang, Q. Fang, A low-cost light-emitting diode induced fluorescence detector for capillary electrophoresis based on an orthogonal optical arrangement, Talanta, 78 (2009) 1155-1158.

[167] S. Nakamura, The Roles of Structural Imperfections in InGaN-Based Blue Light-Emitting Diodes and Laser Diodes, Science, 281 (1998) 956-961.

[168] R.C. Sze, W.R. Bennett, Spontaneous-Emission Profiles of Argon-Ion Laser Transitions, Physical Review A, 5 (1972) 837-853.

[169] V.A. Galievsky, A.S. Stasheuski, S.N. Krylov, Improvement of LOD in Fluorescence Detection with Spectrally Nonuniform Background by Optimization of Emission Filtering, Anal. Chem., 89 (2017) 11122-11128.

APPENDIX A. CAPILLARY ELECTROPHORETIC ONLINE COUPLED ENZYME ASSAY

Introduction

Capillary electrophoresis (CE) has emerged in recent years as an analytical technique with applications in pharmaceuticals research [1, 2], especially for assay development to study enzyme kinetics and inhibition [1, 3]. This is attributed to the low sample consumption (nL), fast separation, and high separation efficiency in CE [4]. In a CE enzyme assay, the reaction mixture can be incubated prior to being injected to the capillary for subsequent separation (offline assay) or all involved steps including mixing, incubation, and separation can occur inside the capillary (online assay). The reaction progress is then monitored by detecting the formation of products and/or depletion of substrates.

The first CE online enzyme assay was reported by Bao et al. [5]. Since then, a wide variety of enzymes have been assayed using this technique [1, 6]. Based on the physical states of the enzymes, CE online enzyme assays can be classified into two categories: homogeneous and heterogenous assays. In a homogeneous assay, all assay reagents including the enzyme are in aqueous form. Alternatively, for a heterogeneous assay, the enzyme is normally immobilized onto the capillary surface, incorporated in a polymer network, or immobilized onto a solid support to form immobilized microenzyme reactors (IMERs). Compared to free enzymes, the immobilized enzymes are more stable upon exposure to heat or different pHs [1]. In addition, immobilized enzymes can be reused, making heterogeneous assays more cost-efficient. Magnetic beads (MBs) have been used widely as the solid supports for enzyme immobilization owing to their high surface to volume ratio, reusability, and the ease of manipulating the location of the microreactors using an external magnetic field [1]. Most MB-based assays were developed on CE with air-based cooling systems [1,

7-12]. The orientation of the magnets along the capillary was studied by both simulations and experiments [7, 9, 12, 13]. The two magnets configurations have been commonly adopted: repulsive arrangement at either 20^{o} or 30^{o}, and attractive arrangement at 90^{o} (perpendicular) to the capillary. Experimental results indicated that relative to the attractive arrangement at 90^{o}, the pair of magnets when positioned in repulsive configuration at 30^{o} resulted in lower enzyme activity but higher reproducibility [7, 13]. In addition to the magnet positions, the chemistry of the functional groups on the MBs is also important for the formation and retention of the MBs inside the capillary [8]. Recently, attempts have been made to develop CE online assays in liquid-based cooling system, in which the coolant tubing made it difficult to align the magnets in proximity to the capillary, posing as an obstacle for the magnet holder design [13, 14]. Ramana et al. reported the ensemble of 1×1×1 mm magnets along the capillary and inside the coolant tubing [14]. In another study, the same group compared the online assays developed on the air-based and liquid coolant-based systems. In the latter system, the magnets were positioned outside the coolant tubing, in attractive orientation, and at an angle of 30^{o} to the capillary [13]. The capturing efficiency of the MBs in the liquid coolant-based CE system was lower compared to the air-based system owing to the longer distance between magnet-magnet and magnet-capillary.

Enzyme assays are based on the detection of either substrate depletion or product formation. However, for some enzymatic reactions, it is not convenient to detect the substrates and products. In such cases, in addition to the primary enzymes, coupling enzymes are also utilized for indirect detection of the substrates or products. Such assays, which are referred to as coupled enzyme assays, have been used widely in biomedical research [15]. Traditional coupled assays are usually carried out in

cuvettes or plate readers, which are prone to spectral interference since the measured signal is attributed to not only the final product but also other assay components. The use of CE for coupled enzyme assays can minimize the spectral interference by separating the assay components prior to detection. Furthermore, small amounts of assay reagents (nL-μL) are needed for the CE assay compared to the conventional coupled assays (μL-mL).

In CE, fluorescence detection is the second common detection method, yet offers the lowest limit of detection. Lasers have been used as the light sources for fluorescence detection in CE owing to its high power, monochromatic, collimated, and coherent output. Since its first introduction by Zare and coworkers [16], CE with laser-induced fluorescence detection (CE-LIF) has been applied to study biological samples including peptides and proteins [17]. The quest for cheaper, more stable excitation sources for fluorescence detection has extended to light-emitting diodes (LEDs).

In this work, a CE coupled online assay was developed on a commercial CE system with liquid coolant. Lactate dehydrogenase (LDH) was used as a coupling enzyme for the indirect detection of pyruvate, which is a product form in the puruvate kinase (PK)-catalyzed reaction:

$$\text{ADP} + \text{phosph(enol)pyruvate} \xrightarrow{\text{Pyruvate kinase}} \text{ATP} + \text{Pyruvate}$$

$$\text{Pyruvate} + \text{NADH} \xrightarrow{\text{Lactate Dehydrogenase}} \text{Lactate} + \text{NAD}^+$$

For this assay, LDH was immobilized onto the MBs, which formed the MB plug inside the capillary in the presence of the external magnetic field. The reaction progress was monitored based on the depletion of NADH, which was detected as a negative peak by fluorescence detection using an LED as the excitation source.

Materials and Methods

Chemicals

Puruvate kinase, L-lactic dehydrogenase from rabbit muscle, pyruvate, NADH, NAD^+, MES, 1-ethyl-3-(3-dimethylaminopropyl) carbodiimide (EDC), sodium hydroxide, potassium bicarbonate, potassium citrate, magnesium chloride, and HEPES were purchased from Sigma-Aldrich (St. Louis, MO). The Superparamagnetic beads (Dynabeads M-270, 2.8 μm diameter, 30 mg/mL, 2 x 10^9 beads functionalized with carboxylic acid) were purchased from Invitrogen Dynal (Oslo, Norway). Solutions were prepared using ultrapure water (>18 MΩ, Barnstead Nanopure, ThermoFisher, Marietta, Ohio, USA). Buffer solutions were filtered through 0.2 μm membranes (Whatman, Hilsboro, OR, USA) before use.

Instrumentation

A P/ACE MDQ with a LIF detector module from Beckman Coulter (Brea, CA, USA) was used for the CE coupled enzyme assays. Data were collected and analyzed using 32 Karat 5.0 software from Beckman Coulter. Fused-silica capillary (50 μm id, 360 μm od) was purchased from Polymicro Technologies (Phoenix, Arizona, USA). A short segment of the polyimide coating on the capillary was removed to create a detection window using a MicroSolv CE window maker (Eatontown, NJ, USA). The capillary total length was 42.5 cm, with an effective length of 32.5 cm (from the injection end to the detection window). The 365-nm LED was purchased from Ocean Optics (Winter Park, FL, USA). An optical fiber with a fiber core diameter of 200 μm and numerical aperture of 0.29 (Ocean Optics, Dunedin, FL, USA) was coupled to the LED by the SMA-905 connector. The maximum LED output power measured at the end of the optical fiber was 0.5 mW. The band pass filter (475 nm, 25 nm band width, OD4, 12.5 mm diameter) was purchased from Edmund Optics, Inc. (Barrington, NJ, USA).

LED emission spectral characterization was performed using an Avantes-2408 spectrometer (Broomfield, CO, USA). The optical filters were characterized using a Varian Cary Eclipse UV-Vis spectrophotometer (Victoria, Australia). The excitation and emission spectra of the NADH were collected using a Varian Cary Eclipse fluorescence spectrophotometer (Victoria, Australia).

Magnet Configuration

The block magnets (1/2×1/4×1/4 in, NdFeB rare earth magnets, N52 magnetization, surface field 7123 Gauss, Brmax 1.48 T, with the polarization along the longest dimension) were purchased from K&J Magnetics (Pipersville, PA, USA). The coolant tubing was modified by inserting a 5.5-cm tubing of smaller size (1/8 inch od, 1/16 inch id) between two pieces of the original coolant tubing (3/8 inch od, 1/8 inch id). The connections between two tubing types were secured by zip tights. When the liquid coolant circulated in the modified cartridge, no leakage was detected. The magnets were positioned against the edges of the smaller coolant tubing as shown in Figure A1. As such, the magnets could be brought closer while the position of the capillary inside the coolant tubing was controlled more accurately. The magnets were separately glued onto two rectangular pieces of plastic (2.7×2.0 cm), which were then fixed onto a rectangular piece of plastic (2.7×4.0 cm) by the nylon bolts. This design allowed the two magnets to be arranged in repulsive orientation, at 20^{o} to the capillary, and 14.7 cm from the capillary inlet.

CE Conditions

For the CE assay, NADH was prepared in the buffer containing 30.0 mM HEPES, 2.5 mM $KHCO_3$, 3.0 mM $MgCl_2$ at pH 7.50 daily due to the instability of NADH. The resulting NADH-containing buffer was used as both the sample and separation buffers. Other assay components (pyruvate, MBs) were also prepared in the NADH-

containing buffer. The capillary was conditioned by rinsing with NaOH, water, and then buffer for 10.0 min at 20.0 psi each. For the NADH separation experiment, the sample was injected at 0.5 psi for 10s, followed by separation at 20.0 kV (470 V/cm). The current conducted in the capillary was at 20.2 μA. The temperatures of both the sample tray and the capillary were set at 25 ˚C.

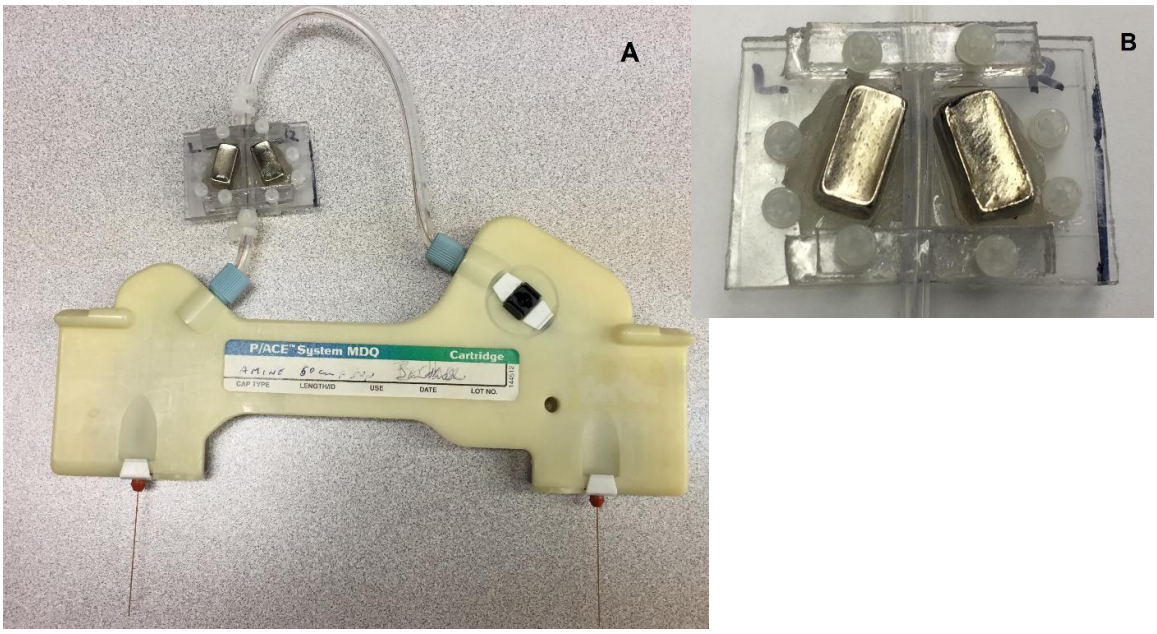

Figure A1. Magnet holder set up for the coolant liquid-based catridge.

Enzyme Immobilization on MBs

The enzyme immobilization onto the MBs was carried out following the two-step procedure suggested by the manufacturer, including the activation of the MB surface with EDC and immobilization of the enzyme. Initially, 100 μL MBs (2×10^9 beads/mL, or 30 mg beads/mL) was washed twice with 0.01 M NaOH and three times with cold deionized water. Subsequently, 200 μL EDC (72.77 mg/mL, prepared in cold water) was added to the MBs, and the mixture was incubated for 30 min at room temperature, on a rocking platform. After the incubated was completed, the supernatant was removed, and the MBs were washed again with cold deionized water and 50 mM MES

buffer (pH 5.0). Following the MB surface activation by EDC, 60 µL LDH (1.0 mg/mL, prepared in 50 mM MES buffer pH 5.0) and 60 µL MES buffer were added to the MBs, and the mixture was incubated at room temperature for 1 hour. Finally, the MBs were washed with PBS buffer to remove the free enzyme in excess and block the unreacted carboxylic acid. The MBs was resuspended to the concentration of 2×10^9 beads/mL in 100 µL PBS buffer and stored at 2-8^{o}C for later use. The working MB solution was prepared by washing the MBs in NADH-containing solution for three time before diluting the stock enzyme-immobilized MB solutions by 20 times in the NADH-containing buffer to obtain the final concentration of 1×10^8 beads/mL.

Results and Discussion

Characterization of NADH, the LED, and the Optical Filter

The excitation and emission spectra of NADH, the transmission spectrum of the band pass filter and the emission spectrum of the LED are shown in Figure A2. The maximum excitation and emission wavelengths of NADH are at 339 nm and 464 nm, respectively whereas the LED emitted light in a wide range of wavelength, with the peak at 365 nm. Consequently, the overlap between the LED emission spectrum and NADH excitation spectrum (Figure A2) enabled the fluorescence detection of NADH using the LED as the excitation source. The band pass filter, which had the maximum transmittance of 97.2%, coincided with the NADH emission spectrum right at its peak. In addition to the passing band being far apart from the LED emission peak, the narrow band width was an important feature of the band pass filter since it limited the stray light from the LED to reach the detector.

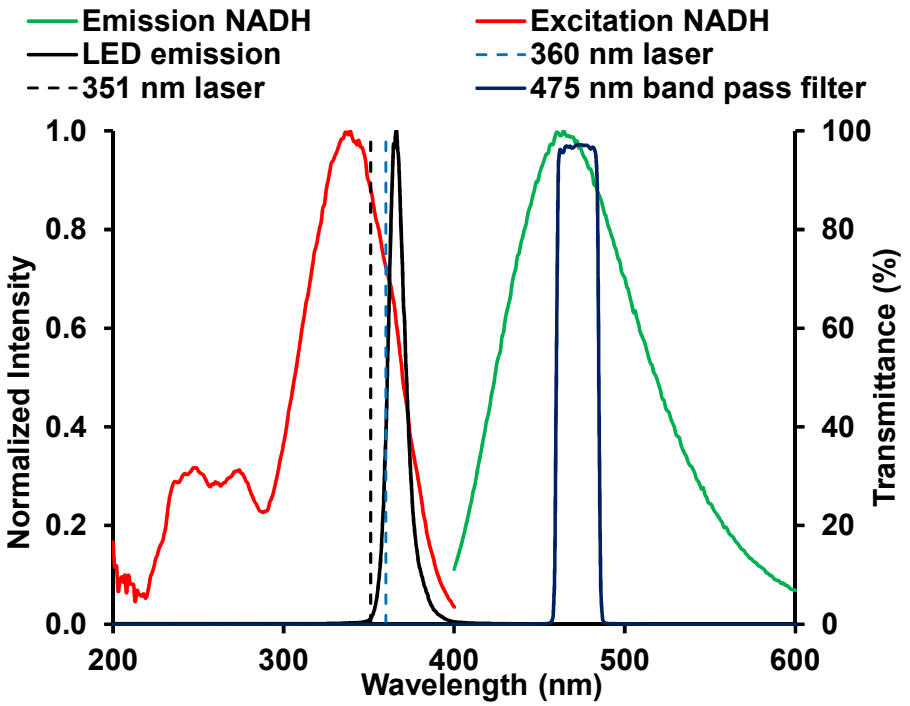

Figure A2. Excitation and emission spectra of NADH, emission spectrum of the LED, and transmission spectrum of the band pass filter

CE Separation and Detection of NADH

NADH was separated by CE in the separation buffer containing 30.0 mM HEPES, 2.5 mM $KHCO_3$, 3.0 mM $MgCl_2$ at pH 7.50 and detected by fluorescence detection. The limit of detection for NADH was 17.2 μM, which was 43 times higher than the LOD reported by Henken et al [18]. Previously, Henken et al. reported the detection of NADH using multiple laser lines at 351-360 nm as the excitation source, with the output power of 3.0 mW, and a 365 nm band pass filter [18]. Eventually, the LED light source output power, the overlap between the light source emission and fluorophore excitation spectra as well as the band pass filter were all attributed to the high LOD. First, the LED that was used as the excitation source for the fluorescence detection of NADH in this project had the maximum output power of 0.5 mW, which was 6-fold lower than the laser. Second, based on the overlap of the LED emission and NADH excitation spectra, the adjusted excitation intensity calculated for this

source-fluorophore was 0.555. For the laser lines at 351 nm and 360 nm, the adjusted excitation intensities were 0.724 and 0.882, respectively. Therefore, the excitation of NADH was 1.3 to 1.5-fold less effective when using the LED. Third, although the band pass filter with a narrow width (central wavelength at 475 nm, 25 nm band width) enabled the collection of NADH fluorescence near the emission peak, a small tail of the LED emission still passed through the filter (Figure A3). The LED emission at long wavelengths (442-515 nm) made up 0.09% of the fluorescence signal.

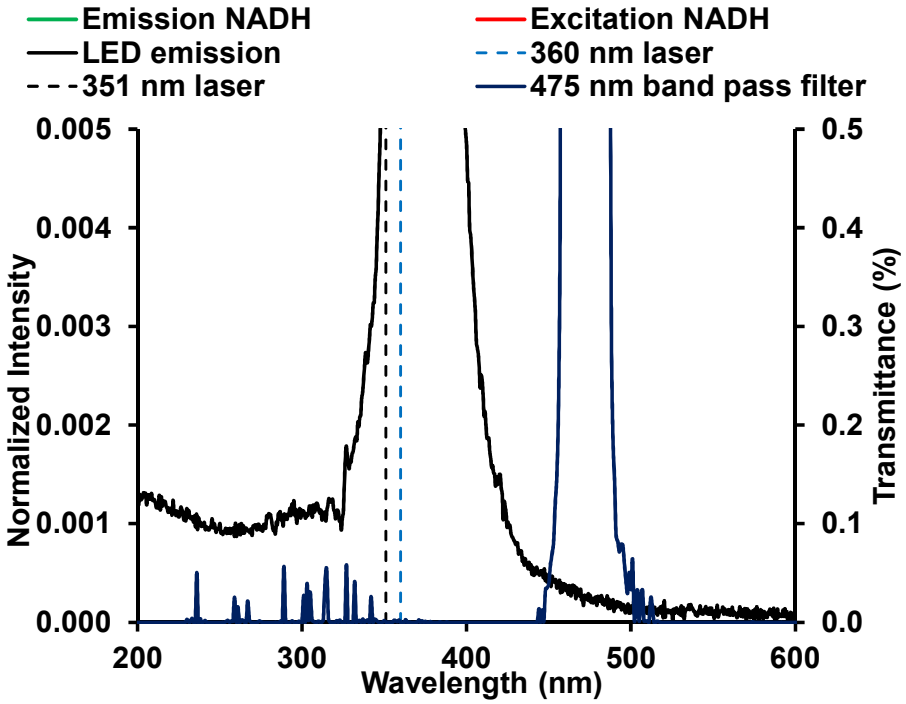

Figure A3. The zoom-in spectra of the LED and band pass filter

For the LDH online enzyme assay, the concentration of NADH in the separation buffer affects not only the product formation but also the background signal. According to Shi et al., in the online assay of immobilized LDH, when the NADH concentration was at and above 0.25 mM, the NADH consumption peak height approached maximum [10]. To study the effect of NADH concentration in the separation buffer on the NADH consumption peak, the electropherograms obtained with two separation

buffers containing 0.25 mM and 1.0 mM NADH were compared. Figure A4 shows the separation of the samples whose NADH concentrations were 100 µM lower than the concentration of NADH in the separation buffers. The CE separation of 900 µM NADH in the separation buffer containing 1.0 mM NADH resulted in a negative peak of NADH. Similarly, 100 µM NADH when separated in the separation buffer containing 0.25 mM NADH was also detected as a negative peak, but without the big artifact peak in the front. Therefore, the separation buffer containing 30.0 mM HEPES, 2.5 mM $KHCO_3$, 3.0 mM $MgCl_2$, and 0.25 mM NADH at pH 7.50 was used for further development of the LDH online assay.

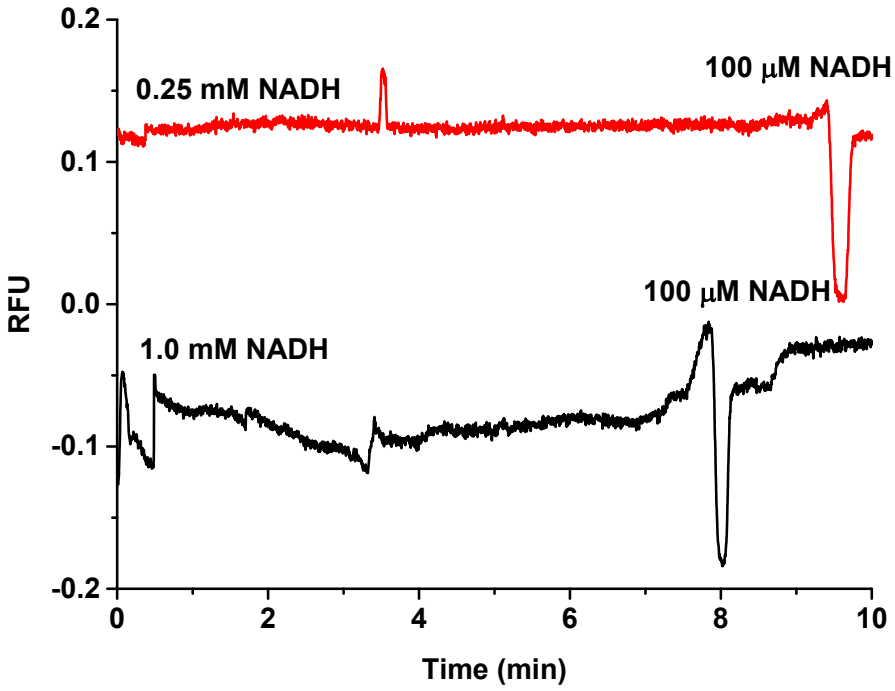

Figure A4. Electropherograms for the separation of 100 µM NADH in the separation buffer containing 0.25 mM NADH (red) and 900 µM NADH in the separation buffer containing 1.0 mM NADH (black).

The calibration curve for direct detection of NADH was $y=0.0017x - 0.0071$ ($R^2 = 0.997$). However, for the coupled assay, NADH was detected as a negative peak due to NADH consumption. Therefore, it was practical to establish the calibration curve

of the depleted NADH. Figure A5 shows the calibration of NADH, provided that the concentration of NADH in the sample was 25-200 μM lower than the concentration of NADH in the separation buffer.

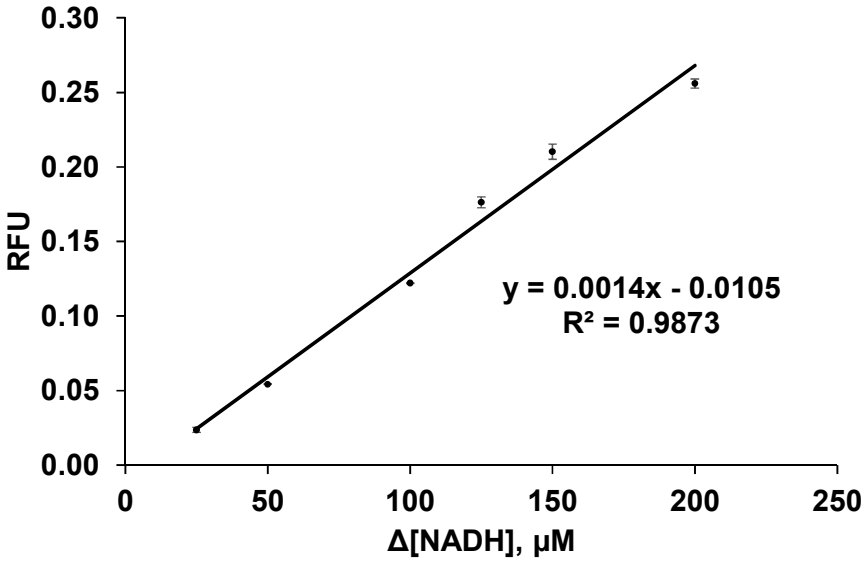

Figure A5. Calibration curve of NADH

Offline Assay of the Immobilized Enzyme

In order to test the activity of the immobilized LDH, the LDH-immobilized MBs (at the final concentration of 2×10^7 beads/mL) were incubated with 1.0 mM pyruvate in a buffer containing 30.0 mM HEPES, 2.5 mM $KHCO_3$, 3.0 mM $MgCl_2$, and 0.25 mM NADH at pH 7.50. Following the hydrodynamic injection at 0.5 psi for 10.0 s, the reaction mixture was separated at 20.0 kV (470 V/cm) in the separation buffer that contained 30.0 mM HEPES, 2.5 mM $KHCO_3$, 3.0 mM $MgCl_2$, and 0.25 mM NADH at pH 7.50. The control contained all components except for the LDH-immobilized MBs. The electropherograms for the offline assay of the LDH-immobilized MBs are shown in Figure A6.

Upon the incubation of the LDH-immobilized MBs with pyruvate in the NADH-containing buffer, a negative peak corresponding to the consumption of NADH was

observed. This NADH peak height increased as the reaction time extended from 3 min to 20 min. This result indicated that the immobilized LDH on the MBs was active.

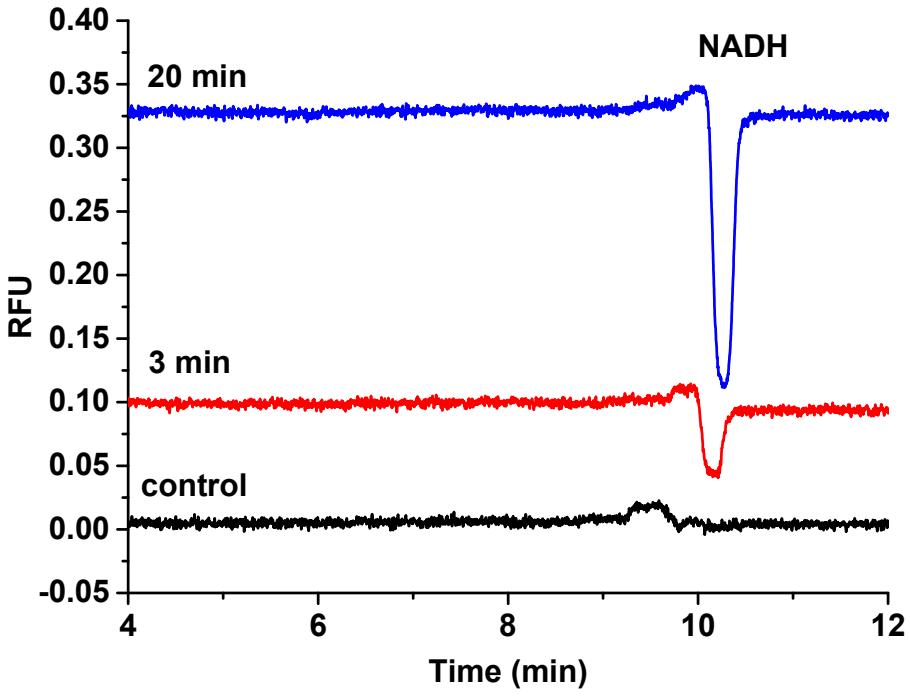

Figure A6. Offline assay of the LDH-immobilized MBs

Online Assay of the Immobilized Enzyme

The formation and retention of the MB plugs inside the capillary was qualitatively studied under the microscope, on a homebuilt CE system. After the LDH-immobilized MBs (1×10^8 beads/mL) were manually injected to the capillary using a syringe, a plug of MBs were observed. Subsequently, upon the application of 10 kV (235 V/cm) for 30 min and 20 kV (470 V/cm), the MB plug still remained in the capillary in between the two magnets.

For the online assay, both the sample buffer and the separation buffer contained 30.0 mM HEPES, 2.5 mM $KHCO_3$, 3.0 mM $MgCl_2$, and 0.25 mM NADH at pH 7.50, which is also referred to as the NADH-containing buffer hereafter. Pyruvate and the MBs for the online assay were prepared in the NADH-containing buffer.

Initially, the LDH-immobilized MBs (1×10^8 beads/mL) were injected to the capillary at 0.5 psi for 60.0 s. Low pressure (0.5 psi) was applied for 10.0 min to transport the MBs to the magnetic field. Afterwards, 1.0 mM pyruvate was injected to the capillary under 0.5 psi for 10.0 s. The plug of pyruvate was moved under 0.5 psi for 4.2 min to the IMER position where the reaction was let incubated for 10.0 min. Finally, the assay components were separated, and the NADH which was consumed was detected as a negative peak, as shown in Figure A7.

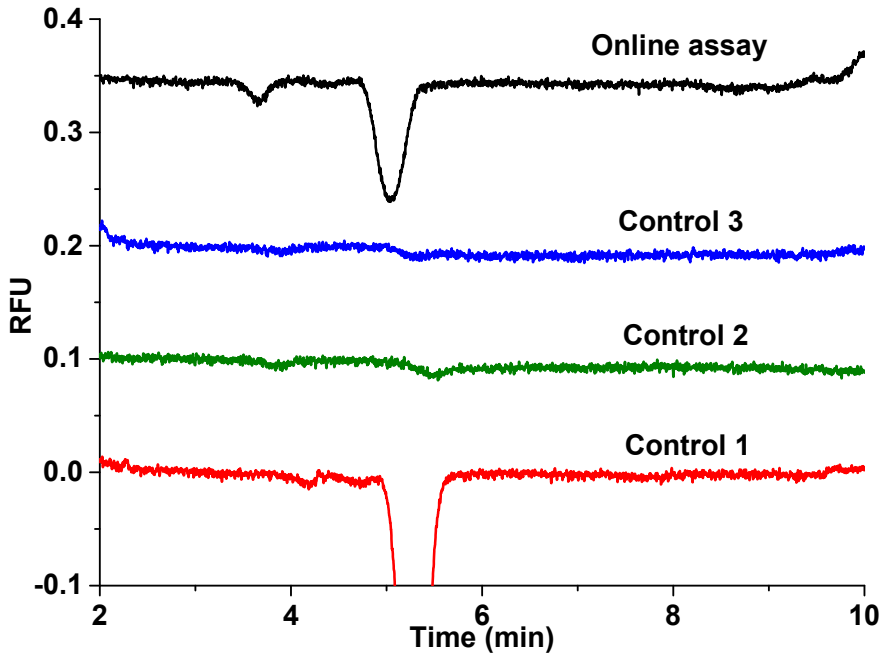

Figure A7. Online assay of LDH. The MBs were hydrodynamically injected at 0.5 psi for 60.0s and moved to the magnetic field under 0.5 psi for 10.0 min. The 1.0 mM pyruvate substrate was injected at 0.5 psi for 10.0s, then moved to the IMER position under 0.5 psi for 4.2 min. After 10.0 min incubation, the reaction was stopped upon the application of 20.0 kV (470 V/cm). The separation buffer contained 30.0 mM HEPES, 2.5 mM $KHCO_3$, 3.0 mM $MgCl_2$, and 0.25 mM NADH at pH 7.50.

In control 1, the NADH-free buffer was injected as a sample to determine the migration time for NADH which was at 5.2 min in the online assay. Compared to the separation of NADH in Figure A4 and Figure A6, the peak of NADH in the online assay presented in Figure A7 was broader while the migration time of NADH was 2 fold

shorter as a result of the additional step involving the transport of the pyruvate plug to the IMERs position under pressure. In control 2, following the same procedure described for the online assay, instead of the pyruvate, the NADH-containing buffer was injected and separated. In addition, in the absence of the MBs, the sample containing 1.0 mM pyruvate and 0.25 mM NADH was injected to the capillary as control 3. In both control 2 and control 3, no negative peak for NADH was observed. For the online assay, a negative peak corresponding to the NADH consumption was observed, indicating that the immobilized LDH was active in the online assay.

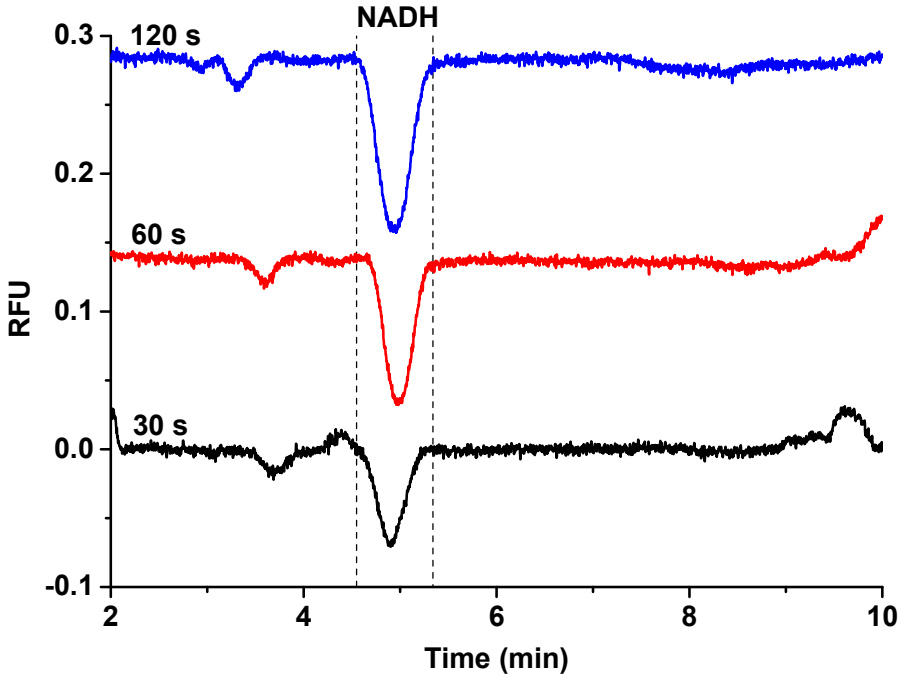

Figure A8. Dependence of NADH peak height on the LDH-MBs injection time. The MBs were injected at 0.5 pi for 30s, 60s, and 120 s. Other experimental conditions were the same as described in Figure A7.

The amount of MBs injected to the capillary is an important factor that affects the assay response. The dependence of the NADH peak on the duration of MB injection is shown in Figure A8. At the same MBs stock concentration, the number of MBs injected to the capillary depends on the pressure and injection time. Under the

injection pressure of 0.5 psi, as the MBs injection time was increased from 30 to 120 s, the NADH peak height increased accordingly. The dependence of NADH peak height on the concentration of the pyruvate substrate was shown in Figure A9. The pyruvate concentration at 1.0 mM yielded higher NADH peak height than the assay with 0.5 mM pyruvate.

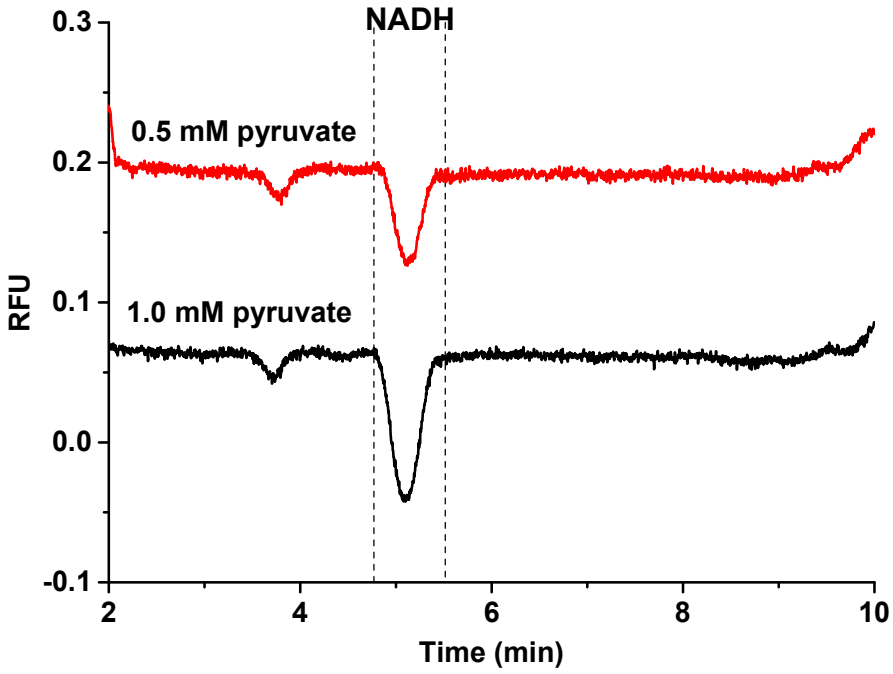

Figure A9. Dependence of the NADH peak height on the concentration of the pyruvate substrate. The 0.5 mM and 1.0 mM pyruvate substrate solutions were injected hydrodynamically at 0.5 psi. Other experimental conditions were the same as described in Figure A7.

Conclusion

A CE online assay of LDH was developed on a liquid coolant-based system. In this assay, LDH was immobilized onto MBs, which were subsequently held inside the capillary by a pair of magnets. The online LDH assay was studied based on the detection of the NADH consumption, which was detected as a negative peak using fluorescence detection. An LED was utilized as the excitation source for NADH detection, yielding the LOD of 17.2 μM. The primary data showed that the LDH-

immobilized MBs retained inside the capillary and exhibited enzyme activity in the online assay. This work served as a basis for the CE online coupled assay that uses lactate dehydrogenase and pyruvate kinase as the coupling enzymes and can be extended for online coupled assays that use multiple coupling enzymes.

References

[1] J. Schejbal, Z. Glatz, Immobilized-Enzyme Reactors Integrated with Capillary Electrophoresis for Pharmaceutical Research, J. Sep. Sci., 41 (2018) 323-335.

[2] L. Suntornsuk, Recent advances of capillary electrophoresis in pharmaceutical analysis, Analytical & Bioanalytical Chemistry, 398 (2010) 29-52.

[3] G.K.E. Scriba, F. Belal, Advances in Capillary Electrophoresis-Based Enzyme Assays, Chromatographia, 78 (2015) 947-970.

[4] J.P. Landers, Handbook of capillary and microchip electrophoresis and associated microtechniques, CRC Press, Boca Raton, 2008.

[5] J. Bao, F.E. Regnier, Ultramicro Enzyme Assays In A Capillary Electrophoretic System, J. Chromatogr. A, 608 (1992) 217-224.

[6] S. Huang, P. Paul, P. Ramana, E. Adams, P. Augustijns, A. Van Schepdael, Advances in Capillary Electrophoretically Mediated Microanalysis for On-line Enzymatic and Derivatization Reactions, Electrophoresis, 39 (2018) 97-110.

[7] J. Schejbal, R. Řemínek, L. Zeman, A. Mádr, Z. Glatz, On-line coupling of immobilized cytochrome P450 microreactor and capillary electrophoresis: A promising tool for drug development, J. Chromatogr. A, 1437 (2016) 234-240.

[8] R.L. Henken, R. Chantiwas, S.D. Gilman, Influence of immobilized biomolecules on magnetic bead plug formation and retention in capillary electrophoresis, Electrophoresis, 33 (2012) 827-833.

[9] A.-L. Gassner, M. Abonnenc, H.-X. Chen, J. Morandini, J. Josserand, J.S. Rossier, J.-M. Busnel, H.H. Girault, Magnetic forces produced by rectangular permanent magnets in static microsystems, Lab on a Chip, 9 (2009) 2356-2363.

[10] J. Shi, W. Zhao, Y. Chen, L. Guo, L. Yang, A replaceable dual-enzyme capillary microreactor using magnetic beads and its application for simultaneous detection of acetaldehyde and pyruvate, Electrophoresis, 33 (2012) 2145-2151.

[11] H.-X. Chen, J.-M. Busnel, A.-L. Gassner, G. Peltre, X.-X. Zhang, H.H. Girault, Capillary electrophoresis immunoassay using magnetic beads, ELECTROPHORESIS, 29 (2008) 3414-3421.

[12] L.G. Rashkovetsky, Y.V. Lyubarskaya, F. Foret, D.E. Hughes, B.L. Karger, Automated microanalysis using magnetic beads with commercial capillary electrophoretic instrumentation, J. Chromatogr. A, 781 (1997) 197-204.

[13] P. Ramana, J. Schejbal, K. Houthoofd, J. Martens, E. Adams, P. Augustijns, Z. Glatz, A. Schepdael, An improved design to capture magnetic microparticles for capillary electrophoresis based immobilized microenzyme reactors, Electrophoresis, 39 (2018) 981-988.

[14] P. Ramana, E. Adams, P. Augustijns, A. Van Schepdael, Trapping Magnetic Nanoparticles for In-line Capillary Electrophoresis in a Liquid Based Capillary Coolant System, Talanta, 164 (2017) 148-153.

[15] R.A. Copeland, Evaluation Of Enzyme Inhibitors In Drug Discovery: A Guide For Medicinal Chemists And Pharmacologists, John Wiley & Sons, Inc., Hoboken, New Jersey, 2013.

[16] E. Gassmann, J.E. Kuo, R.N. Zare, Electrokinetic separation of chiral compounds, Science, 230 (1985) 813-814.

[17] A.M. García-Campaña, M. Taverna, H. Fabre, LIF detection of peptides and proteins in CE, Electrophoresis, 28 (2007) 208-232.

[18] R. Henken, Studies of Enzyme Kinetics and Inhibition Through Capillary Electrophoretic Enzyme Assays, Louisiana State University, Louisiana State University, 2013.

APPENDIX B. LETTER OF PERMISSION

JOHN WILEY AND SONS LICENSE TERMS AND CONDITIONS

Mar 13, 2019

This Agreement between Thu Nguyen ("You") and John Wiley and Sons ("John Wiley and Sons") consists of your license details and the terms and conditions provided by John Wiley and Sons and Copyright Clearance Center.

License Number	4547120099435
License date	Mar 13, 2019
Licensed Content Publisher	John Wiley and Sons
Licensed Content Publication	Electrophoresis
Licensed Content Title	Capillary electrophoretic assay of human acetyl-coenzyme A carboxylase 2
Licensed Content Author	Thu H. Nguyen, Grover L. Waldrop, S. Douglass Gilman
Licensed Content Date	Mar 13, 2019
Licensed Content Volume	0
Licensed Content Issue	0
Licensed Content Pages	7
Type of use	Dissertation/Thesis
Requestor type	Author of this Wiley article
Format	Print and electronic
Portion	Full article
Will you be translating?	No
Title of your thesis / dissertation	Improving Coupled Enzyme Assays With Capillary Electrophoresis
Expected completion date	May 2019
Expected size (number of pages)	160
Requestor Location	Thu Nguyen 640 Choppin Hall Louisiana State University BATON ROUGE, LA 70803 United States Attn: Thu Nguyen
Publisher Tax ID	EU826007151
Total	0.00 USD
Terms and Conditions	

TERMS AND CONDITIONS

This copyrighted material is owned by or exclusively licensed to John Wiley & Sons, Inc. or one of its group companies (each a"Wiley Company") or handled on behalf of a society with which a Wiley Company has exclusive publishing rights in relation to a particular work (collectively "WILEY"). By clicking "accept" in connection with completing this licensing transaction, you agree that the following terms and conditions apply to this transaction (along with the billing and payment terms and conditions established by the Copyright

Clearance Center Inc., ("CCC's Billing and Payment terms and conditions"), at the time that you opened your RightsLink account (these are available at any time at http://myaccount.copyright.com).

Terms and Conditions

- The materials you have requested permission to reproduce or reuse (the "Wiley Materials") are protected by copyright.

- You are hereby granted a personal, non-exclusive, non-sub licensable (on a stand-alone basis), non-transferable, worldwide, limited license to reproduce the Wiley Materials for the purpose specified in the licensing process. This license, **and any CONTENT (PDF or image file) purchased as part of your order,** is for a one-time use only and limited to any maximum distribution number specified in the license. The first instance of republication or reuse granted by this license must be completed within two years of the date of the grant of this license (although copies prepared before the end date may be distributed thereafter). The Wiley Materials shall not be used in any other manner or for any other purpose, beyond what is granted in the license. Permission is granted subject to an appropriate acknowledgement given to the author, title of the material/book/journal and the publisher. You shall also duplicate the copyright notice that appears in the Wiley publication in your use of the Wiley Material. Permission is also granted on the understanding that nowhere in the text is a previously published source acknowledged for all or part of this Wiley Material. Any third party content is expressly excluded from this permission.

- With respect to the Wiley Materials, all rights are reserved. Except as expressly granted by the terms of the license, no part of the Wiley Materials may be copied, modified, adapted (except for minor reformatting required by the new Publication), translated, reproduced, transferred or distributed, in any form or by any means, and no derivative works may be made based on the Wiley Materials without the prior permission of the respective copyright owner.**For STM Signatory Publishers clearing permission under the terms of the STM Permissions Guidelines only, the terms of the license are extended to include subsequent editions and for editions in other languages, provided such editions are for the work as a whole in situ and does not involve the separate exploitation of the permitted figures or extracts,** You may not alter, remove or suppress in any manner any copyright, trademark or other notices displayed by the Wiley Materials. You may not license, rent, sell, loan, lease, pledge, offer as security, transfer or assign the Wiley Materials on a stand-alone basis, or any of the rights granted to you hereunder to any other person.

- The Wiley Materials and all of the intellectual property rights therein shall at all times remain the exclusive property of John Wiley & Sons Inc, the Wiley Companies, or their respective licensors, and your interest therein is only that of having possession of and the right to reproduce the Wiley Materials pursuant to Section 2 herein during the continuance of this Agreement. You agree that you own no right, title or interest in or to the Wiley Materials or any of the intellectual property rights therein. You shall have no rights hereunder other than the license as provided for above in Section 2. No right, license or interest to any trademark, trade name, service mark or other branding ("Marks") of WILEY or its licensors is granted hereunder, and you agree that you shall not assert any such right, license or interest with respect thereto

- NEITHER WILEY NOR ITS LICENSORS MAKES ANY WARRANTY OR REPRESENTATION OF ANY KIND TO YOU OR ANY THIRD PARTY, EXPRESS, IMPLIED OR STATUTORY, WITH RESPECT TO THE MATERIALS

OR THE ACCURACY OF ANY INFORMATION CONTAINED IN THE MATERIALS, INCLUDING, WITHOUT LIMITATION, ANY IMPLIED WARRANTY OF MERCHANTABILITY, ACCURACY, SATISFACTORY QUALITY, FITNESS FOR A PARTICULAR PURPOSE, USABILITY, INTEGRATION OR NON-INFRINGEMENT AND ALL SUCH WARRANTIES ARE HEREBY EXCLUDED BY WILEY AND ITS LICENSORS AND WAIVED BY YOU.

- WILEY shall have the right to terminate this Agreement immediately upon breach of this Agreement by you.
- You shall indemnify, defend and hold harmless WILEY, its Licensors and their respective directors, officers, agents and employees, from and against any actual or threatened claims, demands, causes of action or proceedings arising from any breach of this Agreement by you.
- IN NO EVENT SHALL WILEY OR ITS LICENSORS BE LIABLE TO YOU OR ANY OTHER PARTY OR ANY OTHER PERSON OR ENTITY FOR ANY SPECIAL, CONSEQUENTIAL, INCIDENTAL, INDIRECT, EXEMPLARY OR PUNITIVE DAMAGES, HOWEVER CAUSED, ARISING OUT OF OR IN CONNECTION WITH THE DOWNLOADING, PROVISIONING, VIEWING OR USE OF THE MATERIALS REGARDLESS OF THE FORM OF ACTION, WHETHER FOR BREACH OF CONTRACT, BREACH OF WARRANTY, TORT, NEGLIGENCE, INFRINGEMENT OR OTHERWISE (INCLUDING, WITHOUT LIMITATION, DAMAGES BASED ON LOSS OF PROFITS, DATA, FILES, USE, BUSINESS OPPORTUNITY OR CLAIMS OF THIRD PARTIES), AND WHETHER OR NOT THE PARTY HAS BEEN ADVISED OF THE POSSIBILITY OF SUCH DAMAGES. THIS LIMITATION SHALL APPLY NOTWITHSTANDING ANY FAILURE OF ESSENTIAL PURPOSE OF ANY LIMITED REMEDY PROVIDED HEREIN.
- Should any provision of this Agreement be held by a court of competent jurisdiction to be illegal, invalid, or unenforceable, that provision shall be deemed amended to achieve as nearly as possible the same economic effect as the original provision, and the legality, validity and enforceability of the remaining provisions of this Agreement shall not be affected or impaired thereby.
- The failure of either party to enforce any term or condition of this Agreement shall not constitute a waiver of either party's right to enforce each and every term and condition of this Agreement. No breach under this agreement shall be deemed waived or excused by either party unless such waiver or consent is in writing signed by the party granting such waiver or consent. The waiver by or consent of a party to a breach of any provision of this Agreement shall not operate or be construed as a waiver of or consent to any other or subsequent breach by such other party.
- This Agreement may not be assigned (including by operation of law or otherwise) by you without WILEY's prior written consent.
- Any fee required for this permission shall be non-refundable after thirty (30) days from receipt by the CCC.
- These terms and conditions together with CCC's Billing and Payment terms and conditions (which are incorporated herein) form the entire agreement between you and WILEY concerning this licensing transaction and (in the absence of fraud) supersedes

all prior agreements and representations of the parties, oral or written. This Agreement may not be amended except in writing signed by both parties. This Agreement shall be binding upon and inure to the benefit of the parties' successors, legal representatives, and authorized assigns.

- In the event of any conflict between your obligations established by these terms and conditions and those established by CCC's Billing and Payment terms and conditions, these terms and conditions shall prevail.

- WILEY expressly reserves all rights not specifically granted in the combination of (i) the license details provided by you and accepted in the course of this licensing transaction, (ii) these terms and conditions and (iii) CCC's Billing and Payment terms and conditions.

- This Agreement will be void if the Type of Use, Format, Circulation, or Requestor Type was misrepresented during the licensing process.

- This Agreement shall be governed by and construed in accordance with the laws of the State of New York, USA, without regards to such state's conflict of law rules. Any legal action, suit or proceeding arising out of or relating to these Terms and Conditions or the breach thereof shall be instituted in a court of competent jurisdiction in New York County in the State of New York in the United States of America and each party hereby consents and submits to the personal jurisdiction of such court, waives any objection to venue in such court and consents to service of process by registered or certified mail, return receipt requested, at the last known address of such party.

WILEY OPEN ACCESS TERMS AND CONDITIONS

Wiley Publishes Open Access Articles in fully Open Access Journals and in Subscription journals offering Online Open. Although most of the fully Open Access journals publish open access articles under the terms of the Creative Commons Attribution (CC BY) License only, the subscription journals and a few of the Open Access Journals offer a choice of Creative Commons Licenses. The license type is clearly identified on the article.

The Creative Commons Attribution License

The Creative Commons Attribution License (CC-BY) allows users to copy, distribute and transmit an article, adapt the article and make commercial use of the article. The CC-BY license permits commercial and non-

Creative Commons Attribution Non-Commercial License

The Creative Commons Attribution Non-Commercial (CC-BY-NC)License permits use, distribution and reproduction in any medium, provided the original work is properly cited and is not used for commercial purposes.(see below)

Creative Commons Attribution-Non-Commercial-NoDerivs License

The Creative Commons Attribution Non-Commercial-NoDerivs License (CC-BY-NC-ND) permits use, distribution and reproduction in any medium, provided the original work is properly cited, is not used for commercial purposes and no modifications or adaptations are made. (see below)

Use by commercial "for-profit" organizations

Use of Wiley Open Access articles for commercial, promotional, or marketing purposes requires further explicit permission from Wiley and will be subject to a fee.

Further details can be found on Wiley Online Library

http://olabout.wiley.com/WileyCDA/Section/id-410895.html

Other Terms and Conditions:

v1.10 Last updated September 2015

Questions? customercare@copyright.com or +1-855-239-3415 (toll free in the US) or +1-978-646-2777.

VITA

Thu Hoai Nguyen was born in Vietnam. She attended Vietnam National University in Hanoi, Vietnam where she majored in Chemistry. As an undergraduate student, she worked on her thesis under Prof. Ta Thi Thao. In summer 2011, she worked as an undergraduate researcher under the mentorship of Dr. Alexander Scheeline at the University of Illinois at Urbana-Champaign. After graduating from Vietnam National University, she joined the Chemistry graduate program at Louisiana State University in 2013. In summer 2018, she worked at SC Johnson & Son, Inc. in Racine, WI as an RD&E intern.